CHALMERS

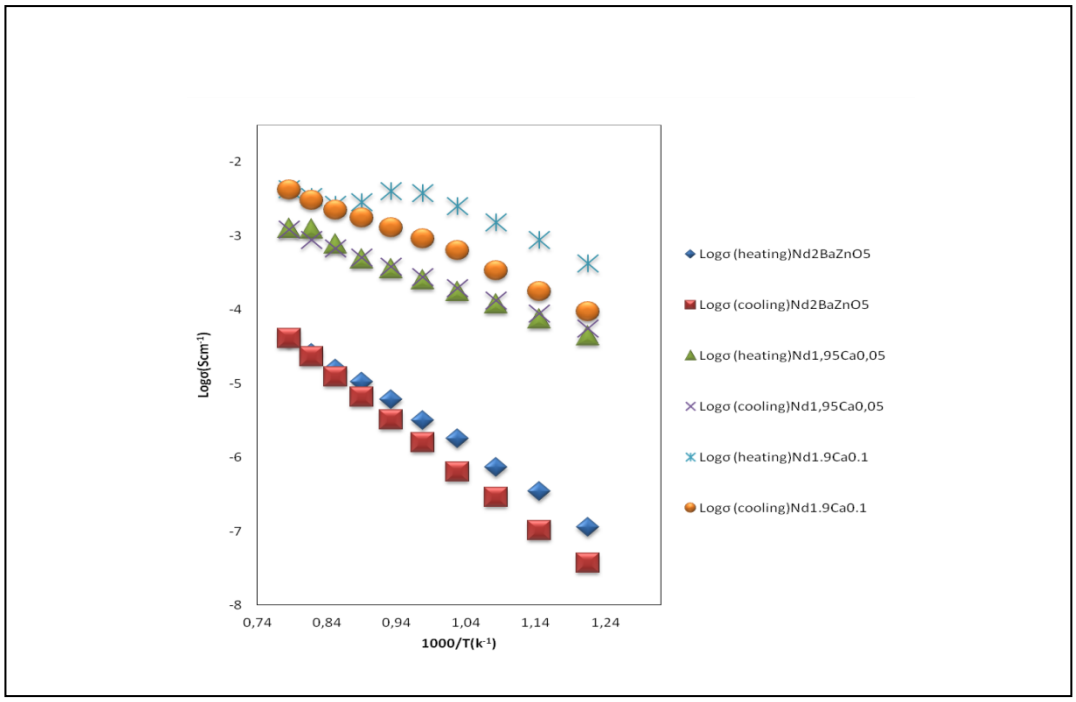

IONIC CONDUCTING OXIDE MATERIALS FOR CLEAN ENERGY APPLICATIONS: SYNTHESIS, STRUCTURE AND CONDUCTIVITY

Master's Thesis in the Master Degree Programme, Biotechnology

MD. KHAIRUL HOQUE

Department of Chemical and Biological Engineering
Division of Environmental Inorganic Chemistry
CHALMERS UNIVERSITY OF TECHNOLOGY
Gothenburg, Sweden, 2012
Master's thesis 2012:11

2012/11

IONIC CONDUCTING OXIDE MATERIALS FOR CLEAN ENERGY APPLICATIONS:

SYNTHESIS, STRUCTURE AND CONDUCTIVITY

MD. KHAIRUL HOQUE

Department of Chemical and Biological Engineering
Division of Environmental Inorganic Chemistry
CHALMERS UNIVERSITY OF TECHNOLOGY
Gothenburg, Sweden, 2012

Abstract

The main intent of the study was to find a suitable material with high oxide ion conductivity or proton conductivity which is chemically stable based on pyrochlore and other complex oxide systems. In particular how acceptor doping increased proton or oxide ion conductivity was examined in this thesis. Another purpose of the study was to investigate how the phase transition and other properties of brownmillerite structure based materials changes in humid condition.

In this thesis the following materials were investigated, pyrochlore structure based materials ($Nd_{2-x}Ca_xInMO_{7-\delta}$ where M=Nb,Ta $0\leq x\leq 0.05$), brownmillerite structure based materials($Ba_2In_{2-x}MO_{5-\delta}$ where M=Ga,Y and $0\leq x\leq 0.85$) and the zinc containing complex oxide system $R_{2-x}Ca_xBaZnO_{5-\delta}$ where R=La,Nd ; $0\leq x\leq 0.3$. These materials were successfully synthesized by solid state sintering method.

Rietveld refinement of X-ray diffraction (XRD) on $R_{2-x}Ca_xBaZnO_{5-\delta}$ confirmed these materials possessed tetragonal structure with I4/mcm space group. Changes in the unit cell parameter with Ca^{2+} introduction was proven by Rietveld analysis. XRD on hydrated samples proved that these materials were not stable in wet condition. Thermogravimetric analysis (TGA) results showed higher than expected mass losses for this system. The oxide ion conductivity of these materials increased with increase of doping level under dry Argon according to impedance spectroscopy data and the reached a maximum of ~0.01 Scm^{-1} at 1000 °C. The conductivity was also seen to increase further in dry oxygen, indicating significant p-type (electron hole) conductivity.

Brownmillerite structure based materials ($Ba_2In_{2-x}MO_{5-\delta}$ where M=Ga, Y and $0\leq x\leq 0.85$) possessed a structure with Ibm2 space symmetry up to $x \leq 0.5$ according to XRD. The unit cell volume expanded with increase of doping (ionic radius Y^{3+}=0,92Å) level and contracted with increase of dopant (ionic radius Ga^{3+}=0, 62Å).PXRD of hydrated Brownmillerite showed a structural transformation from orthorhombic to tetragonal. TGA result confirmed that these materials were fully hydrated.

Pyrochlore structure based materials ($Nd_{2-x}Ca_xInMO_{7-\delta}$ where M=Nb, Ta $0 \leq x \leq 0.05$) adopt a cubic structure with Fd-3m space group according to XRD and Rietveld refinement. These materials are not good ionic conductors according to the measured conductivity.

In summary this work provides a wider understanding of the influence of the acceptor doping on oxide ion conductivity and/or proton conductivity.

Key words: X-ray Diffraction (XRD), Rietveld refinement, Proton Conductivity, Oxide ion Conductivity, impedance spectroscopy, Thermogravimetric analysis. (TGA)

DEDICATION

I dedicate this project work to my father Late Md. Anwarul Hoque and mother Selina Nargis.I also want to dedicate this work to my brother Parash and sisters, Kohinoor, Nipu, popy and my wife mousumi.

Table of content

Abstract ..... **i**

DEDICATION ..... **iii**

Chapter1 ..... **1**

1.1 Introduction 1

1.1.1 Overview of fuel cells 1

1.1.2 Solid oxide fuel cells 2

1.1.3 Acceptor doping for proton and oxide ion conductivity 3

1.1.4 Aim of the thesis 4

1.2 Motivations 4

1.2.1 Technological approach 4

1.2.2 Fundamental approach 5

1.2.3 Oxide ion conductors 6

Chapter 2 ..... **8**

Overview of solid state conductors **8**

2.1 Oxide ion conductors 8

2.1.1 Fluorite structured oxides 8

2.1.2 Perovskite-structured oxides 9

2.1.3 New oxide ion conductors 9

2.2. Proton conductors 10

2.2.1 Perovskite-structured oxides 11

2.2.2 Perovskite related oxides 12

2.2.3 Phosphates 12

2.2.4 Solid acids 12

2.2.5 New types of proton conductors 13

Chapter 3 ..... **14**

Experimental sections **14**

3.1 Sample preparation 14

3.1.1 The solid state sintering method 14

3.1.2 Wet chemical route 14

3.1.2.1 .Sol gel 14

3.1.2.2. Precipitation method 15

3.1.3 Hydrated samples 15

3.1.4 Vacuum dried samples 15

3.1.5 Samples for Impedance measurements 16
3.2. Characterization Methods 16
3.2.1 Thermogravimetric Analysis (TGA) 16
3.2.2 Diffraction 17
3.2.2.1 X-Ray powder Diffraction 18
3.2.3 The Rietveld Refinement Method 19
3.2.4 Impedance Spectroscopy (IS) 19
Chapter 4 22
Pyrochlore structure based materials 22
Chapter 5 27
Brownmillerite structure based materials 27
Chapter 6 40
Ln_2BaZnO_5 systems 40
Conclusion 59
Appendix I 60
Appendix II 63
Acknowledgements 64
References 65

Chapter1

1.1 Introduction

A secure and consistent supply of energy is needed for modern society to lead a comfortable and better daily life. Nowadays a main challenge facing the world is to find new cleaner and sustainable sources of energy. Our natural recourses of energy are limited but the population is increasing day by day. Because of increasing awareness of environmental factors and limited supply of energy recourses, we have to think about alternative ways of using clean energy sources. Fuel cells are electrochemical devices that directly convert chemical energy in fuel into electrical energy in a clean and sustainable way. This is based on the chemical reaction between hydrogen introduced (at the anode) and oxygen (at the cathode) to produce water and electricity.

1.1.1 Overview of fuel cells

Depending on the electrolyte materials fuel cells are categorized as polymer electrolyte fuel cells (PEMFC), alkaline fuel cells (AFC), phosphoric acid fuel cells (PAFC), molten carbonate fuel cells (MCFC) and solid oxide fuel cells (SOFC). The above mentioned fuel cells have the same principal but they differ when it comes to properties like fuel, the operating temperature and the mobile ions for ionic conduction (1). For example the charge carrier in AFC are hydroxyl groups that move in the electrolyte, in PEMFC and PAFC protons(H^+) move, in MCFC carboxyl groups(CO_3^{2-}) flow in the electrolyte and in SOFC oxide ion(O^{2-}) and protons(H^+) are the mobile ionic species. Schematics of SOFCs utilizing oxide-ion conducting and proton conducting electrolytes are shown in Fig. 1(a) and (b), respectively,

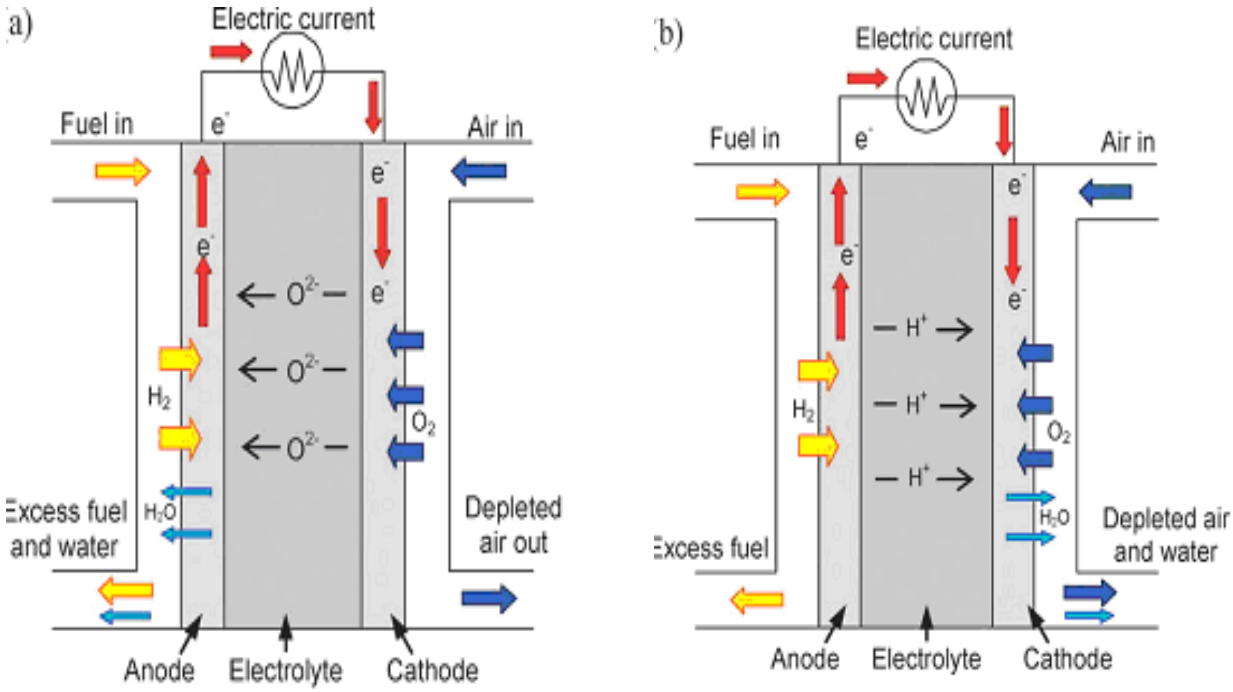

Figure 1: Schematic diagram of the processes taking place in a solid oxide fuel cell (SOFC) during operation; (a) oxide-ion conducting electrolyte, and (b) proton conducting electrolyte.(2)

1.1.2 Solid oxide fuel cells

Based on the electrolyte materials SOFC are categorized as oxide-ion conducting fuel cell and proton conducting fuel cell (Figure 1). A SOFC based on an oxide ion conductor has advantages such as, high efficiency, low emissions and relatively low cost. SOFC operates at high temperature T>800^{0}C results corrosion and long start up times. Efficiency (about 45-55%) is low due to water vapour produced at the anode as less fuel utilization, thermal insulation needed to retain heat that limits applications for transportation. There is a high interest in the synthesis of new materials for SOFC application in the intermediate temperature range (200-700^{0}C). Perovskite oxides, such as $BaZr_{0.9}Y_{0.1}O_{3-\delta,}$ have been the focus of research into proton conducting materials and these show higher ionic conductivity than oxide ion conductors at intermediate temperatures.

1.1.3 Acceptor doping for proton and oxide ion conductivity

Partial substitution of an acceptor doping creates oxygen vacancy into the materials. This oxygen vacancy is important to successfully incorporate protons in a material. When these materials are exposed to humidified atmosphere hydroxyl ion fills the oxygen vacancy and proton forms a covalent bond with oxygen in the structure, these phenomena can be describe by Kröger-Vink notation as follows,

$$H2O\ (g) + V0^{\cdot} + O_o^{x} = 2OH_o^{\cdot}$$

In oxidizing atmospheres formation of electronic holes due to compensate oxygen vacancy according to,

$$^{1}/_{2}\,O_2 + V_o^{\bullet\bullet} \leftrightarrow O_o^{\,x} + 2h^{\bullet}$$

At low oxygen partial pressure reduction can also take place (3), (4),

$$O_o^{\,x} \leftrightarrow {}^{1}/_{2}\,O_2 + V_o^{\bullet\bullet} + 2\acute{e}$$

For oxide ion conductors acceptor doping also create vacancy on the oxide ion sublattice. At higher temperature (above 800^0C) this high vacancy concentration with high mobility enhances very high oxide ion conductivity in this material. For example Zr^{4+} is substitute by Y^{3+} in $Zr_{1-x}Y_xO_{2-x/2}$ where x=0.1 higher oxide ion conductivity was observed at temperature above 800^0C (5).

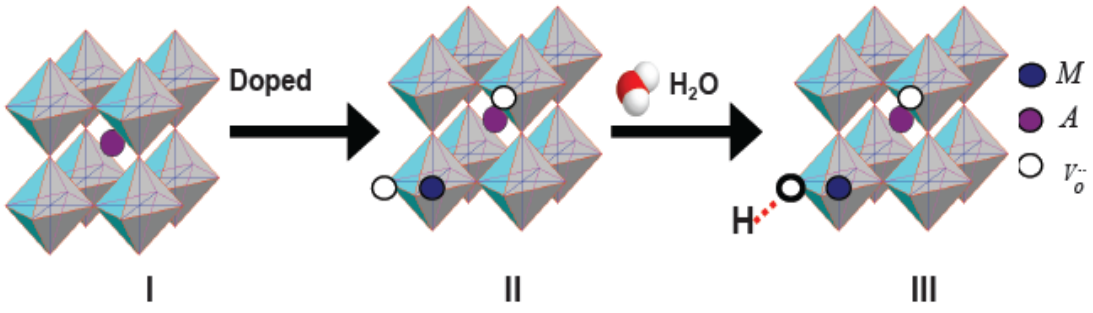

Figure 2**:** A schematic picture of formation of and filling of an oxygen vacancy by acceptor doping: I) Perfect lattice, II) Introduction of oxygen vacancies, III)
Formation of proton defect (6).

1.1.4 Aim of the thesis

The main intent of the study was to find a suitable material with high ionic conductivity which is chemically stable based on pyrochlore and complex oxide system. Another purpose of the study is to investigate how the phase transition and other property of brownmillerite structure based materials changes in humid condition. How the acceptor doping increase proton or oxide ionic conductivity was examined in this thesis. These can be future materials for clean energy application.

In this thesis for research purpose the following materials investigated which are as follows, pyrochlore structure based materials($Nd_{2-x}Ca_xInMO_{7-\delta}$ where M=Nb,Ta $0\leq x\leq 0.05$), brownmillerite structure based materials($Ba_2In_{2-x}MO_5$ where M=Ga,Y and $0\leq x\leq 0.85$) and complex oxide system $R_{2-x}Ca_xBaZnO_{5-\delta}$ where R=La,Nd ; $0\leq x\leq 0.3$.

In order to investigate the property of the materials following techniques such as solid state routes for material synthesis, powder x-ray diffraction, impedance spectroscopy, thermogravimetric analysis, differential scanning calorimetry, Rietveld analysis and z-view program were used in this thesis.

1.2 Motivations

1.2.1 Technological approach

Proton conductors are generally preferred compared to aqueous electrolyte fuel cell due to greater corrosion robustness and resistance (7).SOFC operates at high temperature ($T>800^0C$) though high operating temperature has some technical problems such as long startup times, high temperature corrosion on these materials, low efficiency and thermal insulation is needed for these system(8),(9).SOFC operating at lower temperatures can the overcome above mentioned problems with high temperature SOFC. Low temperature fuel cells are polymer membrane electrolyte fuel cell(PEMFC) with proton conducting Nafion (perfluorosulfonic polymer) as the best electrolyte although these have some problems such

as the requirement of expensive platinum catalysts, low electrical efficiency .A desirable alternative is fuel cell operating in an intermediate temperature range (200-700^{0}C).

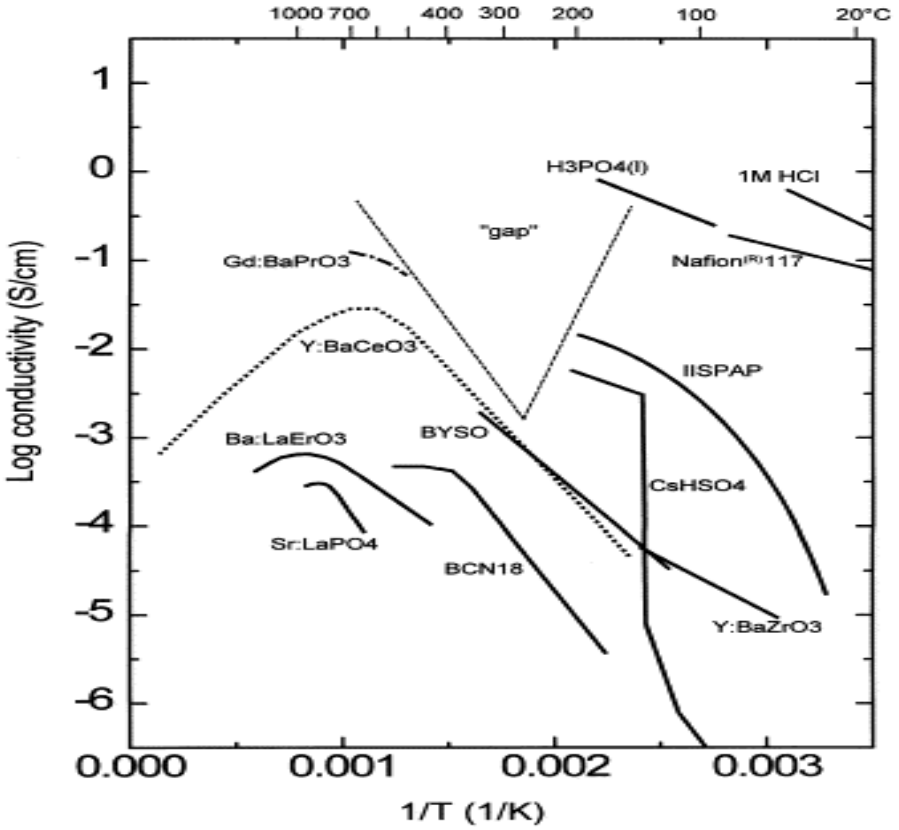

Figure3: Proton conductivity in selected materials, Imidazole-intercalated sulfonated polyaromatic polymer (IIPAP); dotted lines is calculated estimate of BYSO: $Ba_2YSnO_{5.5}$; Y: $BaCeO_3$. (7)

Norby (7) shows (figure 3) the presence of a gap in the intermediate temperature range where no materials show high proton conductivity. In^{3+} doped SnP_2O_7 possessed high proton conductivity (10^{-1} S·cm^{-1} at 250^{0}C under wet atmosphere) (10).

1.2.2 Fundamental approach

Proton conductivity of several perovskite has been reported for several years of them Y doped $SrCeO_3$ and $BaCeO_3$ were shown to have high proton conductivity. Proton conductivity of pyrochlore oxides and fluorite oxides have been investigated in figure 4 such as $Ln_2Zr_{2-x}Y_xO_{7-\delta}$ where (Ln=La, Nd, Gd, Sm) Proton conductivity of various oxides has been summarized in figure 4.

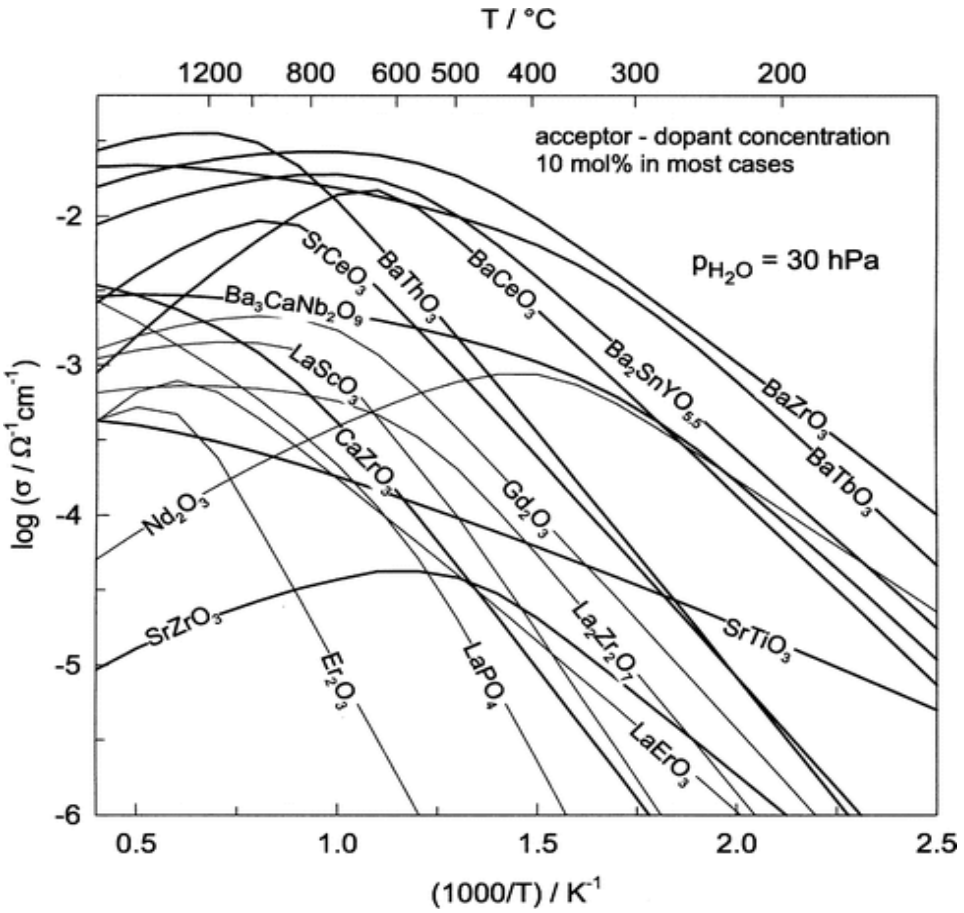

Figure 4: Kreuer's summary of proton conductivity of various oxides which are based on motilities and concentrations calculated by Norby and Larring. (11), (12)

Perovskite oxides have highest proton conductivities than pyrochlore oxides.Pyrochlores' show proton conductivity ~ 1-2 lower order magnitude lower than best performing perovskite. Therefore, in this study we focused on pyrochlore structure based materials $Nd_{2-x}Ca_xInMO_{7-\delta}$ where M=Ta, Nb.

This study also focused on new type of materials with $Ln_{2-x}Ca_xBaZnO_{5-\delta}$ structure based where Ln=Nd, La and brownmillerite structure based materials $Ba_2In_{2-x}MxO_{5-\delta}$ where M=Ga,Y which are derivative of ABO_3 type perovskite oxides.

1.2.3 Oxide ion conductors

Developing and discovering highly ionic conductive and chemically stable electrolyte materials is one of the main roles of materials science. There are several oxide ions conductive materials have been discovered over the last decade. Well known oxide ion

conductors with different conduction mechanism such as Yttria stabilized zirconia (YSZ), cerium –gadolinium oxide (CGO), $La_{0.9}Sr_{0.1}Ga_{0.8}Mg_{0.2}O_{2.85}$ (LSGM), $La_{10}(SiO_4)_6O_3$ (Si-apatite), $La_2Mo_2O_9$ (LAMOX) (Figure 3)of them CGO and YSZ adopt fluorite type crystal structure.YSZ is the most common electrolyte materials but operates at high temperature (typically 800-1000^{0}C)(2).CGO has higher conductivity than YSZ and operates at lower temperature (500-700^{0}C) than YSZ.

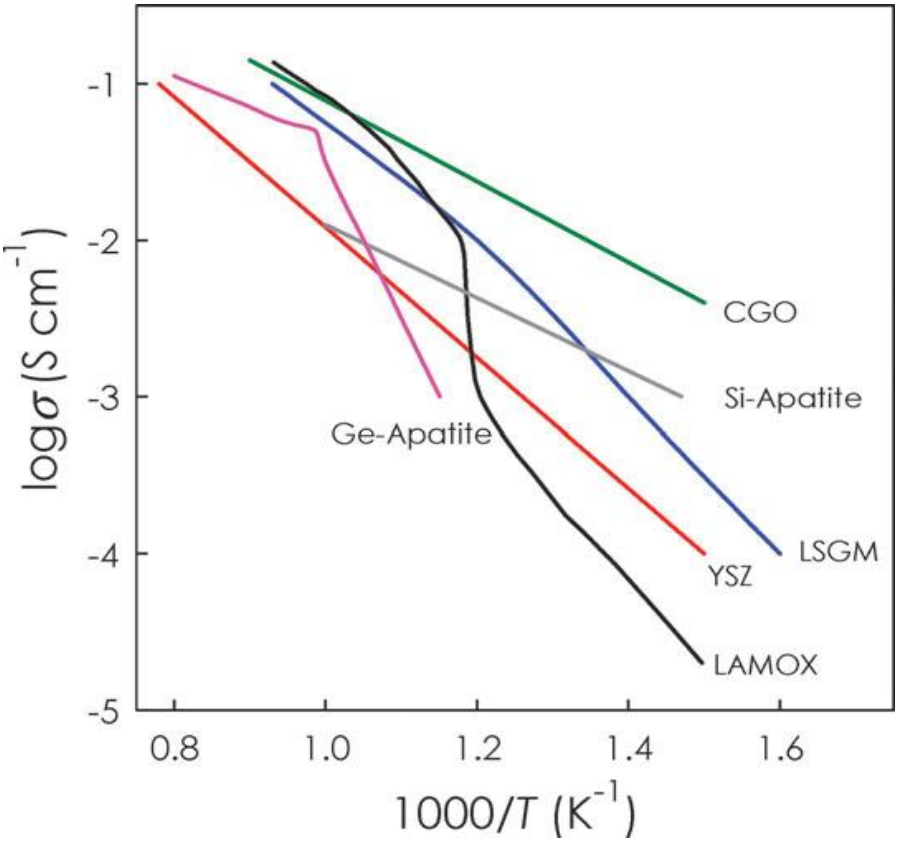

Figure 5: Total conductivity plot of several oxide-ion conductors as function of inverse temperature. (13)

The material LSGM is perovskite structure based oxide exhibits higher ionic conductivity than YSZ. Ge-apatite, Si-apatite and LAMOX are new types of oxide ion conductors being studied as SOFC electrolytes (14),(15).

Chapter 2

Overview of solid state conductors

2.1 Oxide ion conductors

Oxide ion conductors can be classified into several categories either on the basis of the transport species or on their working temperature. In this section, structure and conductivity of some conventional and new oxide-ion conductors were discussed briefly.

2.1.1 Fluorite structured oxides

Most of the oxide ion conducting materials has fluorite type crystal structure like AO_2, where A is tetravalent cation. Figure 6 illustrated the fluorite type crystal structure(AO_2).One of the best known fluorite type oxide ion conductor is acceptor doped ZrO_2.Yttria stabilized zirconia (YSZ) is the most widely used electrolyte for SOFCs. This material has good chemical stability and exhibiting good oxide ion conductivity above 700^0C.Other fluorite type oxide ion conductors are cerium-gadolinium oxide (CGO), sammaria doped ceria (SDC), δ-Bi_2O_3 .CGO have higher conductivity than YSZ even at lower temperature (500-700^0C).δ-Bi2O_3 has high fraction of vacancies which is basis for its high ion conductivity. δ-Bi_2O_3 doped with rare earth materials such as, Y, Dy or Er by partially substitute Bi which possess high oxide ion conductivity even at low temperature (16).

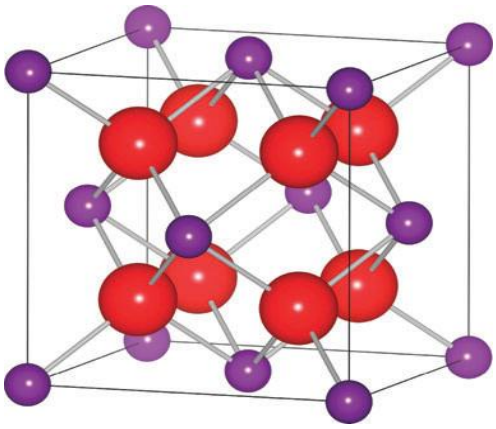

Figure 6**:** Fluorite type crystal structure (AO_2) adopted by ZrO_2 where O^{2-} ions are represented by red circles and small purple represent A^{4+} ions.

2.1.2 Perovskite-structured oxides

Perovskite structure (ABO_3) is a simple crystal structure where A-site cation is large coordinated to twelve anions. B cation is smaller occupying a six-coordinate site and forming BO_6 octahedra.

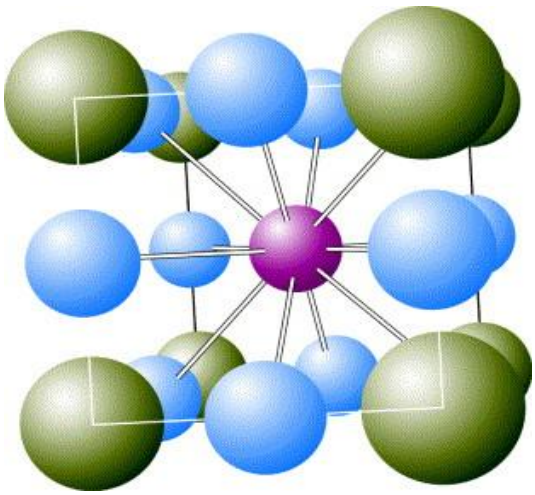

Figure 7: Representation of cubic perovskite (ABO_3) structure, where the red circle represents the A-cation, the green circles represent the B-cations, and the small blue circles are oxygen ions. (17)

Perovskite structure based oxide ion conductors have been used as electrolytes in the Intermediate temperature range (650-800°C) is doped lanthanum gallate, $LaGaO_3$. (Sr, Mg) doped $LaGaO_3$ with composition $La_{0.9}Sr_{0.1}Ga_{0.8}Mg_{0.2}O_{3-\delta}$ (LSGM) is found as high ion conductor which is suitable for ionic applications (18), (19), (20).This material exhibit higher ionic conductivity than some of the existing fluorite-type oxides YSZ even at lower temperature. The purpose of acceptor doping on both La with Sr and Ga site with Mg is to create oxygen vacancy to aid rapid oxide ion conductivity. Another type of perovskite structure oxide ion conductors are $BaCeO_3$(21), $NdGa_{0.9}Mg_{0.1}O_{2.95}$(22), $Gd_{0.85}Ca_{0.15}AlO_{2.925}$(23).

2.1.3 New oxide ion conductors

In 2000 the group of Lacorre developed the LAMOX family of oxide ion conductors based on patent material $La_2Mo_2O_9$ (LAMOX).There is α-β phase transition was found at above 600^0C with the latter ionic conductivity of 6×10 $Scm^{-1}$was found at 800^0(24).The compound has one of the complex crystal structure with 312 crystallo-graphycally distinct sites. Figure 8

illustrated the structure of β-LAMOX is emphasizing the coordination environments of the anions where [La–Mo–O1] tetrahedral units is surrounded by oxide ions on O2 and O3 sites. LAMOX has a high oxide ion conductivity to be considered as a practical material for solid electrolyte application.

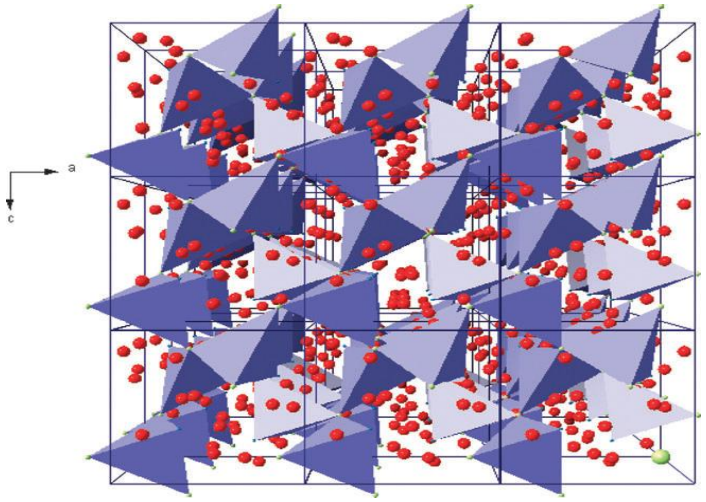

Figure 8: A rigid framework of β-$La_2Mo_2O_9$ with [La–Mo–O1] units with O_2 and O_3 sites.

Apatite-type oxides are most fascinating of the new materials being studied as alternative SOFC electrolytes which are recently discovered. In 1990 fast oxide ion conductivity was discovered in silicate based apatites $Ln_{9.33}(SiO_4)_6O_2$ where (Ln=La, Nd)(25), (26).

The BIMEVOX families of oxide ions are good conductors which are based on fluorite-related oxide Bi_2O_3 .A typical composition of this type of oxide ($Bi_2Mg_xV_{1-x}O_{5.5-3x/2-\delta}$) showed ionic conductivity of the order of 0.1 S cm^{-1} at 600°C (27)

2.2. Proton conductors

30 years ago the field of solid state conductors emerged. Proton conducting oxides are important for both academics and technologies. Proton transport depends on the structural and physical properties of the materials.

2.2.1 Perovskite-structured oxides

In 1980 Iwahara and co-workers discovered high-temperature proton conductivity in oxide materials doped strontium and barium cerates which are perovskite structure based. The perovskite-type cerates and zirconates become well established proton conductors after twenty years of active investigation (28).Some well-known proton conductors are illustrates in figure 9. Undoped $SrCeO_3$, $BaCeO_3$, $CaZrO_3$ and $SrZrO_3$ exhibit low proton conductivity. $BaCeO_3$ with 10mol% Y doped ($BaCe_{0.9}Y_{0.1}O_3$) exhibits high proton conductivity. This material is one of the best proton conductors. Y-doped $BaZrO_3$-based oxides (BZO) are highly stable with high proton conductivity that exceeds best oxide ion conductivity at temperature below 700^0C (Figure 9).

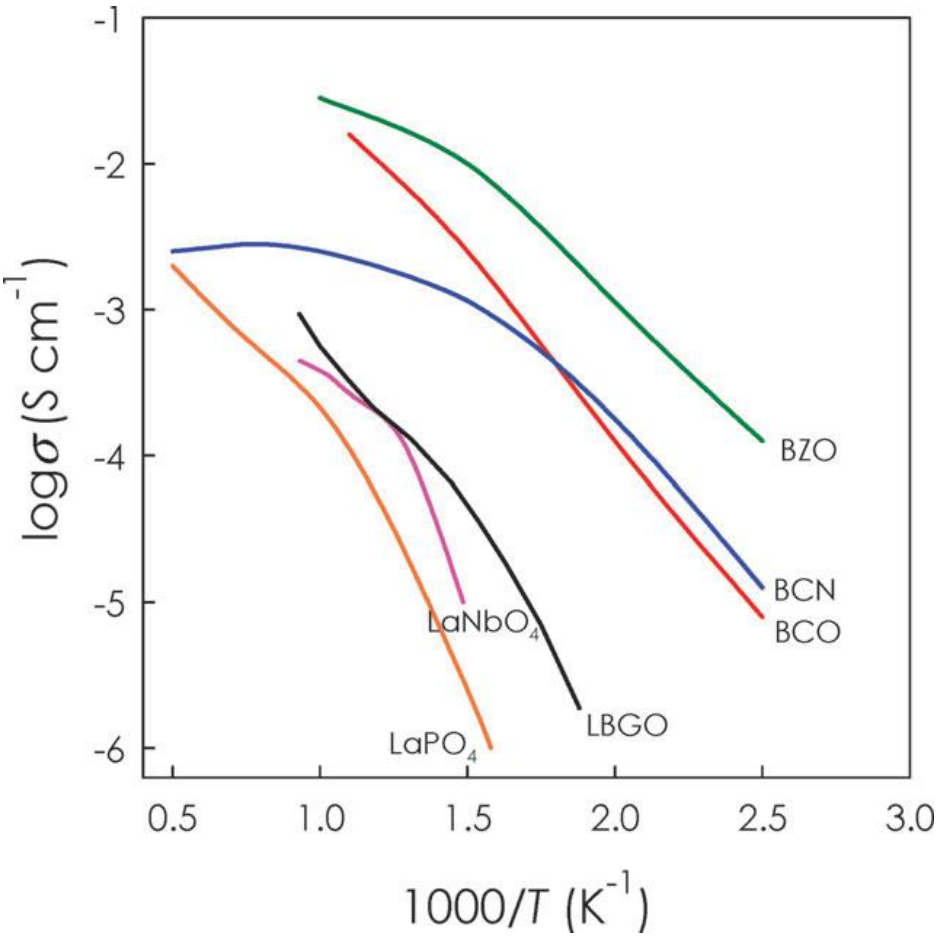

Figure 9: Well know proton conductors such as $BaCe_{0.9}Y_{0.1}O_3$ (BCO); $BaZr_{0.8}Y_{0.2}O_3$ (BZO); $La_{0.9}Sr_{0.1}PO_4$; $Ba_3Ca_{1.18}Nb_{1.82}O_{8.73}$ (BCN); $La_{0.99}Ca_{0.01}NbO_4$; $La_{0.8}Ba_{1.2}GaO_{3.9}$ (LBGO) with their total conductivity (2).

2.2.2 Perovskite related oxides

Perovskite related oxides $Sr_{6-2x}Nb_{2+2x}O_{11+3x}$, $Sr_{6-2x}Ta_{2+2x}O_{11+3x}$, and $(Ba_{1-y}Cay)_6Nb_2O_{11}$ showed purely proton conductivity at 600^0C .The value of conductivity is very low (less than 10^{-3} S cm^{-1}). One of the known best materials $Ba_3Ca_{1.18}Nb_{1.82}O_{8.73}$ (also known as BCN18) for proton conductivity which is comparable with other best proton conductors BZO,BCO(figure 9).

Perovskite-related materials $Ba_2In_2O_5$ initially proposed as an oxide-ion conductor later considered its ability to conduct protons (29). This material is also known as brownmillerite structure based materials. This material is also studied in this thesis. High conductivity phase of this material is stabilized by replacing either Ba or In (or sometimes both). $(Ba_{1-x}La_x)_2In_2O_{5+x}$ system where x=0.1 showed proton conductivity of 1.12×10^{-5} S cm^{-1} at 400^0C. Investigation of these materials has substantial opportunities for developing higher proton conductors (2).

2.2.3 Phosphates

Phosphates are relatively high temperature proton conductors. In 1990s the compound $LaPO_4$ was proposed as proton conductor (30). $LaPO_4$ with Ca and Sr doped exhibit protonic conductivity of 6×10^{-5} S cm^{-1} and 3×10^{-4} S cm^{-1} respectively at ~800^0C.Other phosphates lanthanum polyphosphate (LaP_3O_9) and lanthanum oxophosphate $La_7P_3O_{18}$ have shown protonic conduction in humid condition about 3×10^{-4} S cm^{-1}at 700^0C (2).

2.2.4 Solid acids

Inorganic solid acids such as $CsHSO_4$ and CsH_2PO_4 have showed high proton conductivity at moderate temperatures (120-300^0C).These structures are consisting of SO_4 and PO_4. CsH_2PO_4 has super atomic disorder phase that's why electrolyte based on this material has been demonstrated for both H_2/O_2 and methanol fuel cells for continuous power generation (2).

2.2.5 New types of proton conductors

Niobates and tantalates are more stable proton conducting materials. High conductivities in the niobates and tantalates are obtained at relatively low doping level compare to perovskite structure based materials. $La_{0.99}Ca_{0.01}NbO_4$ has been reported to have the high conductivity (Figure 9).La containing niobates have higher proton mobility than other Re based niobates.

Although the conductivity of these materials are low compared to perovskite types cerates ,these materials represent a promising family of materials capable of operating in CO2 containing atmosphere for use as thin film electrolytes for SOFCs(2).

General formula of gallium based oxides is $La_{1-x}Ba_{1+x}GaO_{4-x/2}$ .Gallium based oxide with composition $La_{0.8}Ba_{1.2}GaO_{3.9}$ has shown high proton conductivity at intermediate temperature (figure 9).

Chapter 3

Experimental sections

The experimental section comprises two parts one is sample preparation and another is characterization methods. Both sections describes briefly in bellow section.

3.1 Sample preparation

Crystalline solids can be prepared as ceramics, films, powders, nano-particles and single crystals. Sample preparation depend on thermodynamics stability of the compounds (2).solid state sintering method is most common method because of its simplicity. Other method like sol-gel and milling procedure can be used in order to decrease sintering temperature. Various synthesis method of making is described here briefly.

3.1.1 The solid state sintering method

It is traditional method involves mixing, compacting and firing of reactants to achieve the desired product. The rate of reaction is determined by kinetics and change of free energy. This method is slow but simple. Sometimes further compacting and firing is needed in order to obtain complete pure samples. The compacting and firing enhance solid state diffusion.

3.1.2 Wet chemical route

3.1.2.1 .Sol gel

An important synthesis route is based on sol gel chemistry and modified pechini routes (33).Wet chemical routes have some advantages over solid state sintering method: this process reduces the synthesis temperature and allows development of new fabrication techniques (e.g films, fibers, monoliths)(34).The desired pure phase can be obtained quickly at low temperature

3.1.2.2. Precipitation method

It is very fast and useful in synthesis of solid acids (compounds with intermediate properties between the acid and its salt) where one of the reagents is an aqueous solution and another reagent are dissolve in the acidic solution before adding methanol and ethanol. Finally precipitated desired salt is washed with ethanol and dried before use.

3.1.3 Hydrated samples

As prepared sample were hydrated at different temperature like 400,300,250^{0}C under N2 gas flow that has been pre-saturated with water at 76.2°C.and p(H_2O)= ~0.42atm (figure 10) for several days.

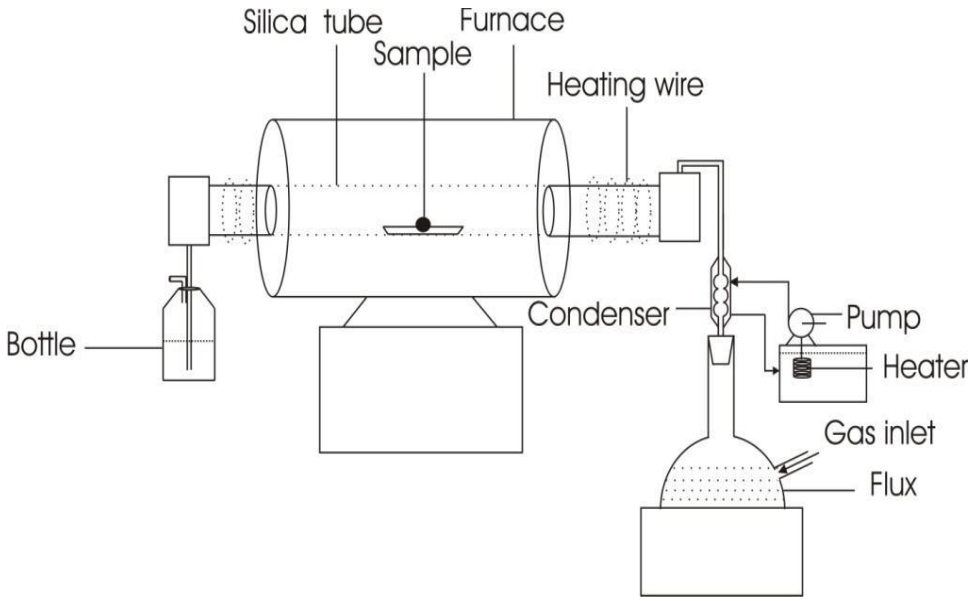

Figure 10: A schematic diagram of the set up used to hydrate samples. (35)

3.1.4 Vacuum dried samples

These dried samples were achieved by annealing the as-prepared samples in vacuum (10^{-6} mbar) at 900^{0}C or sometimes at 800^{0}C overnight. The samples were carefully removed from the vacuum and transferred to a controlled atmosphere.

3.1.5 Samples for Impedance measurements

In order to make dense pellets for Impedance measurements, 1.5g of the powder was placed into a 13mm die and 5.5 metric ton pressure was applied to compress powder into a cylindrical pellet. The pellet was sintered at 1100^0C for 10h in air. Circular surface of sintered pellet was coated with platinum ink paste and heated at 1000^0 C for 1h to burn away organic residues.

3.2. Characterization Methods

The characterization methods used in this thesis are Thermogravimetric Analysis (TGA), X-Ray powder Diffraction, The Rietveld Refinement method, and Impedance Spectroscopy (IS) .etc. All these methods are described briefly below.

3.2.1 Thermogravimetric Analysis (TGA)

Thermogravimetric analysis (TGA) is a type of experiment performed on a sample to measure the change in mass of the sample as a function of temperature or time. Change in mass upon heating is a fundamental property of samples Change in mass also explains how the sample undergoes decomposition or absorption/desorption when heated or cooled under controlled atmospheres. This mass change can be quantitatively linked with chemical and physical process such as hydration of a proton conductor (31).

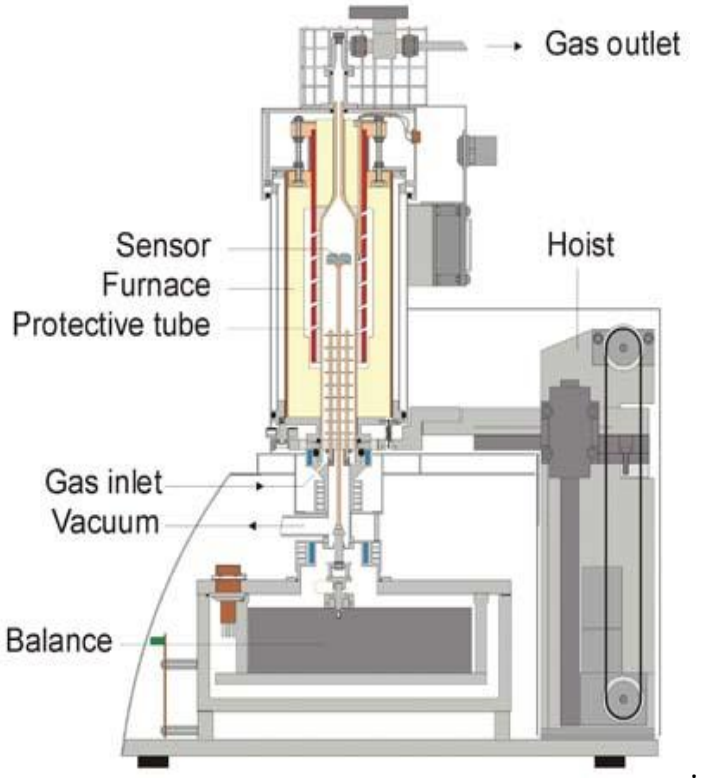

Figure 11: A schematic diagram of the TGA experiment set up of NETZSCH STA 409 PC

In the case of proton conductors the hydrated sample mass loss is greater than as prepared sample because during hydration reaction significant mass increase. The amount of protonic defects formed during hydration process is thus measured by TGA.

The instrument used for TGA experiment was a NETZSCH STA 409 PC (Figure 11).Alumina crucibles were used as sample and reference container.N_2 gas was used as supporting gas. An empty run was performed before a new batch of sample was run and 50-100mg of sample was run under experimental condition. Before each run the top valve is shut and vacuum pump is turned on.TGA chamber is evacuated and refilled with N_2 gas two times. After that the pump is turned off and top valve is opened and the initial condition gas is on for 10 min in order to ensure gas flow equilibrium.

3.2.2 Diffraction

Initially diffraction pattern is used to characterize the compound. Each crystalline compound has its own diffraction pattern. In order to describe the crystal structure it can be divided

into unit cell. Diffraction pattern represent the atomic structure of the compound in terms of the unit cell. Characterization of periodic arrangement of atom is described by integer values h,k,l known as miller indices. When these planes are parallel to each other the distance between the planes is denoted by $\mathbf{d_{hkl}}$.

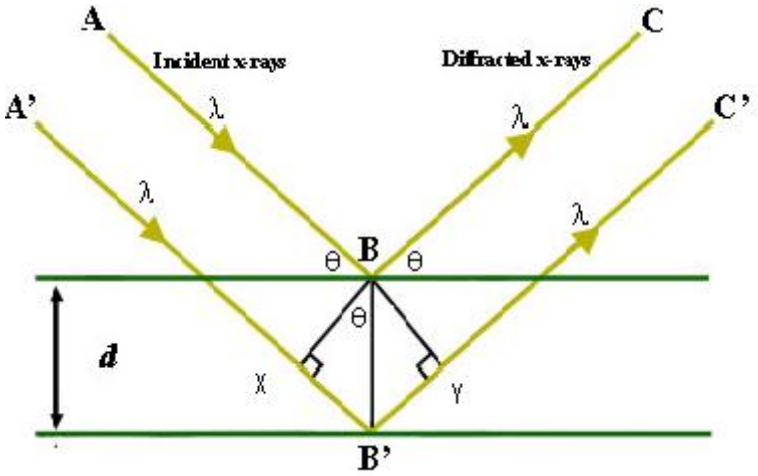

Figure 12: Bragg's Law reflection where path difference is 2dsinϴ and d denotes the inter-planar distance. (31)

Bragg and his son developed a simple theory of diffraction from crystal. Derivation of Baggs law for X-ray diffraction is shown by Figure 12.Two X-ray beam A,A' are reflected from adjacent planes B,B'. Beam A'B'C' has to travel extra distance compared to beam ABC. If the path difference (dsinθ) is equal to integer number (n) of wavelength (**λ**) then constructive interference occurs and a diffraction pattern peak appears according to Braggs equation 1., $\mathbf{2d_{hkl}\sin\theta=n\lambda}$ eq 1 where θ is Braggs angle and d is distance between plane denoted by hkl

Distance between planes d determines peak position in the diffraction pattern and crystal structure of the compound can be studied.

3.2.2.1 X-Ray powder Diffraction

X-Ray powder Diffraction (XRD) is widely used powerful technique for characterization of crystalline solids. It's a quick method to verify sample purity, identify impurity and progress of synthesis. When the x-rays are illuminated on a sample, electrons in the atoms of the sample scatter light and a diffraction pattern is produced. This pattern is collected by a

detector. In this study a Bruker D8 powder diffractometer is used and radiation used was the Cu kα_1 radiation with a wavelength of 1.5406Å. A database of International Centre for Diffraction Data (ICDD) was used to identify the samples.

3.2.3 The Rietveld Refinement Method

Rietveld analysis is a method of refining crystal structure from powder diffraction data (33). This method involves interpretation of not only line position but also of line intensities. In the Rietveld method least-squares refinements is used to fit a calculated pattern with the entire powder diffraction pattern.(32).By changing different parameter such as, lattice parameters, background, temperature factors and position of the atoms the difference between experimental data and that calculated based on the structural model is minimised. The accuracy of the model is judged by reliability factors and lower R value implies convergence of least-square calculation but provides no guarantee that the model is physically meaningful. Good chemical knowledge is also needed to check that desired bond lengths are realistic.

3.2.4 Impedance Spectroscopy (IS)

Impedance spectroscopy (IS) is a good method to characterize the electrical properties of materials and their interface with electrodes (34). A known voltage or current is applied to the electrode and a response current or voltage is observed. The most common and standard electrical stimuli is to apply frequency voltage to the interface and measure the impedance from the phase shift and amplitude. The resulting current has two parts, imaginary and real. Typically, $v(t) = V_m \sin(\omega t)$ is applied to the cell and the resulting steady state current, $i(t) = I_m \sin(\omega t+\theta)$ is measured(4),where v (t), i(t), V_m , I_m, t and θ are respectively voltage function, current function, voltage amplitude, current amplitude, time and phase difference between current and voltage. Impedance and its magnitude can be defined as $Z(\omega) = v(t)/i(t)$ and $|Z(\omega)| = Vm/Im(\omega)$ respectively. Z is complex quantity and can be written as $Z(a) = Z' + jZ''$ where j is imaginary number. According to the figure 13,

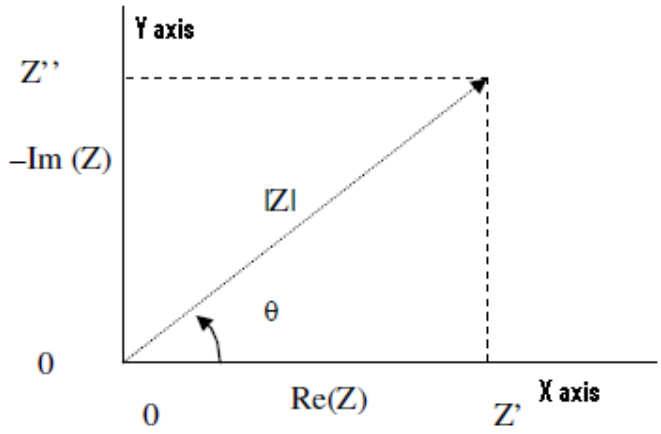

Figure 13: The real and imaginary part of the impedance is represented in vector format (34).

From the figure it can be written Re (Z) ≡ Z' = |Z|cosθ and Im (Z) ≡ Z'' = |Z|sinθ where phase angle $\theta = \tan^{-1}(Z'/Z'')$ and modulus is defined as $|Z| = [(Z')^2 + (Z'')^2]^{1/2}$.

Figure 14 represents schematic diagram of the setup used during the experiment where Probostat cell in the furnace is connected with the with the Solartron 1260 analyzer which is connected with the computer. Smart software is used to control the temperature and analyser.

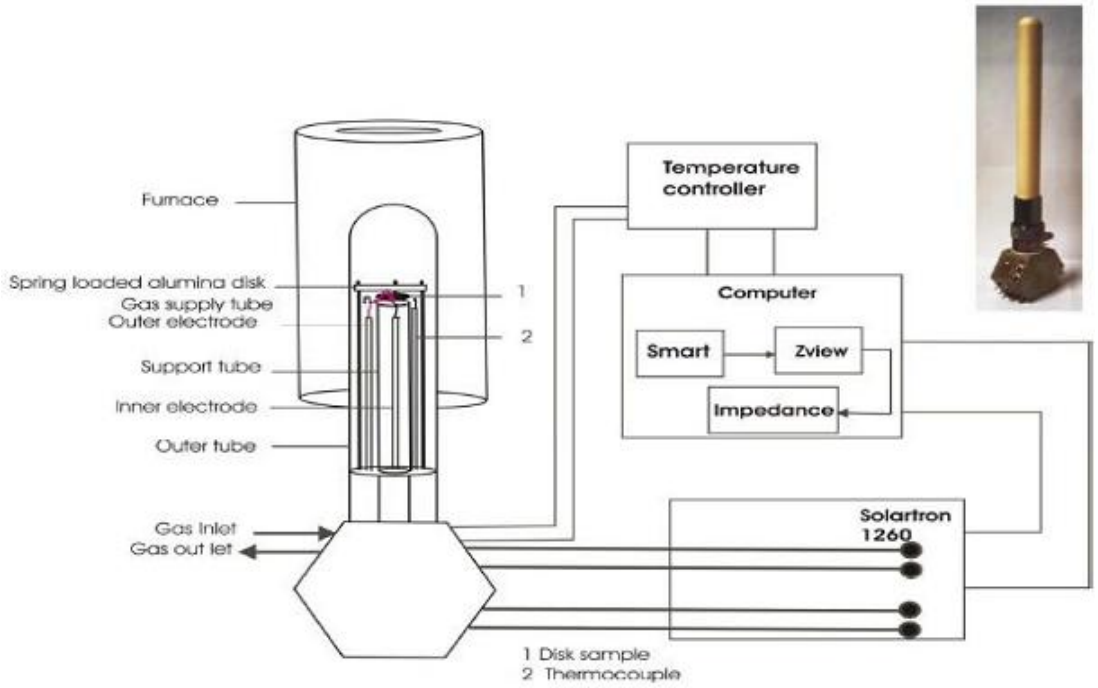

Figure 14: A schematic diagram of Impedance Spectroscopy setup .Insert picture is of the conductivity cell.

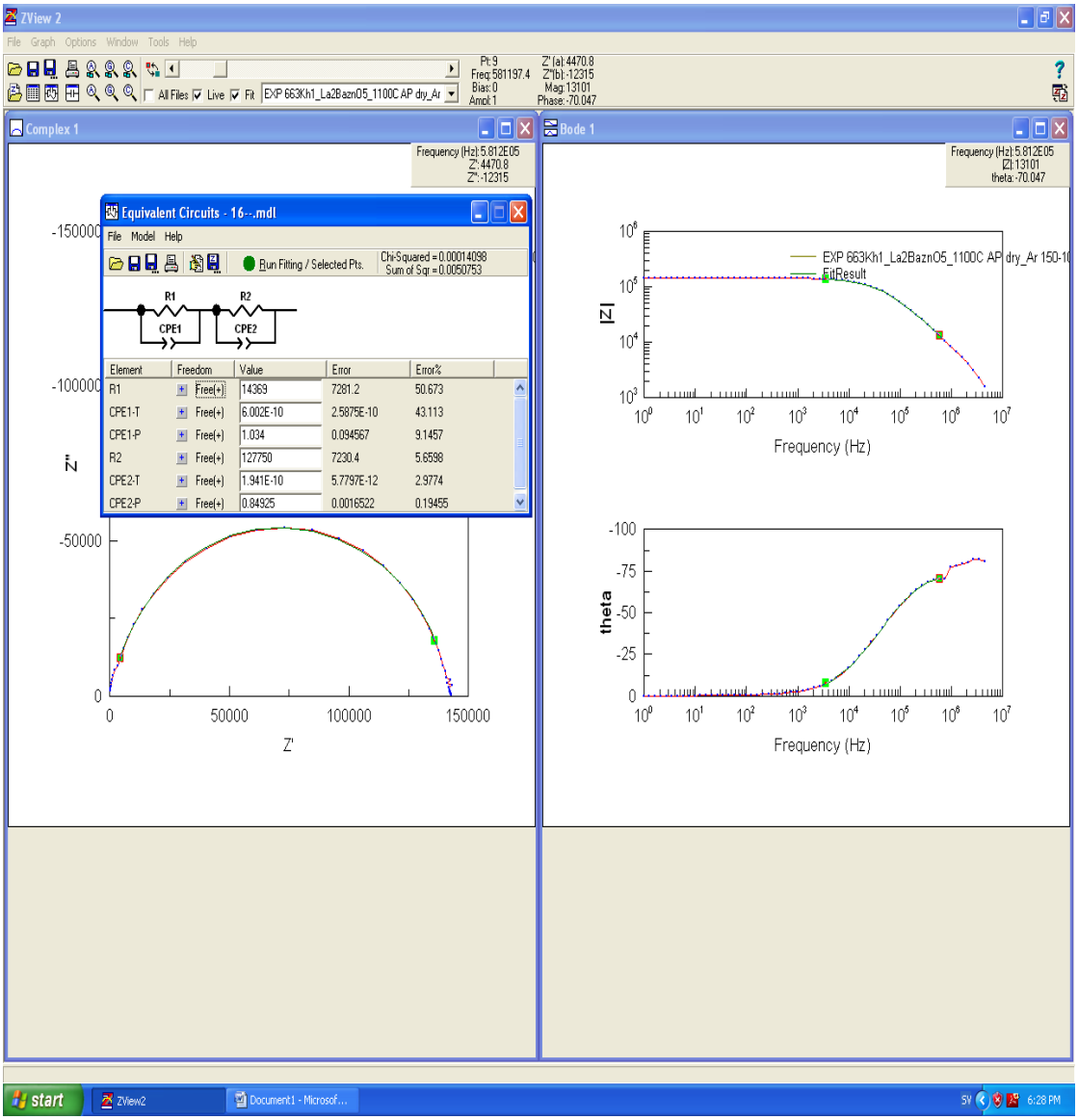

Figure 15**:** Impedance data analysis by z-view software with an insert model. From this semicircle with fitted data total conductivity can be obtained at certain temperature.

A pellet form of sample was run by Solartron 1260 analyzer with smart software. This software generated a dat file and experimental file. By using z-view software these data were analyzed with an insertion z-view model. When model data was fitted with the experimental data then the data was taken and total conductivity was calculated. Activation energy of the system was calculated by using Arrhenius plot of total conductivity.

Chapter 4

Pyrochlore structure based materials

Pyrochlore possess a complex $A_2B_2O_7$-type structure. Sometimes they are written as $A_2B_2O(1)_6O(2)$ to highlight the two types of O anions present. An ideal structure of $A_2B_2O_7$ is given below (figure 16),

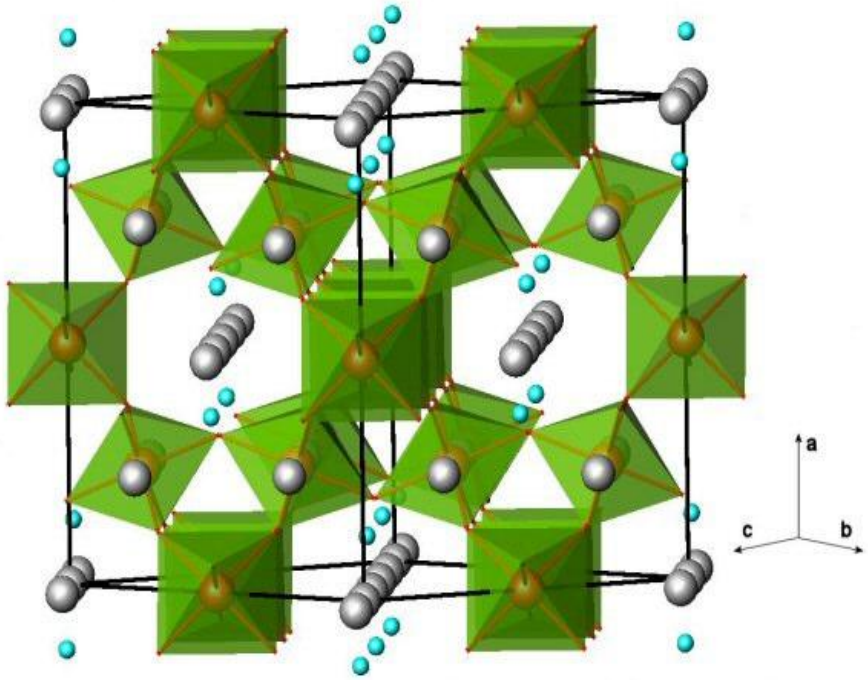

Figure 16: A schematic diagram of $A_2B_2O_7$-type pyrochlore structure where BO_6 octahedra in green, cations in grey and non polyhedra O in cyan (36)

This structure can be viewed as three-dimensional network of interlinked BO_6 octahedra with the A_2O (2) atoms occupying. The B_2O (1)6 and A_2O (2) networks weakly interact through A–O (1).So vacancy can be taken place in the A_2O (2) network.

In this study $Nd_{2-x}Ca_xInMO_{7-\delta}$ where M=Nb,Ta $0 \leq x \leq 0.05$) was investigated. These are $A_2B_2O_7$-type pyrochlore structure where B sites in the $A_2^{3+}B_2^{4+}O_7$ compound are randomly occupied by In^{3+} and Nb^{5+} , In^{3+} and Ta^{5+}ions in a charge balanced manner which leads to slight modification of band structure and crystal structure(37),(38).

These samples were synthesized by conventional solid state sintering method.In_2O_3 (Aldrich), Nb_2O_3 (sigma Aldrich) with 99.99% purity, $CaCO_3$ (merely) with 99%purity Nd_2O_3 (Aldrich) with 99.9% purity and Ta_2O_3 (Aldrich) with 99% purity were used as starting materials.Nd_2O_3 was dried at 800^0C at 1hr before use. These materials were mixed and grinded with mortar. The mixture was pre heated in air at 1200^0C for 10hr.Resulting powder were grinded and made pellet and putted into the furnace at 1400^0C for 24hr.Again resulting samples were grinded and made pellet and heated at 1500^0C for 8hr and 1550^0C for 24hr respectively. Purity of the sample was confirmed by XRD. XRD pattern of these samples after 1550^0C heating is given below,

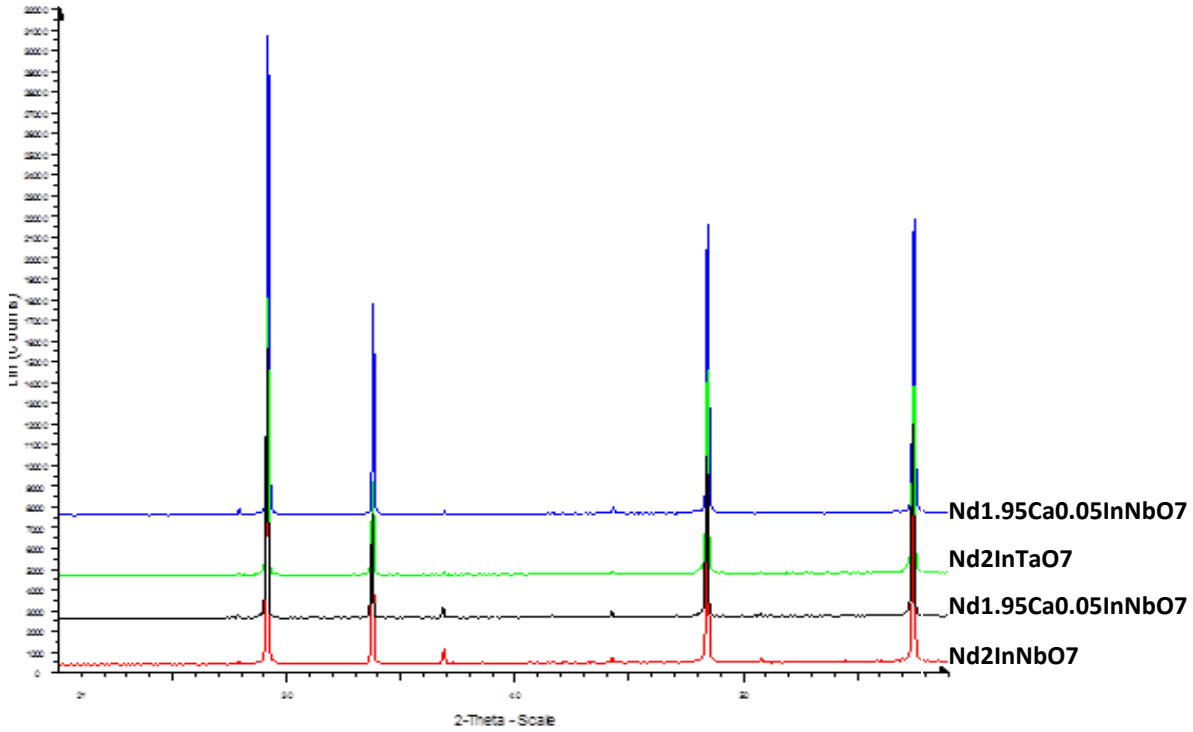

Figure17**:** XRD pattern of $Nd_{2-x}Ca_xInMO_{7-\delta}$ where M=Nb,Ta $0 \leq x \leq 0.05$).These data were investigated on the Bruker D8 diffractmeter.

According to figure 19 these pyrochlore structure based materials adopts cubic structure with space group Fd-3m . Rietveld refinement method is performed on $Nd_2InNbO_{7-\delta}$ and the unit cell parameter was obtained as **a**= 10.6292(1)Å. Unit cell volume, chi squire value and

Rwp value of system was calculated as 1200.8858(1)Å^3, 7.867, 6.75% respectively..Rietveld refinement fit curve is given below,

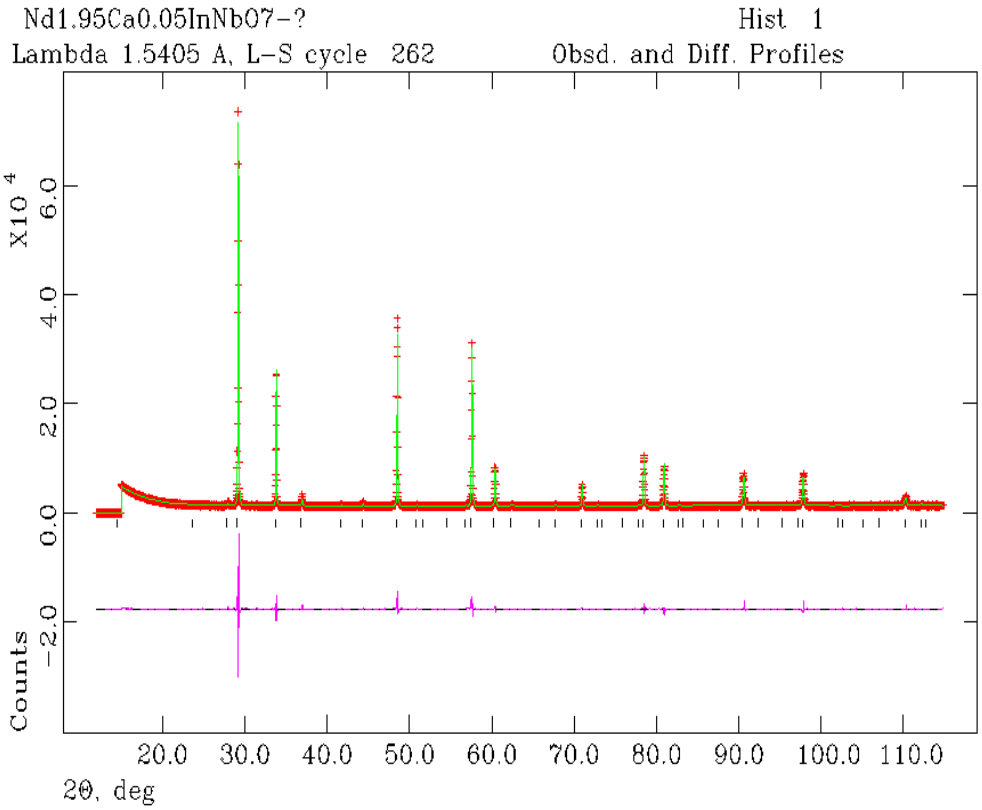

Figure18: Rietveld fit of XRD data for the $Nd_2InTaO_{7-\delta}$. The difference curve (pink), calculated pattern as solid lines and the model (green) on the observed pattern (red);

Table1: Refined Structural parameters of $Nd_{1.95}Ca_{0.05}InNbO_{7-\delta}$ obtained by the Rietveld Structure refinement.

Atom	x	y	Z	Occupancy	UISO
Nd	**0.5**	**0.5**	**0.5**	**0.975**	**0,0004(1)**
In	**0**	**0**	**0**	**0.5**	**0,0189(1)**
Ta	**0**	**0**	**0**	**0.5**	**0,0189(1)**
O	**0.3326**	**0.125**	**0.125**	**1.0**	**0,0690(1)**
O	**0.375**	**0.375**	**0.375**	**1.0**	**0,0821(1)**
Ca	**0.5**	**0.5**	**0.5**	**0.025**	**0.0004(1)**

Table 1 summaries the Rietveld refinement data of $Nd_{1.95}Ca_{0.05}InNbO_7$ Atomic position and occupancy of the atoms is also described. Figure 18 describe how good the Rietveld fit of $Nd_2InNbO_{7-\delta}$ system. The pink curve showed difference between calculated data and experimental data that means less difference. So the data was fitted well.

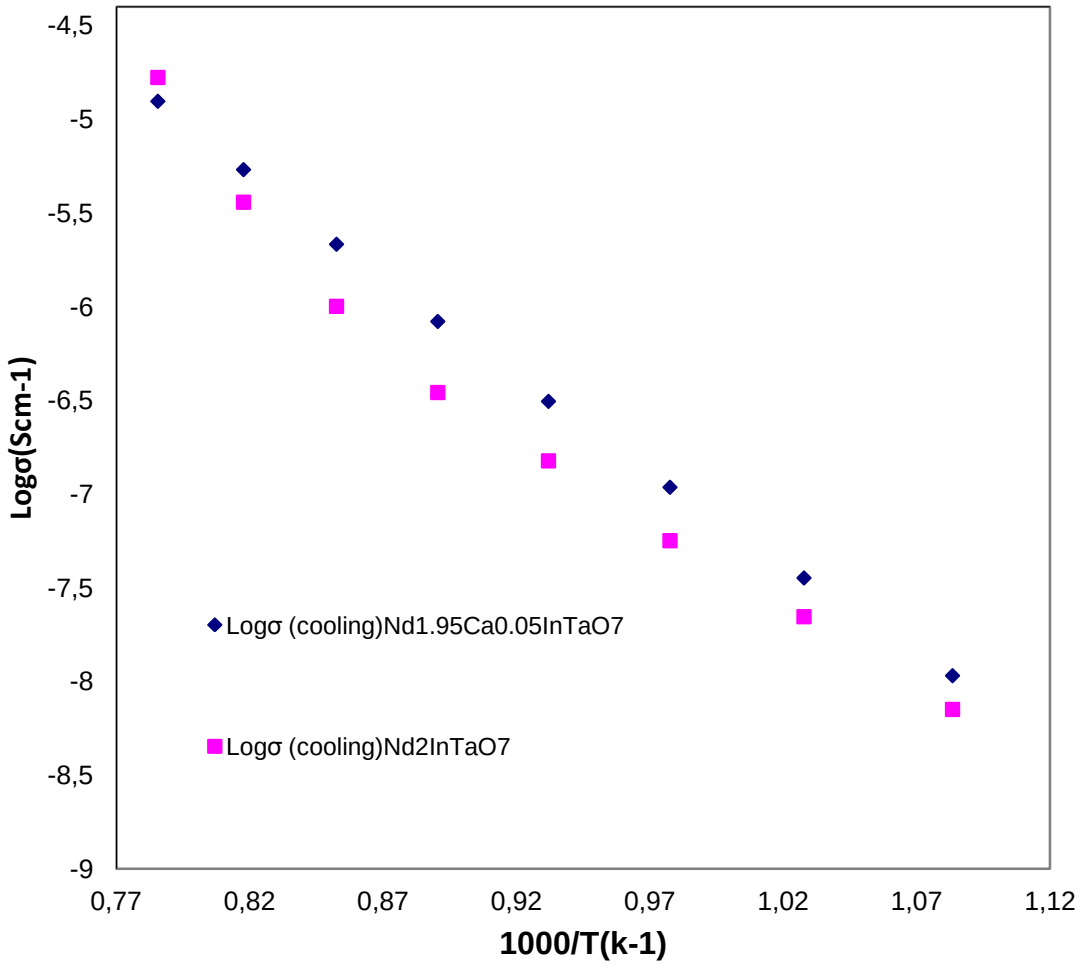

Figure 19: A typical plot of the log of conductivity $Nd_{2-x}Ca_xInTaO_{7-\delta}$ (where x=0, 0.05) as a function of temperature under Dry argon (cooling).

Conductivity of the system $Nd_{2-x}Ca_xInTaO_{7-\delta}$ (where $0 \leq x \leq 0.05$) were investigated and plotted in figure 19. Undoped and doped with Ca^{2+} samples were chosen for conductivity measurement. Conductivity increased slightly with the doping level, however at 1000^0C conductivity of undoped sample was higher than the doped sample. Because of high resistance at lower temperature conductivity data was not taken.

These pyrochlore structure based samples were synthesized successfully. Rietveld analysis confirmed that these materials adopted cubic system with Fd3m space group According to conductivity data these materials are not good oxide ion conductor.Ca^{2+} could not create so much oxygen vacancy as it was expected. May be other dopant need to introduce in order to create oxygen vacancy. Conductivity value of $Nd_{1.95}Ca_{0.05}InTaO_{7-\delta}$ at 650^0C is 1.078×10^{-7} which is very low compare to pyrochlore $NdGdZr_{1.85}Sc_{0.15}O_{7-\delta}$ of $1.89 \times 10^{-4}Scm^{-1}$ conductivity (44)

Chapter 5

Brownmillerite structure based materials

$Ba_2In_2O_5$ is brownmillerite structure based materials. This is one of the well-known perovskite-related oxide ion conductors. At room temperature these materials adopt orthorhombic structure with ordered oxide ion vacancies with InO_6 octahedra and InO_4 tetrahedra (figure20).There are three crystallography distinct oxygen sites.O1in the equatorial sites, O2 in the apical sites of the octahedral and tetrahedral and O3 in the equatorial sites of the tetrahedral (39).In this thesis brownmillerite structure based $Ba_2In_{2-x}M_xO_{5-\delta}$ (where M=Ga,Y and $0 \leq X \leq 0.85$) synthesized and characterized this material by Rietveld refinement method.

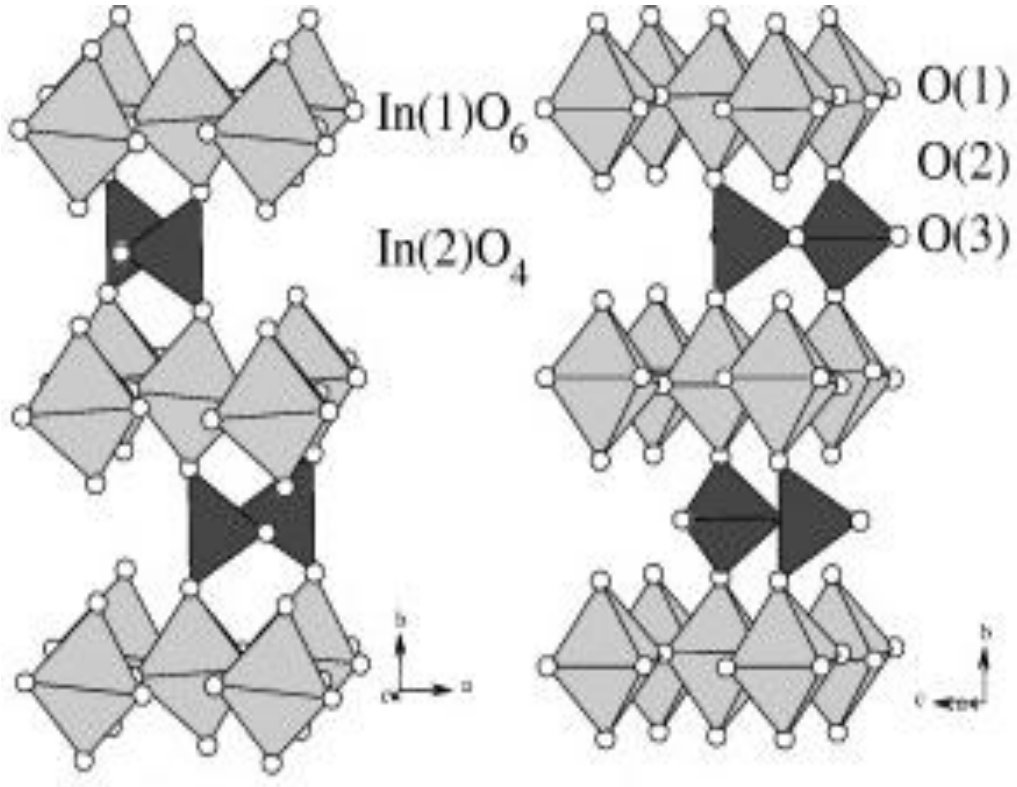

Figure20: Brown millerite structure based $Ba_2In_2O_5$ showing InO_6 and InO_4 (1).

The sample of $Ba_2In_{2-x}M_xO_{5-\delta}$ was synthesized by solid state sintering method. With stochiometric mixture of $BaCO_3$ (Aldrich) with 99.98% purity, In_2O_3 (Aldrich) with 99.99% purity, Ga_2O_3 (Aldrich) with 99.99% purity,Y_2O_3 (Aldrich) with 99.99% .These materials were mixed and grinded and heated at 1000^0C for 16h.After heated at 1000^0C these materials

again grinded and made pellet form finally sintered at 1250C with some intermediate grinding. XRD data were collected at room temperature on a Bruker axs D8 diffractometer. According to XRD results single phase was found at 1250^0C.

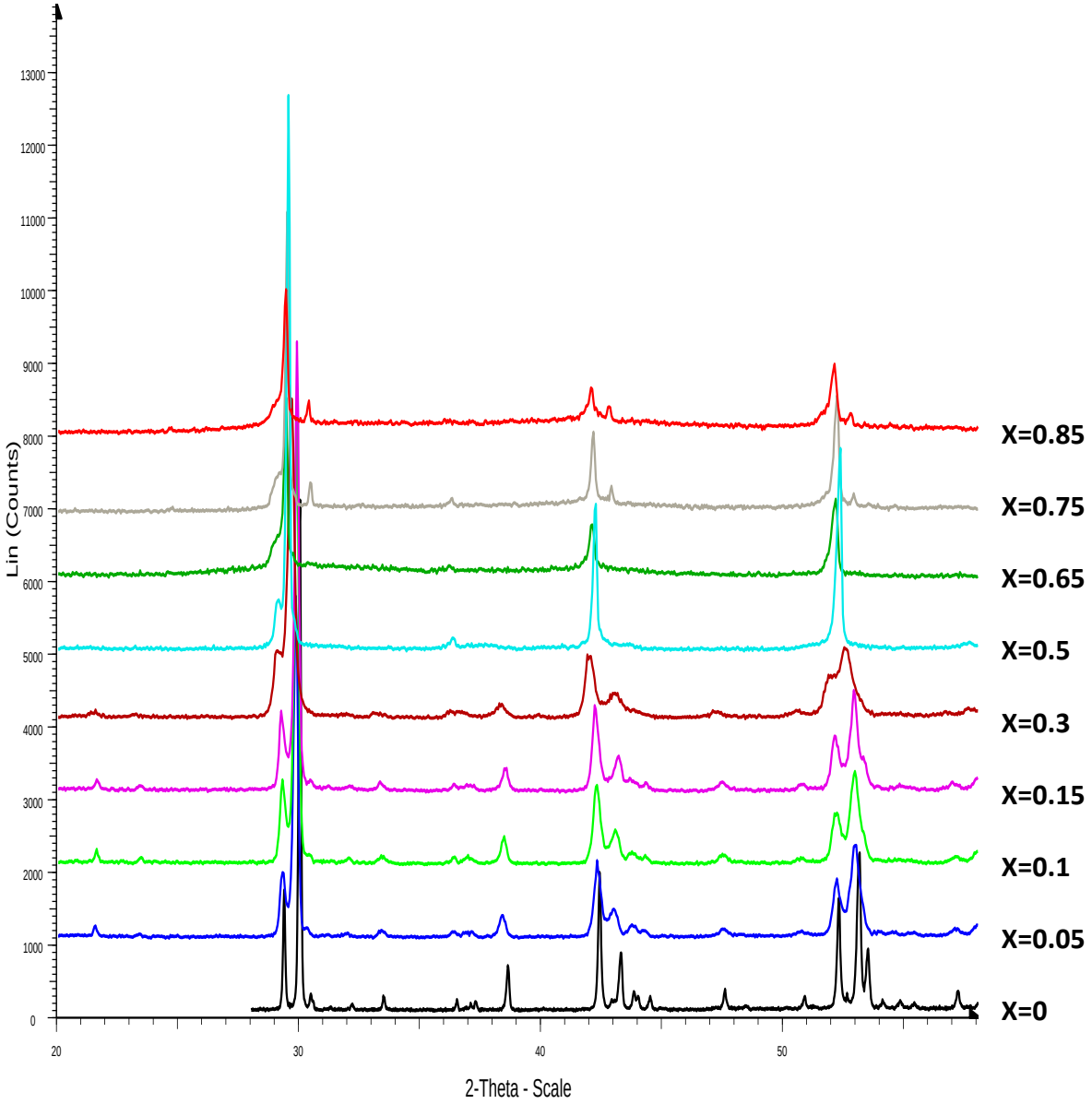

Figure 21: XRD pattern of $Ba_2In_{2-x}Y_xO_{5-\delta}$ where $0 \leq x \leq 0.85$.This data was investigated on the Bruker D8 diffractmeter.Structural change was occurred higher doped ($x \geq 0.5$) materials.

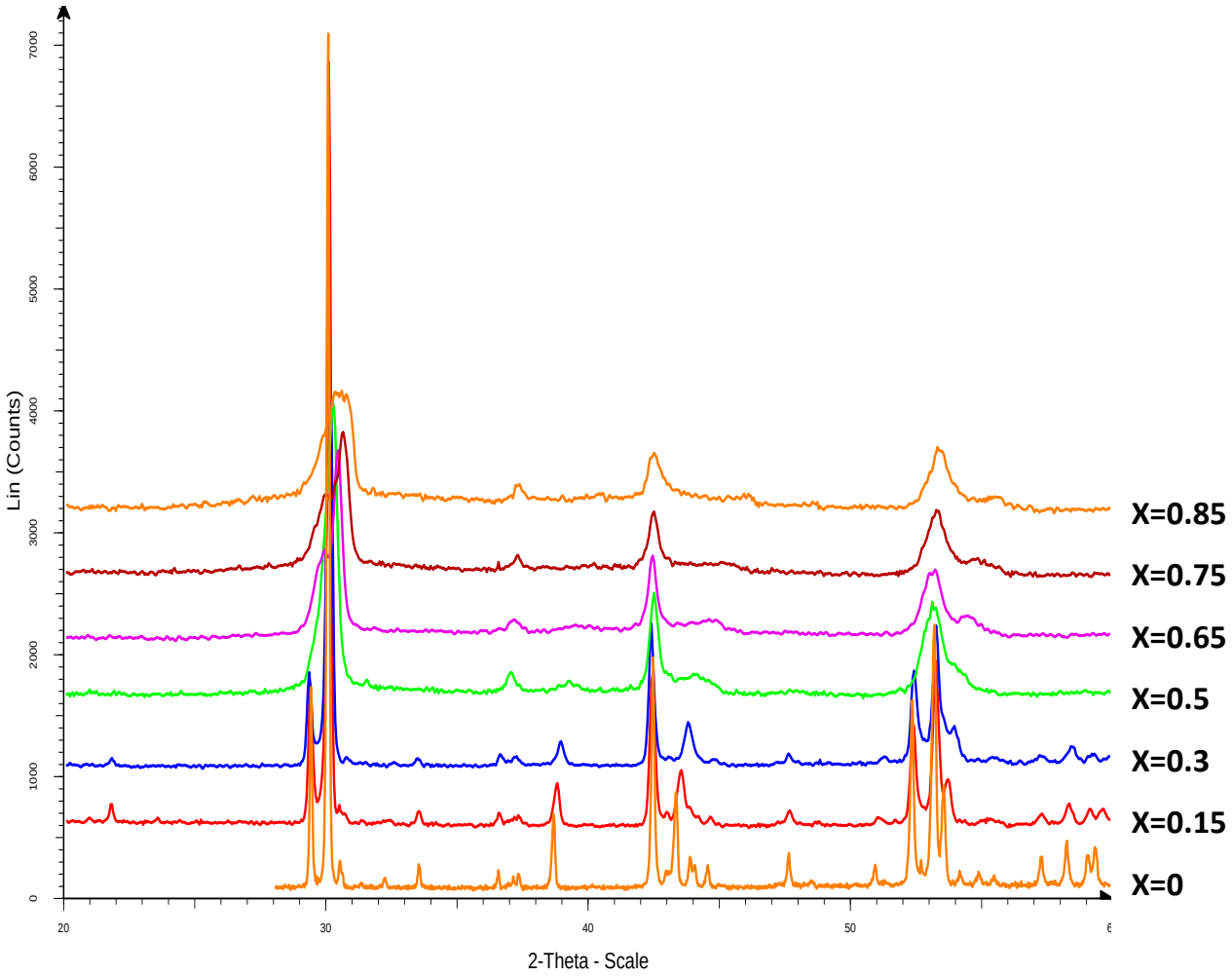

Figure 22: XRD pattern of $Ba_2In_{2-x}Ga_xO_{5-\delta}$ where $0 \leq x \leq 0.85$.This data was investigated on the Bruk D8 diffractmeter.Structural change was occurred higher doped ($x \geq 0.5$) materials.

At room temperature $Ba_2In_{2-x}Ga_xO_{5-\delta}$ and $Ba_2In_{2-x}Y_xO_{5-\delta}$ adopt orthorhombic structure upto $x \approx o.3$.Structual changes clearly observed at x=0.5.Ga doped brownmillerite samples structure transforming from orthorhombic to cubic and Yttrium doped samples structure transforming from orthorhombic to tetragonal structure. Figure 23 showed the XRD pattern for both dopant at x=0.5.According to figure 23 it can be understood that these systems are still transforming.

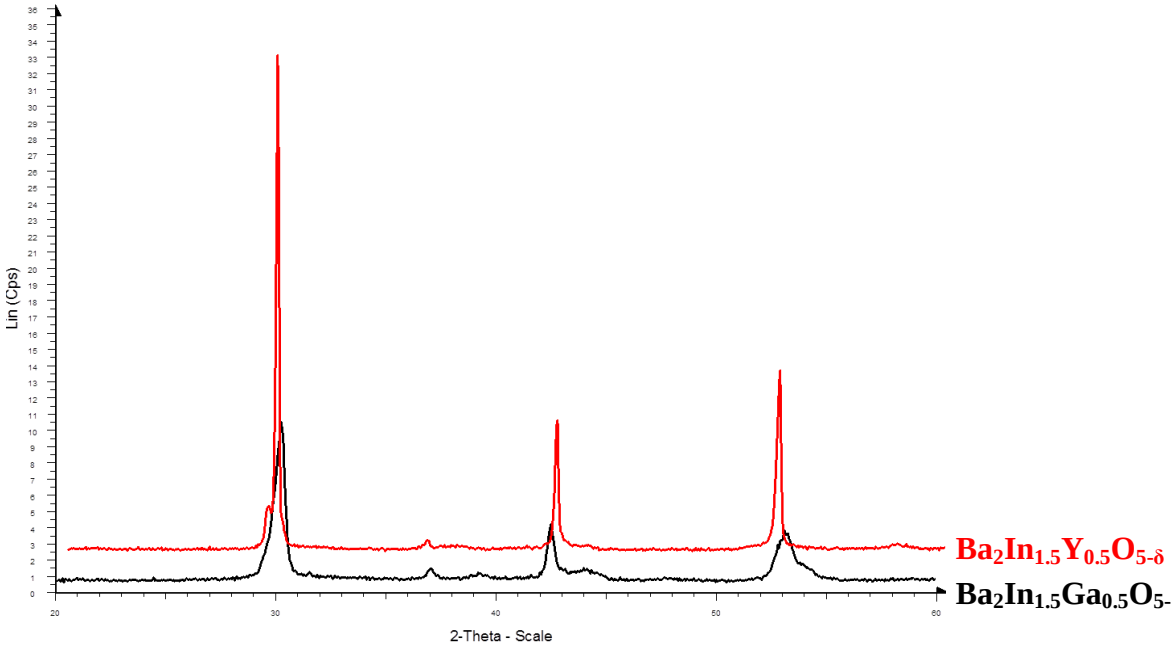

Figure 23: XRD pattern of $Ba_2In_{1.5}Ga_{0.5}O_{5-\delta}$ (Black) and $Ba_2In_{1.5}Y_{0.5}O_{5-\delta}$ (Red).

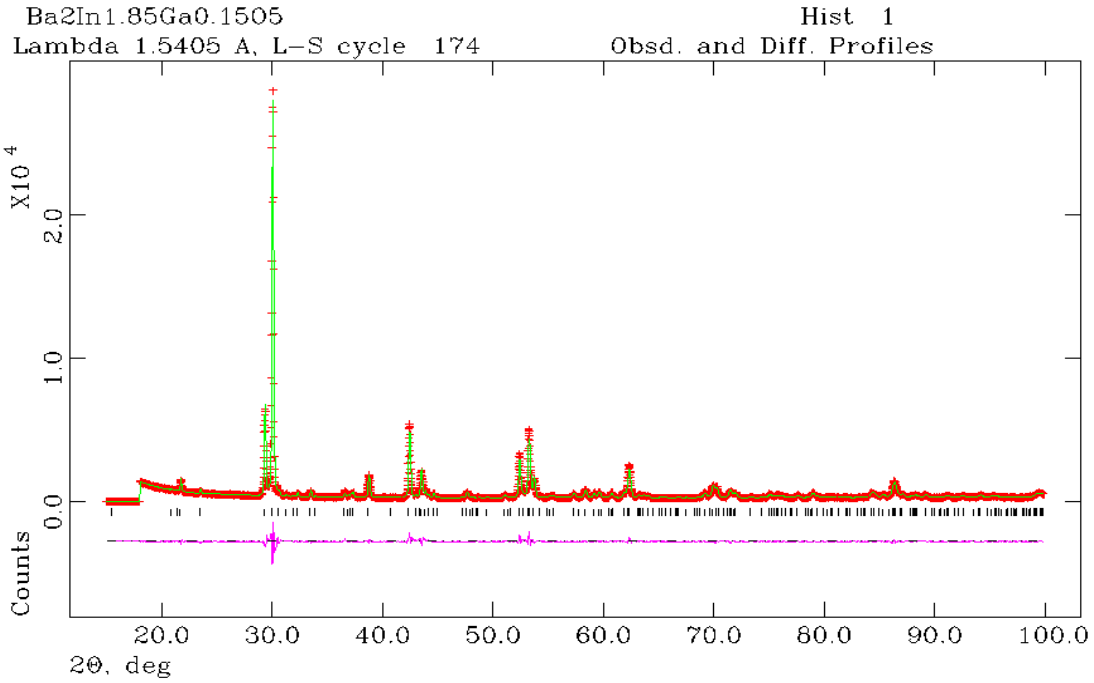

Figure 24: Rietveld fit of XRD data for the $Ba_2In_{1.85}Ga_{0.15}O_{5-\delta}$. The difference curve (pink), calculated pattern as solid lines and the model (green) on the observed pattern (red).Cell parameter a=6, 0982(1)Å;b=16.6486(1)Å;c=5.9633(1)Å ,Unit cell volume =605.433(1)Å3, chi squire χ^2=3.771, Rwp = 8.30%

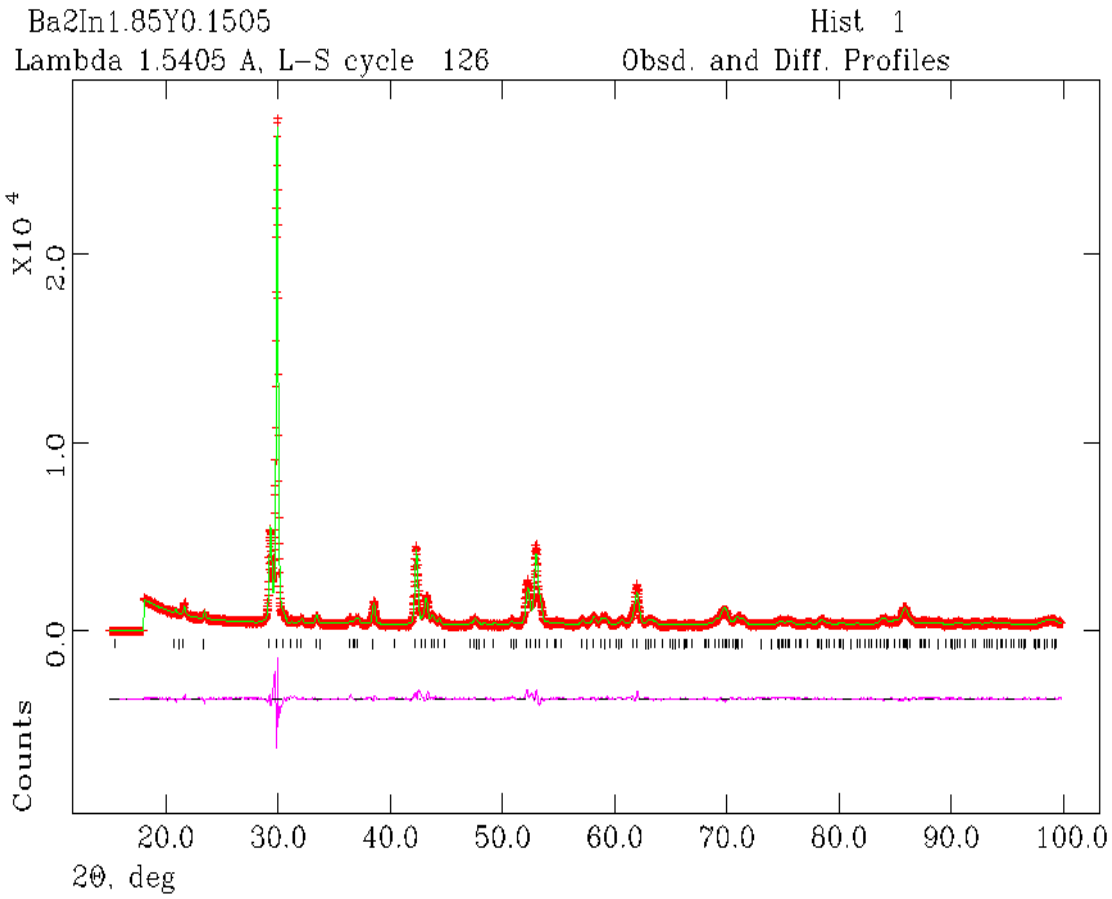

Figure 25: Rietveld fit of XRD data for the $Ba_2In_{1.85}Y_{0.15}O_{5-\delta}$. The difference curve (pink), calculated pattern as solid lines and the model (green) on the observed pattern (red); Cell parameter a=6.1084(1)Å;b=16.7736(1)Å;c=5.9887(1)Å**,**Unit cell volume =613.427(1)Å^3, χ^2=5.409, Rwp = 9.13%

Rietveld analysis was performed on Ba_2In_{2-x} (Ga, Y) $_xO_{5-\delta}$ up to x=0.3 and the unit cell was found to be orthorhombic and space group was Ibm2 (figure24, 25).Cell expansion was also proved by Rietveld analysis. Cell parameter of $Ba_2In_{2-x}(Ga,Y)_xO_{5-\delta}$ system is showed in the table 2.

Table 2: Summary of the Rietveld refinement of XRD patterns collected for the $Ba_2In_{2-x}(Ga,Y)xO_{5-\delta}$ system.

Composition	a	b	c	Chi Square
$Ba_2In_2O_{5-\delta}$	6.0846(1)	16.7807(1)	5.9672(1)	4.893
$Ba_2In_{1.95}Y_{0.05}O_5$	6.0851(1)	16.7946(1)	5.9660(1)	4.921
$Ba_2In_{1.9}Y_{0.1}O_5$	6.0956(1)	16.7822(1)	5.9768(1)	4.554
$Ba_2In_{1.85}Y_{0.15}O_5$	6.1084(1)	16.7736(1)	5.9887(1)	5.490
$Ba_2In_{1.7}Y_{0.3}O_5$	6.1315(1)	16.8466(1)	6.0323(1)	4.802
$Ba_2In_{1.85}Ga_{0.15}O_5$	6.0982(1)	16.6486(1)	5.9633(1)	3.771
$Ba_2In_{1.7}Ga_{0.3}O_5$	6.0926(1)	16.5262(1)	5.9632(1)	6.223

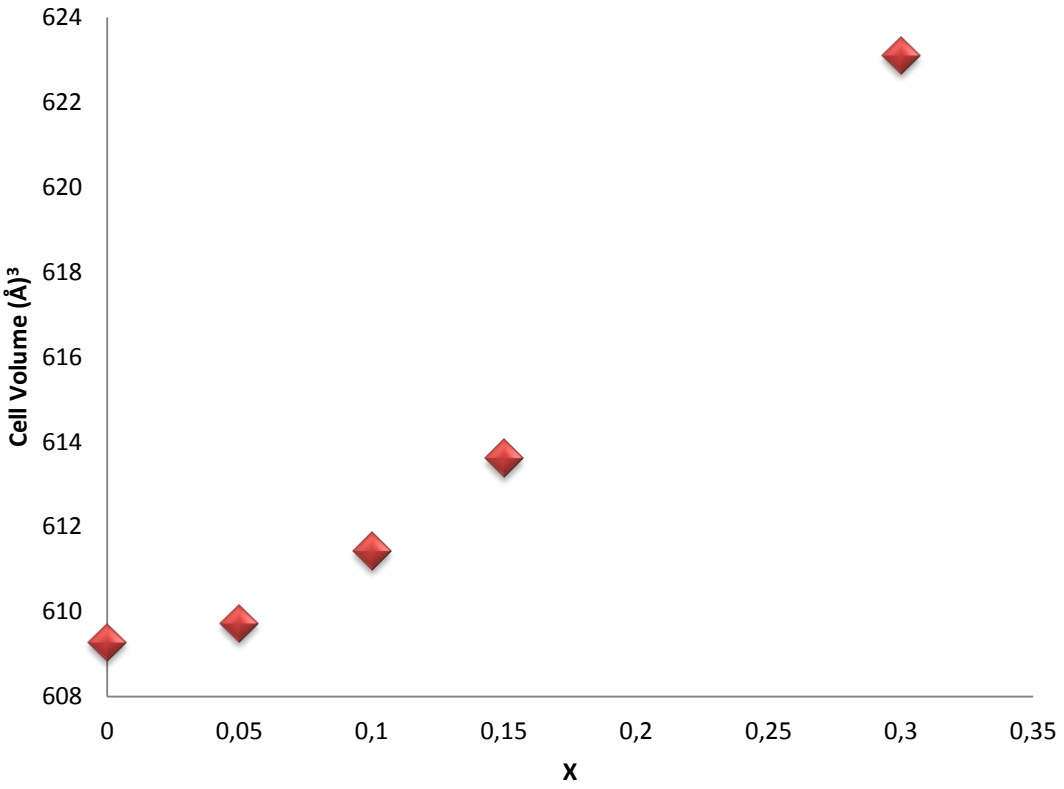

Figure 26: Cell volume function of Y doping concentration curve for $Ba_2In_{2-x}Y_xO_{5-\delta}$ system, where cell volume increase with the increase doping concentration.

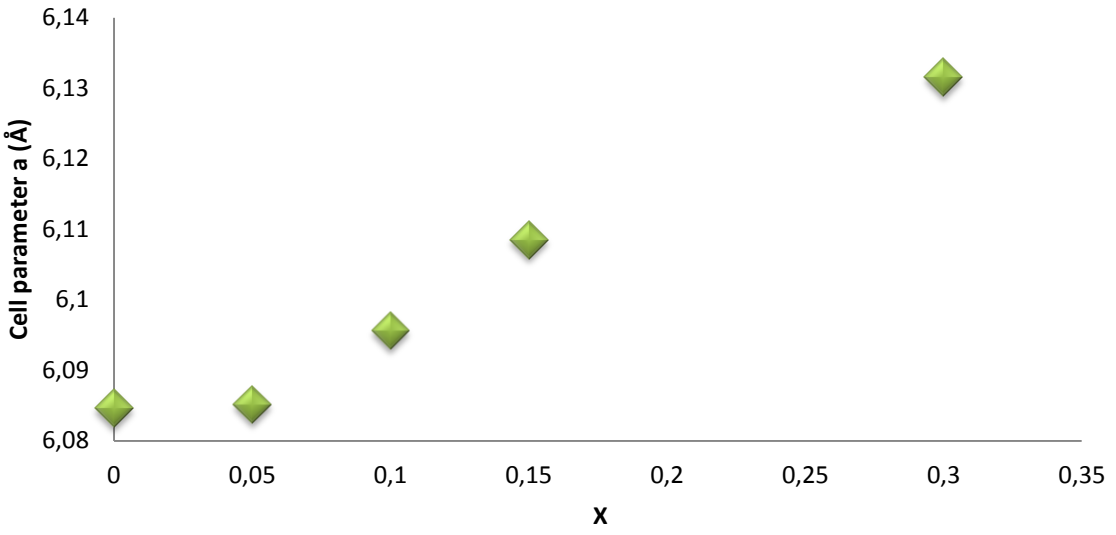

Figure 27**:** Cell parameter function of Y doping concentration curve for $Ba_2In_{2-x}Y_xO_{5-\delta}$ system, where cell parameter (a) increase with the increase of doping concentration.

Ionic radius of Coordination Number (CN) 6 Y^{3+} (0, 9Å) is larger than CN 6 In^{3+} (0, 8Å).With the increase of dopant concentration Y^{3+} cell volume and cell parameter (a) also increased. Cell was expanding according to table 2 and figure 26, 27.

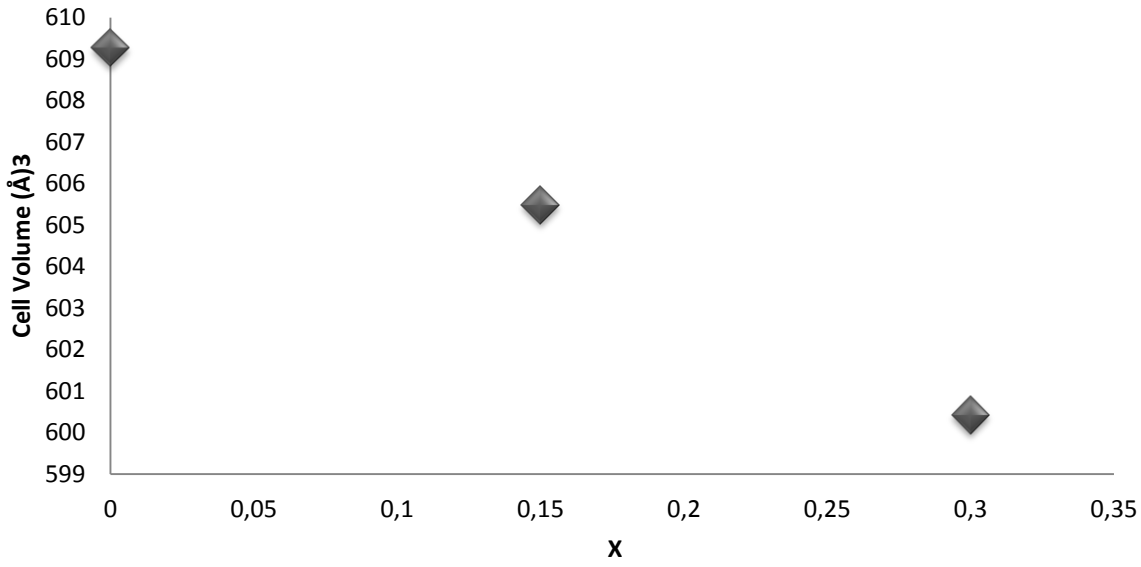

Figure 28: Cell volume function of Ga doping concentration curve for $Ba_2In_{2-x}Ga_xO_{5-\delta}$ system, where cell volume decrease with the increase of doping concentration.

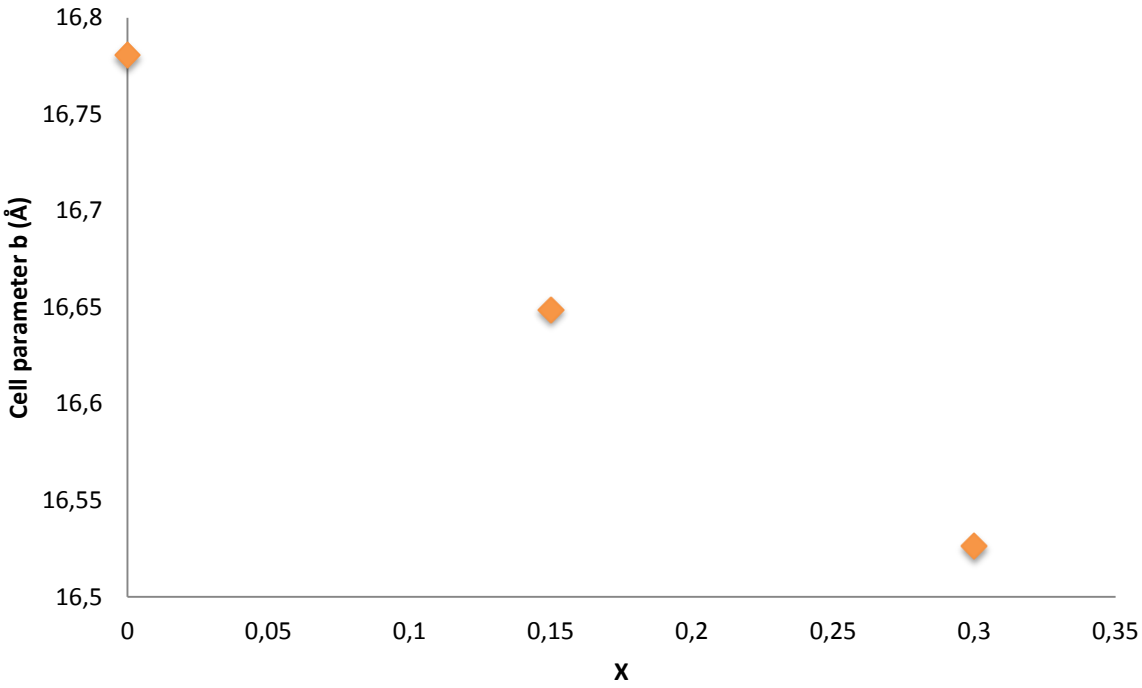

Figure 29: Cell parameter function of Ga doping concentration curve for $Ba_2In_{2-x}Ga_xO_{5-\delta}$ system, where cell parameter (b) decrease with the increase of doping concentration.

Ionic radius of CN4 Ga^{3+} (0, 47Å) is lower than CN 4In^{3+} (0,62Å).For this reason cell volume and cell parameter (b) also decrease with the increase of doping level according to table 1,figure 28,29 The unit cell is contracting with the increasing dopant concentration.

Hydration experiment was run at 275^{0}C and p(H_2O)≈0.42 atm under N_2 gas flow for 3 days and XRD was done on hydrated samples. Vacuum drying was done on all the samples at 700C and 10^{-6}mbar for 1 day and XRD data was collected for these samples. Figure 30 illustrates XRD of $Ba_2In_{1.85}Ga_{0.15}O_{5-\delta}$ (hydrated, vacuum dried, as prepared).

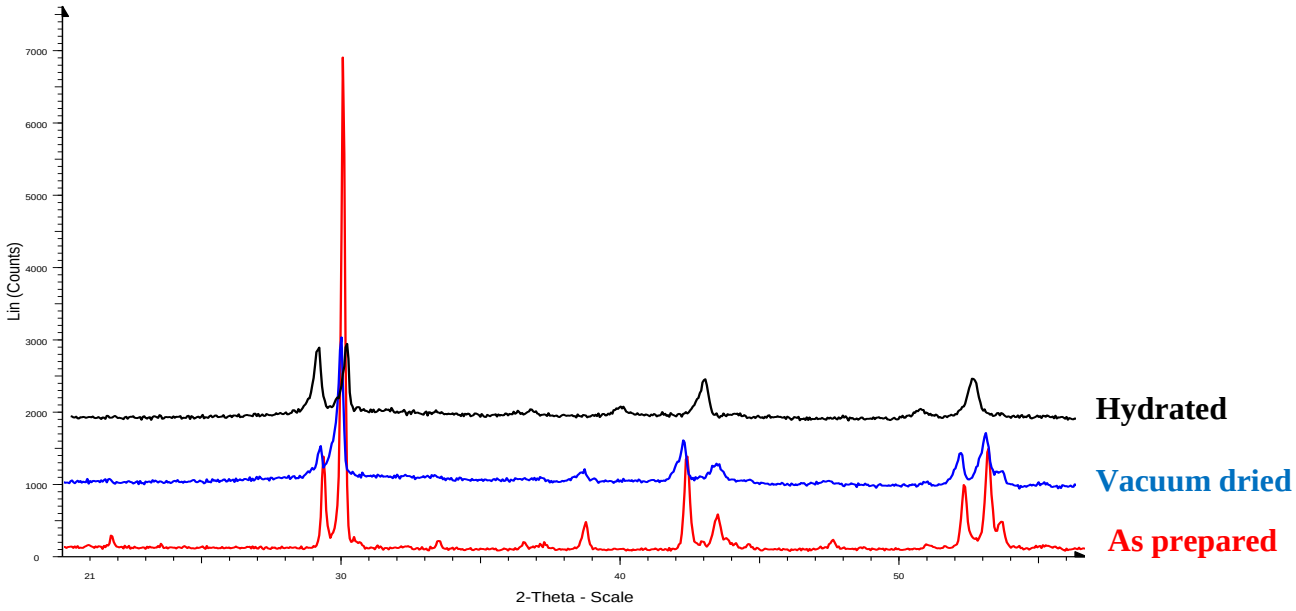

Figure 30: XRD pattern for $Ba_2In_{1.85}Ga_{0.15}O_{5-\delta}$ where red curve is for hydrated sample, blue curve is for as prepare sample and black curve is for vacuum dried .Hydrated $Ba_2In_{1.85}Ga_{0.15}O_{5-\delta}$ adopt tetragonal structure.

Hydrated $Ba_2In_{1.85}Ga_{0.15}O_{5-\delta}$ adopts tetragonal structure with space group P4/mmm. Rietveld refinement was done on hydrated $Ba_2In_{1.85}Y_{0.15}O_{5-\delta}$ in order to extract cell parameters. Rietveld fit curve of $Ba_2In_{1.85}Y_{0.15}O_{5-\delta}$ is plotted in figure 30 and refined atomic positions are described in table 3.

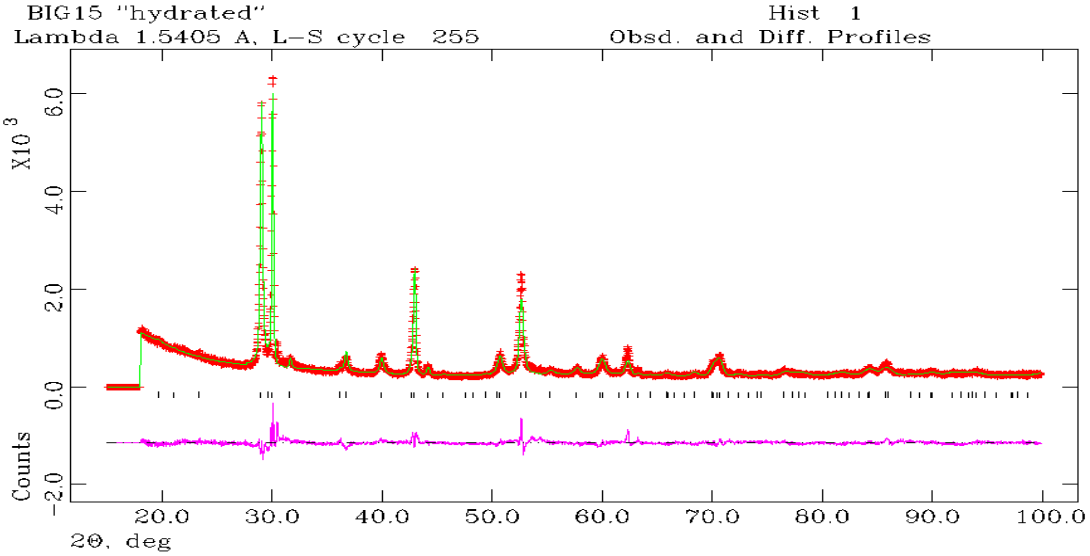

Figure 33**:** Rietveld fit of XRD data for the hydrated $Ba_2In_{1.85}Ga_{0.15}O_{5-\delta}$. The difference curve (pink), calculated pattern as solid lines and the model (green) on the observed pattern (red);where hydrated $Ba_2In_{1.85}Ga_{0.15}O_{5-\delta}$ possessed tetragonal phase. Cell parameter a, b= 4.2142(1)Å, c= 9.0363(1)Å, Unit cell volume =160.48(1)Å^3, χ^2 2=3.564, Rwp = 9.27%.

Table 3: Refined atomic position and site occupancy of hydrated $Ba_2In_{1.85}Ga_{0.15}O_{5-\delta}$.

Atom	X	Y	Z	Occupancy
Ba	**0**	**0**	**0.2908(1)**	**1**
In	**0.5**	**0.5**	**0.5**	**1**
In	**0.5**	**0.5**	**0**	**0.85**
Ga	**0.5**	**0.5**	**0.5**	**0**
O	**0.5**	**0.5**	**0.3324(1)**	**1**
O	**0**	**0.5**	**0.5**	**1**
O	**0.2916(1)**	**0**	**0**	**0.5**
Ga	**0.5**	**0.5**	**0**	**0.15**

Thermogravimetric analysis (TGA) was performed on as prepared and hydrated According to TGA result mass loss was observed 3.02% for $Ba_2In_{1.85}Ga_{0.15}O_{5-\delta}$, 2.83% for $Ba_2In_{1.7}Ga_{0.3}O_{5-\delta}$and 3.01% for $Ba_2In_{1.85}Y_{0.15}O_{5-\delta}$. These brownmillerite structure based materials were almost 99.99% hydrated according to table 4 and figure32.

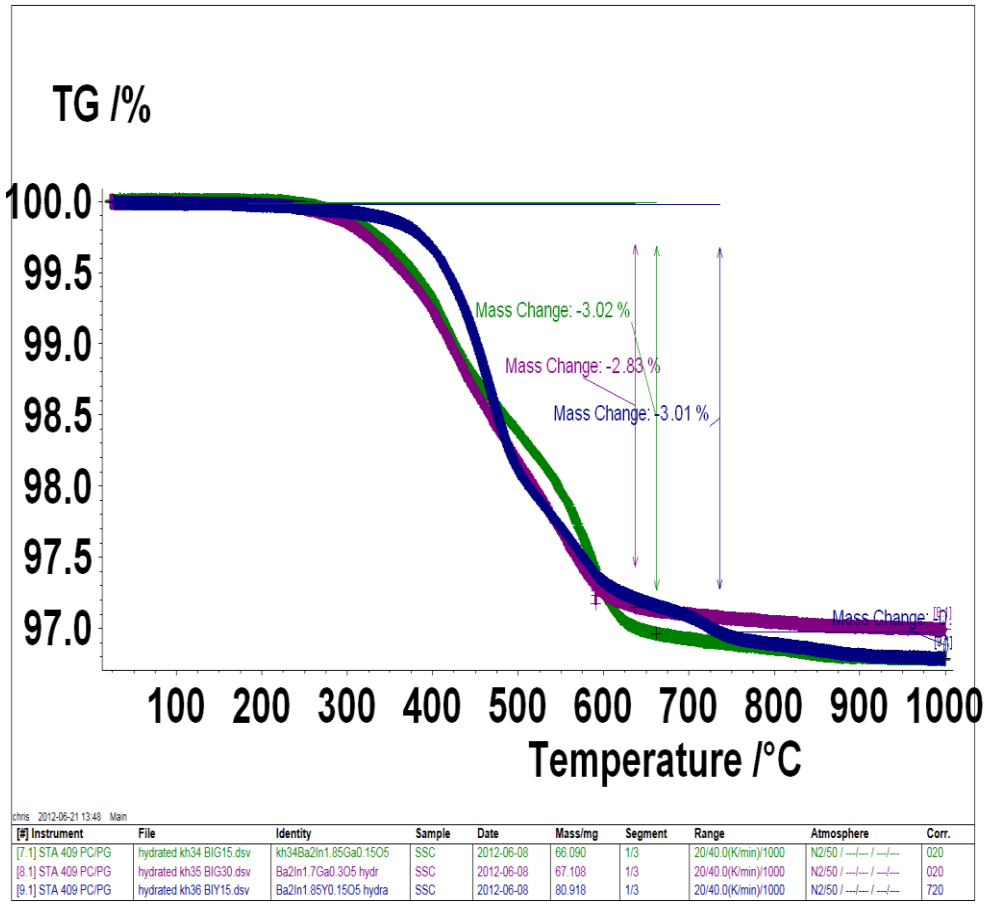

Figure 32**:** TGA data for $Ba_2In_{2-x}(Ga,Y)_xO_{5-\delta}$ system showing amount of mass loss in hydrated samples. Amount of mass loss is consistent with the system.

Table 4**:** Theoretical vs experimental mass loss of hydrated $Ba_2In_{2-x}(Ga,Y)_xO_{5-\delta}$.

Sample	**theoretical mass loss%**	**experimental mass loss%**	**exp/theory%**
$Ba_2In_{1.85}Ga_{0.15}O_{5-\delta}$	**3.025**	**3.02**	**99.83**
$Ba_2In_{1.7}Ga_{0.3}O_{5-\delta}$	**3.059**	**(663C)2.83**	**92.51**
$Ba_2In_{1.85}Y_{0.15}O_{5-\delta}$	**3.012**	**(736C)3.01**	**99.93**

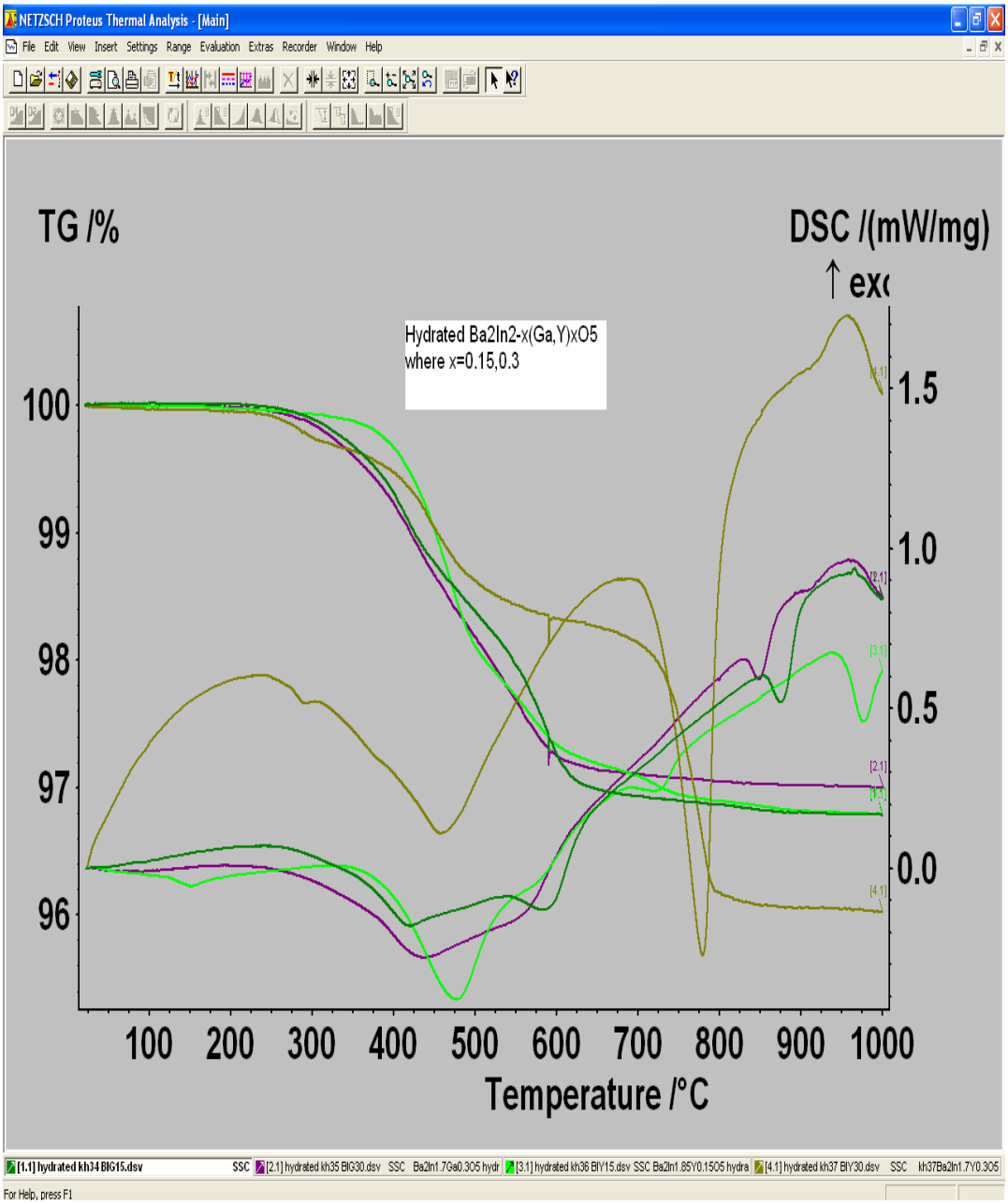

Figure 33: TG-DSC on Hydrated $Ba_2In_{2-x}(Ga,Y)_xO_{5-\delta}$ where TG-DSC curve of $Ba_2In_{1.7}Y_{0.3}O_{5-\delta}$ didn't follow same trend like other hydrated brownmillerite materials.

DSC and TGA curve was plotted together in figure 33.Mass loss was observed between 400-600^{0}C temperature region where DSC Peaks also showed endothermic reaction .This mass loss could be water loss. DSC peaks at higher temperature around 800^{0}C showed structural changes (orthorhombic to tetragonal).TG-DSC curve of $Ba_2In_{1.7}Y_{0.3}O_{5-\delta}$ haven't followed same trend like other hydrated brownmillerite materials.

In summary $Ba_2In_{2-x}(Ga, Y)_xO_{5-\delta}$ were synthesized successfully. These materials possessed brownmillerite structure with Ibm2 space group until x≤0.3.When doping level increase structural changes occurred and structure become orthorhombic to cubic or tetragonal according x-rd pattern. Cell is expanded with increase of dopant (Y^{3+}) concentration and contracted with increase of dopant (Ga^{3+}) concentration. Hydrated brownmillerite possessed a tetragonal structure.

Chapter 6

Ln_2BaZnO_5 systems

$Ln_{2-x}Ca_xBaZnO_{5-\delta}$ family of ternary oxides (where Ln=La,Nd and $0 \leq x \leq 0.3$) Have been analyzed in this thesis. An ideal structure of Ln_2BaZnO_5 is given below,

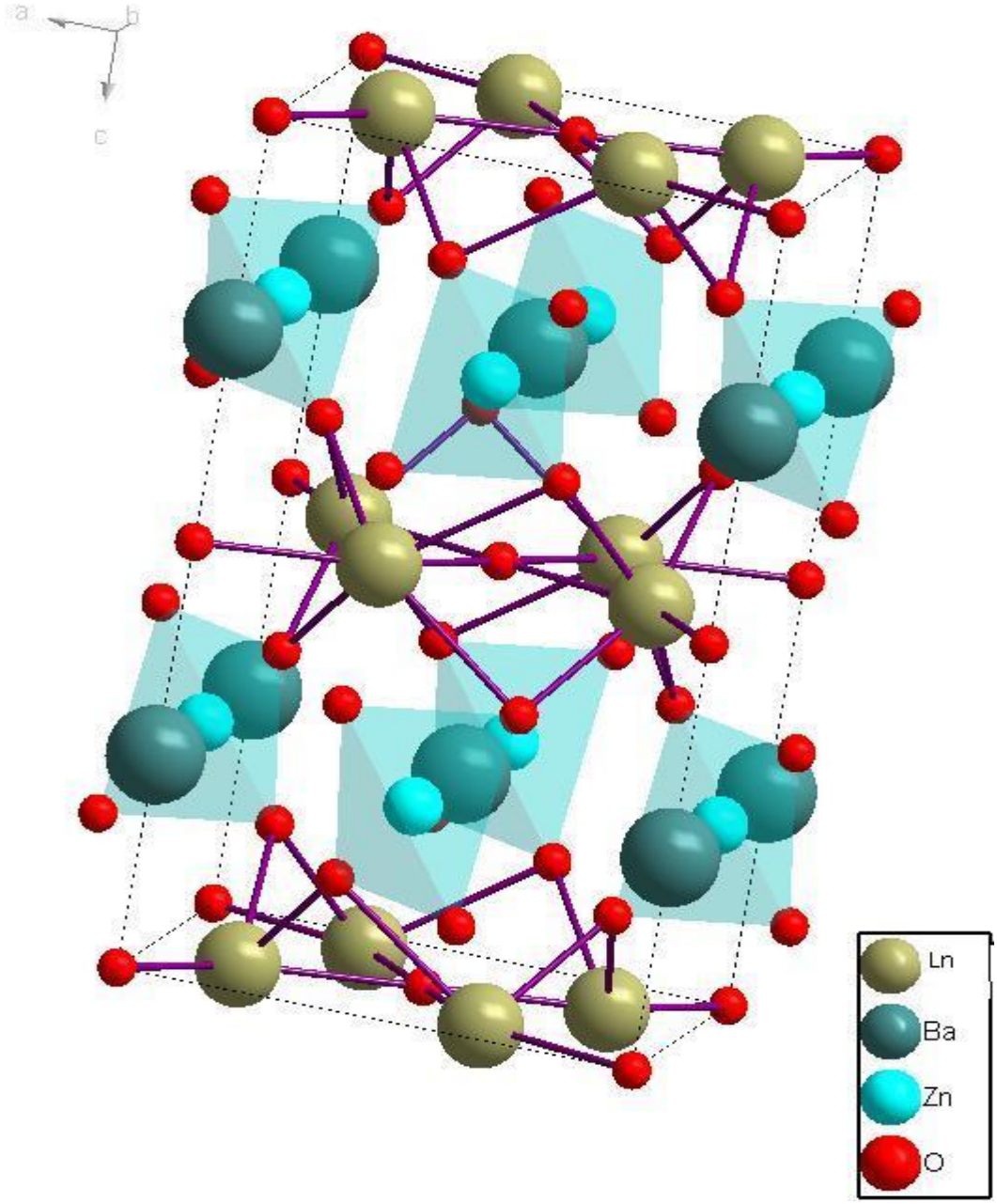

Figure 34: A schematic diagram of Ln_2BaZnO_5 family with complex structure where ZnO_4 tetrahedral in green, Ln in light brown, Ba in bluish grey and non polyhedra O in red.

This structure is one of the complex structures which are crystalline in tetragonal structure where Ln^{3+} ion is surrounded with 8 oxygen ions and Zn^{2+} is surrounded with 4 oxygen ions. LnO_8 polyhedra are linked with one another to form Ln-O layer.O-Ba-O have weak interaction with ZnO_4 network (figure34).So that oxygen vacancy can be found in ZnO_4 network (41).

In this thesis $La_{2-x}Ca_xBaZnO_{5-\delta}$ and $Nd_{2-x}Ca_xBaZnO_{5-\delta}$ ($0 \leq x \leq 0.3$) have been synthesized. The ability to acceptor doping the materials with Ca^{2+} in order to create oxygen vacancies and increase ionic conductivity has been investigated. Both of the systems have same structure with I4/mcm space group (42).

The sample of $La_{2-x}Ca_xBaZnO_{5-\delta}$ and $Nd_{2-x}Ca_xBaZnO_{5-\delta}$ were synthesized by solid state sintering method. La_2O_3 (Aldrich) with 99.95% purity, $CaCO_3$ (merely) with 99% purity, $BaCO_3$ (Aldrich) with 99.98% purity, ZnO (Aldrich) with 99.99% purity, Nd_2O_3 (Aldrich) with 99.9% purity were used as starting materials. Nd_2O_3 was dried at 800^0C at 1hr before use. These materials were mixed and grinded. These mixtures heated at 1000-1100^0C with intermediate grinding. Finally the samples heated at 1100^0C for 24hr.The formation of single phased materials was determined by XRD. After heating the powder (La_2BaZnO_5) at 1000^0C and 1050^0C X-rd was done and some impurity peak was found on the pattern. (Figure 35)Finally pure phase was observed at 1100^0C.

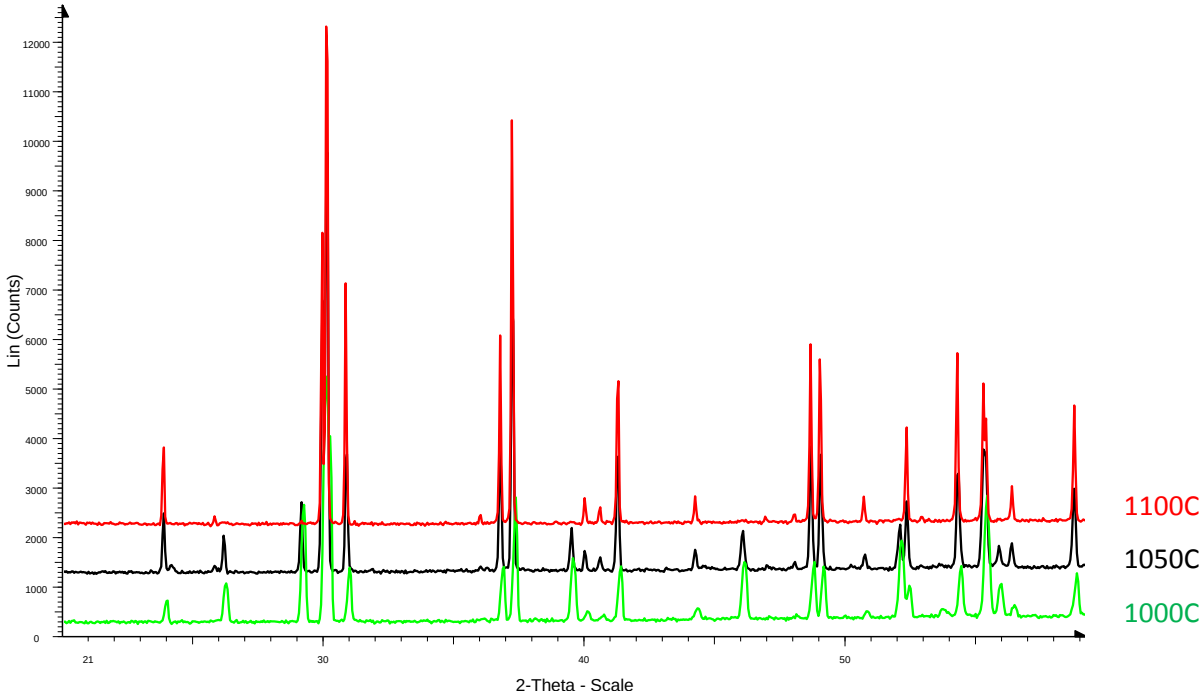

Figure 35: XRD pattern of La_2BaZnO_5 after heating at different temperature. Pure phase was obtained at 1100^0C.Impurity phase was found at lower temperature.

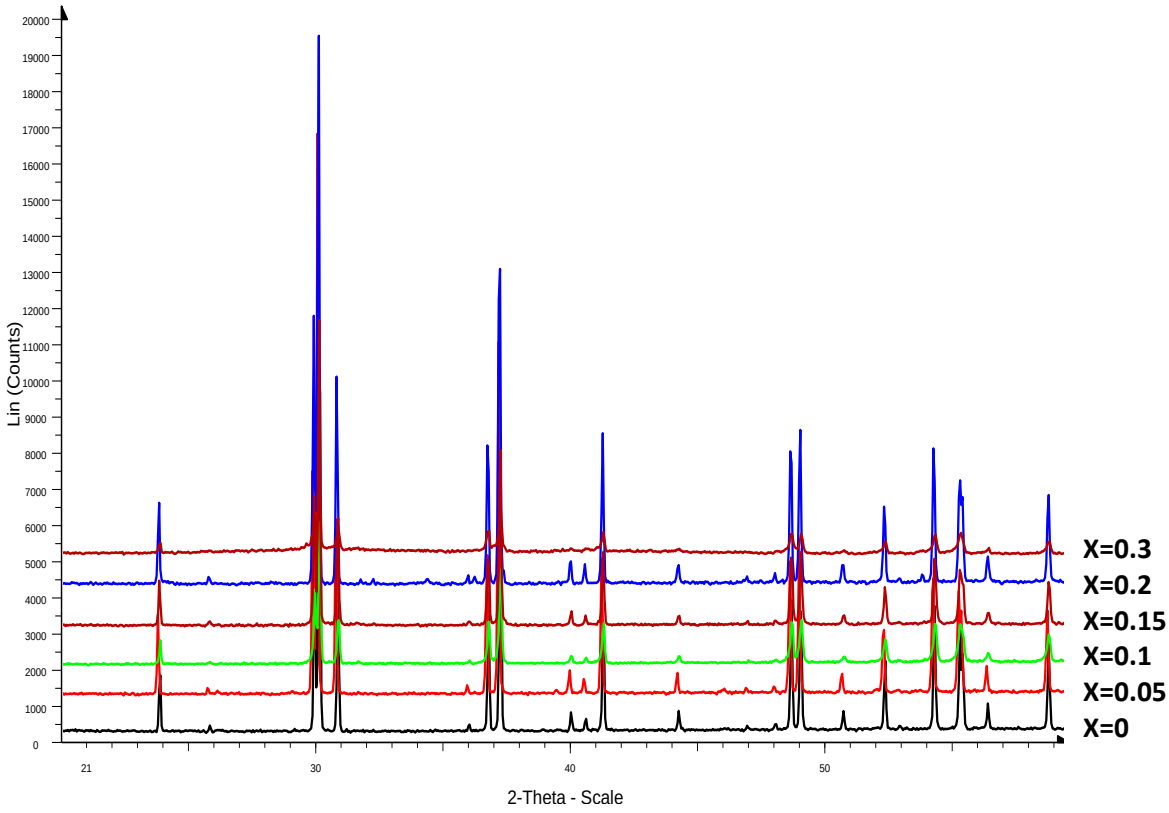

Figure 36: XRD pattern of $La_{2-x}Ca_xBaZnO_{5-\delta}$ where $0 \le x \le 0.3$.These data were investigated on the Bruker D8 diffractmeter.Top pattern has some change of structure (some peak disappeared).

$La_{2-x}Ca_xBaZnO_{5-\delta}$ and $Nd_{2-x}Ca_xBaZnO_{5-\delta}$ both systems (doped+undoped) have followed same pattern At X=0.3 some peaks disappeared and long scan also showed some impurity phase on this system at X=0.3.

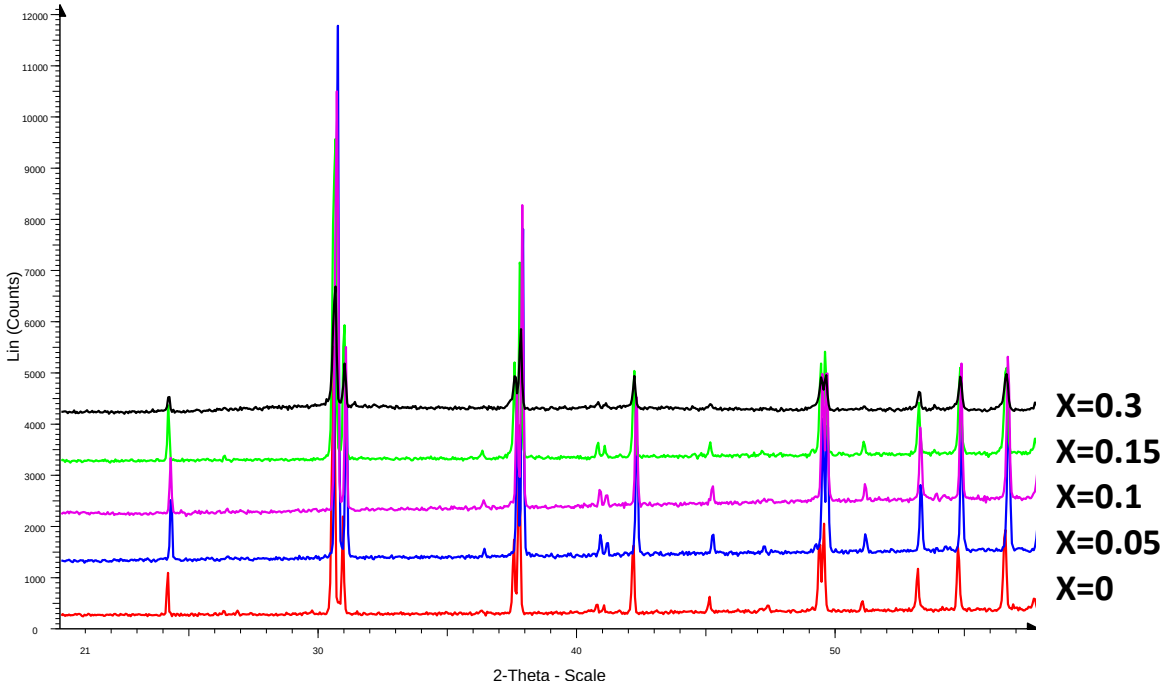

Figure 37: XRD patterns for $Nd_{2-x}Ca_xBaZnO_{5-\delta}$ where $0 \le x \le 0.3$.These data were investigated on the Bruker D8 diffractmeter. Top pattern has some change of structure (some peak disappeared).

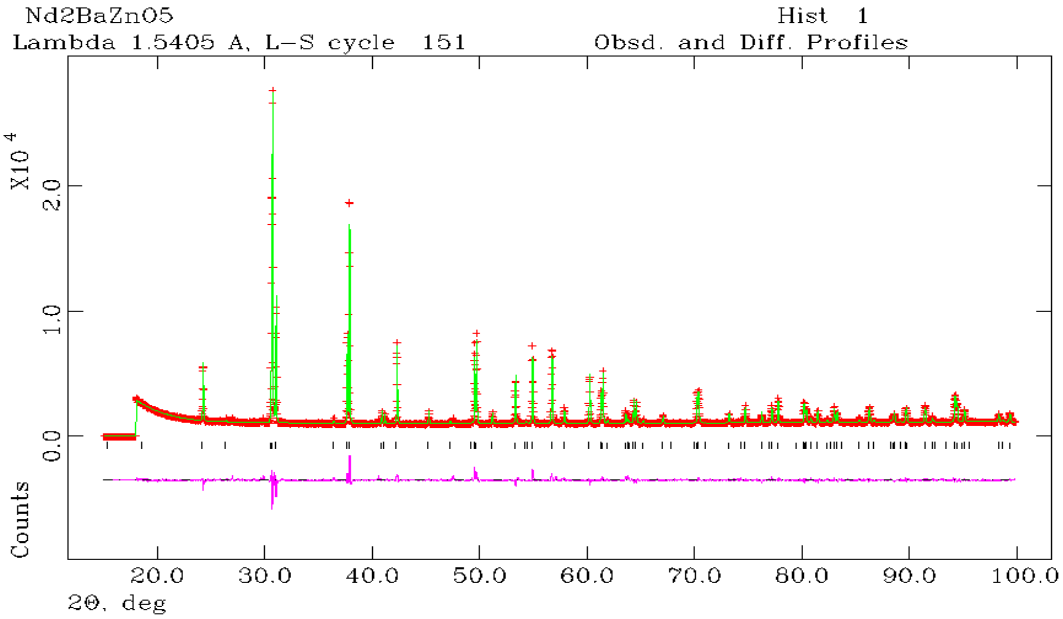

Figure 38: Rietveld fit of XRD data for the Nd_2BaZnO_5. The difference curve (pink), calculated pattern as solid lines and the model (green) on the observed pattern (red). Cell parameter a=b= 6.7607 (1)Å;c= 11.5438 (1)Å ,Unit cell volume =527.63(1)$Å^3$, chi-square c2=3.776, Rwp = 9.51%

Table5: Refined atomic position and site occupancy of Nd_2BaZnO_5

Atom	Position	X	Y	Z	Occupancy
Nd		**0.1720(1)**	**0.6720(1)**	**0**	**1**
Ba		**0**	**0**	**0.25**	**1**
Zn		**0**	**0.5**	**0.25**	**1**
O		**0**	**0**	**0**	**1**
O		**0.3356(1)**	**0.8356(1)**	**0.1285(1)**	**1**

Summary of refined atomic position and site occupancies listed in table 5. Rietveld fit of XRD data for Nd_2BaZnO_5 is showed in figure 38.The graph was well fitted. Reitveld fit curve for $La_{2-x}Ca_xBaZnO_{5-\delta}$ is showed in appendix1 Cell expansion was proved by the Rietveld analysis (table 6).For $La_{2-x}Ca_xBaZnO_{5-\delta}$ system cell parameter and Zn-O bond length is increasing with the increase of doping concentration exception was observed for $La_{1.7}Ca_{0.3}BaZnO_{5-\delta}$ system due to impurity.

Table6: Summary of the Rietveld refinement of XRD patterns collected for the $La_{2-x}Ca_xBaZnO_{5-\delta}$ and $Nd_{2-x}Ca_xBaZnO_{5-\delta}$ system.

composition	a,b (Å)	c (Å)	Zn-O bond length (Å)	Chi-squared
$La_{1.95}Ca_{0.05}BaZnO_{-\delta}$	**6.9077(1)**	**11.5922(1)**	**1.9254(1)**	**4.30**
$La_{1.9}Ca0.1BaZnO_{5-\delta}$	**6.9111(1)**	**11.5942(1)**	**1.9264(1)**	**4.99**
$La_{1.85}Ca0.15BaZnO_{5-\delta}$	**6.9121(1)**	**11.5989(1)**	**1.9287(1)**	**5.484**
$La_{1.7}Ca0.3BaZnO_{5-\delta}$	**6.9110(1)**	**11.5919(1)**	**1.9338(1)**	**5.502**
Nd_2BaZnO_5	**6.7607(1)**	**11.5438(1)**	**2.1060(1)**	**3.776**
$Nd_{1.95}Ca_{0.05}BaZnO_{5-\delta}$	**6.7607(1)**	**11.5461(1)**	**1.9100(1)**	**4.836**
$Nd_{1.9}Ca_{0.1}BaZnO_{5-\delta}$	**6.7608(1)**	**11.5465(1)**	**1.9324(1)**	**2.688**
$Nd_{1.85}Ca_{0.15}BaZnO_{5-\delta}$	**6.7610(1)**	**11.5469(1)**	**1.9454(1)**	**3.736**
$Nd_{1.7}Ca_{0.3}BaZnO_{5-\delta}$	**6.7613(1)**	**11.5475(1)**	**1.9464(1)**	**4.423**

0.5 gm of the entire sample ($La_{2-x}Ca_xBaZnO_{5-\delta}$ and $Nd_{2-x}Ca_xBaZnO_{5-\delta}$ system) was hydrated in a protonation furnace at 400^0C for 2days and for 2 days simultaneously 300^0C for 2 days and 200^0Cfor 2days.Partial pressure was noted as p(H_2O) ~0,42atm. XRD data was collected on hydrated samples. Again Vacuum drying was done on all the as prepared samples at 700C and 10^{-6}mbar for 1 day and XRD data was collected for these samples. From the XRD data of as prepared, hydrated and vacuum dried samples ($La_{2-x}Ca_xBaZnO_{5-\delta}$ and $Nd_{2-x}Ca_xBaZnO_{5-\delta}$) it can be remarked that structure was changed during hydration. Nd $(OH)_3$ and La $(OH)_3$ were formed.(figure 39).XRD pattern of hydrated Nd_2BaZnO_5 is given in appendix 1.

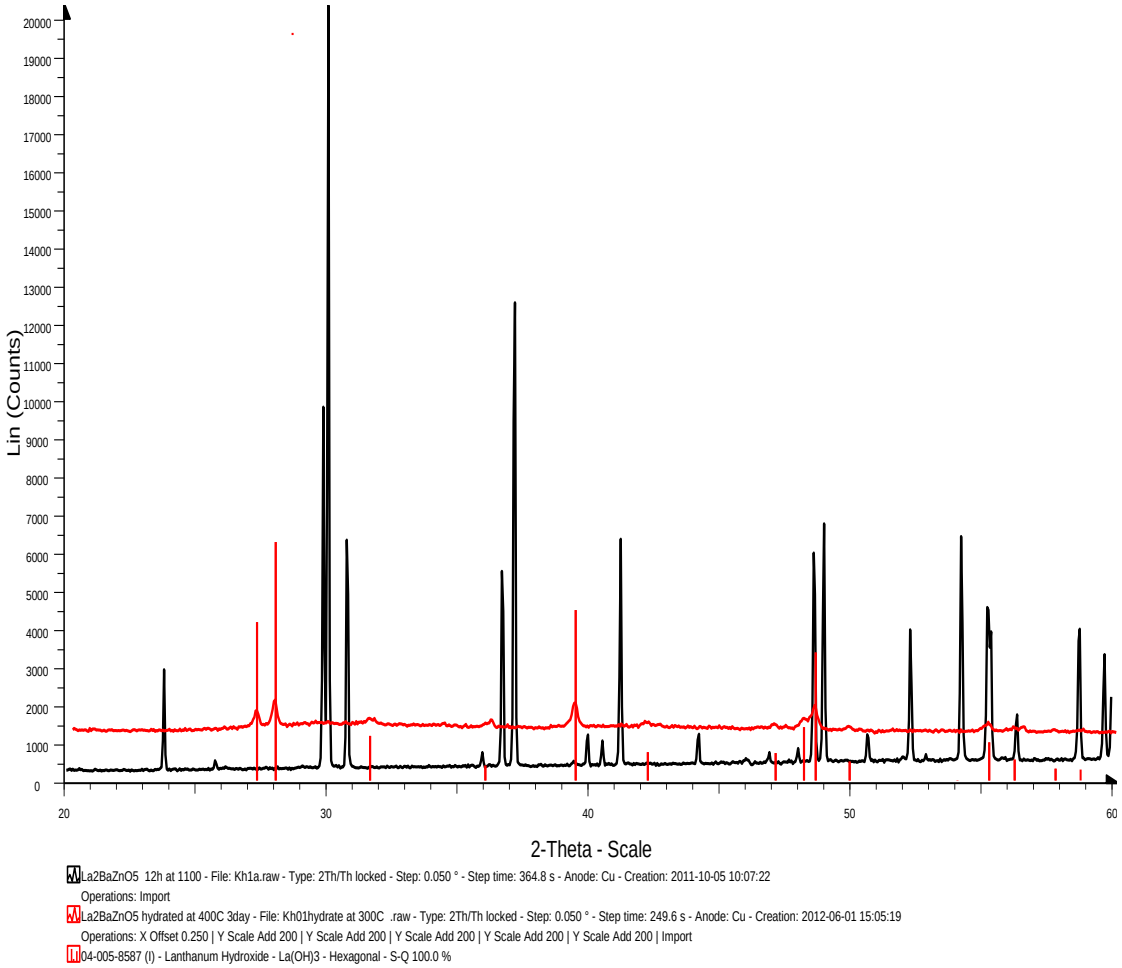

Figure 39: XRD pattern for La_2BaZnO_5 where red curve is for hydrated sample and black curve is for as prepare sample. Hydrated curve is showing some La $(OH)_3$ peaks.

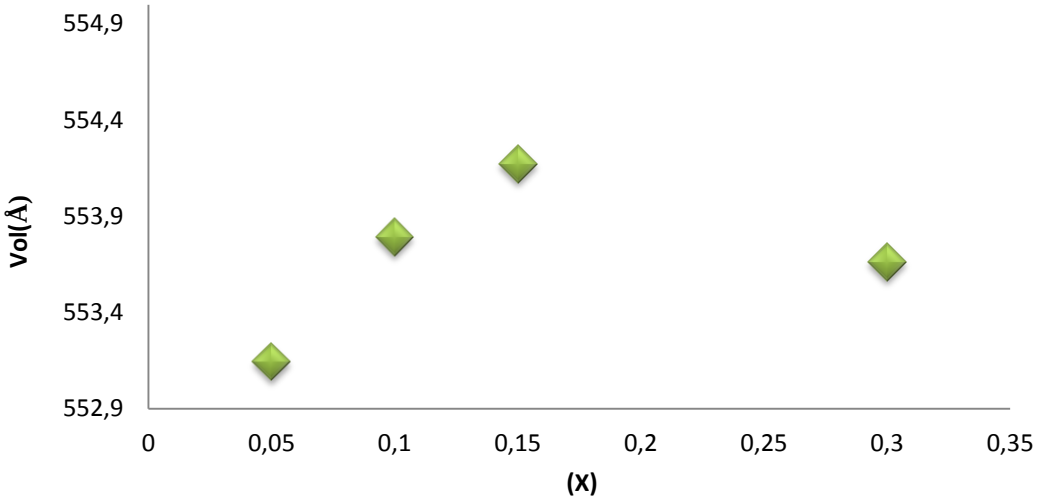

Figure 40: Cell volume function of Ca^{2+} doping concentration (x) curve for $La_{2-x}Ca_xBaZnO_{5-\delta}$ system, where cell volume increase with the increase of doping concentration Exception at X=0.3

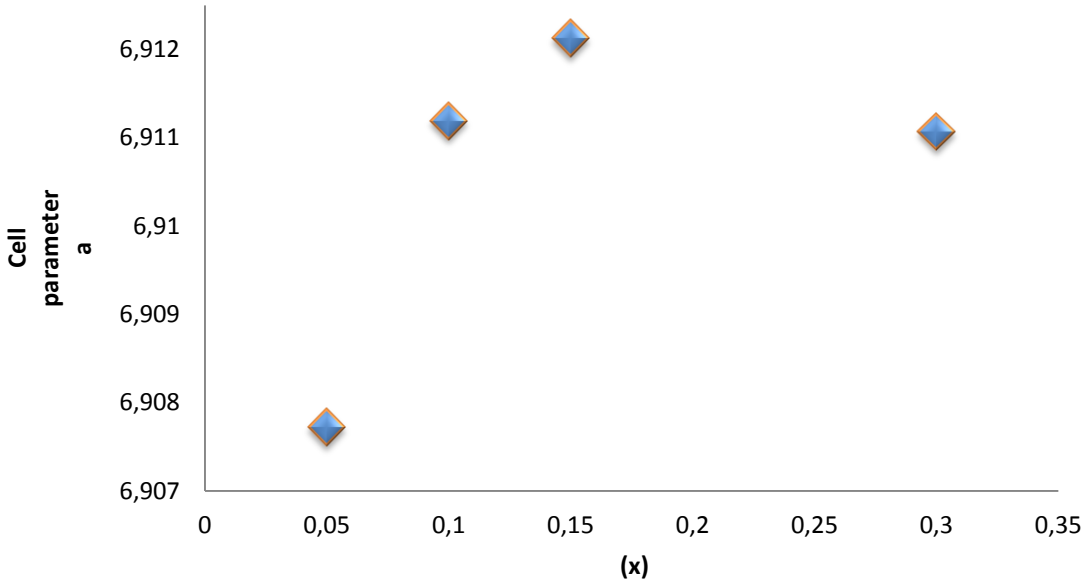

Figure 41: Cell parameter a function of Ca^{2+} doping concentration (x) curve for $La_{2-x}Ca_xBaZnO_{5-\delta}$ system, where value of cell parameter increase with the increase of doping concentration Exception at X=0.3.

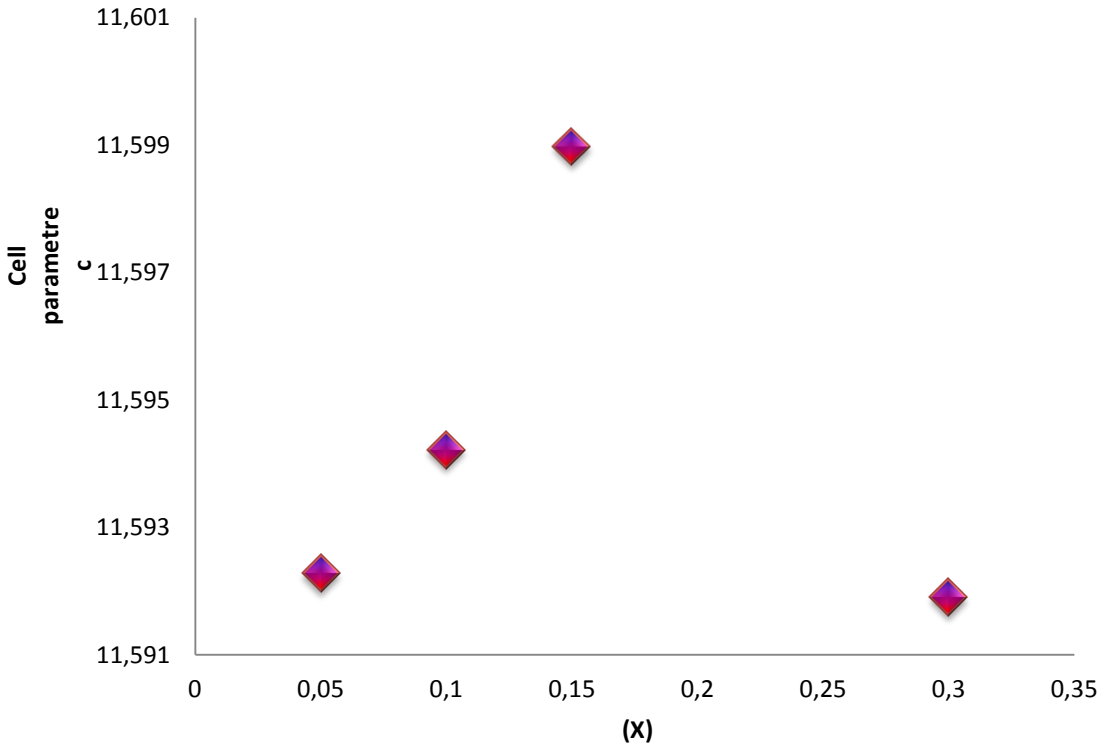

Figure 42: Cell parameter c function of Ca^{2+} doping concentration (x) curve for $La_{2-x}Ca_xBaZnO_{5-\delta}$ system, where value of cell parameter increase with the increasing doping concentration Exception at X=0.3.

Figure 40, 41, 42 illustrates how the cell volume, cell parameter change with increase of Ca doping concentration. These cell parameters are Rietveld refinement value of XRD data. At x=0.05 concentration cell volume was calculated as 553.1438(1)$Å^3$.At higher Ca doped higher cell volume was found except at x=0.3 .the same trend was followed for cell parameters .The value of cell parameter also increase with the increase of Ca doping concentration. The exception was observed at x=0.3 because this sample was not completely pure. Although ionic radius of CN 8 Ca^{2+} (1,12Å) is lower than ionic radius of CN 8 La^{3+}(1.16Å) cell was expanded for these system with Ca doped. It can be explained that Ca^{2+} creates oxygen vacancies and perhaps this leads to cell expansion, alternatively Ca^{2+} may either have replaced Ba^{2+} and some La^{3+} was substituted by Ba^{2+}(CN10 ionic radius 1,52Å), that's why cell parameter and cell volume increased and cell expanded with the increasing doping level

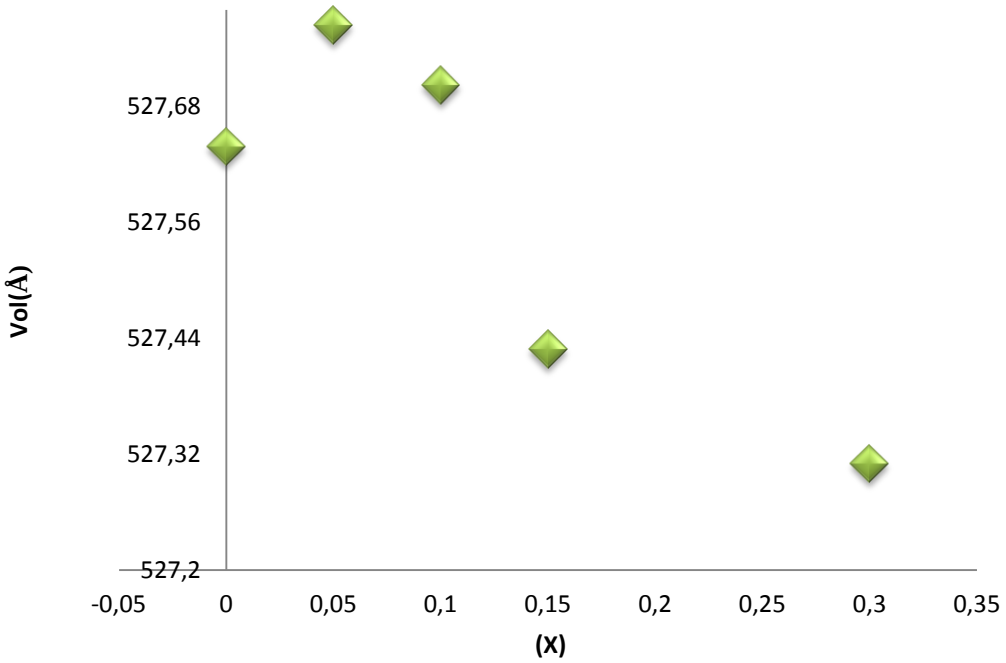

Figure 43: Cell volume function of Ca^{2+} doping concentration (x) curve for $Nd_{2-x}Ca_xBaZnO_{5-\delta}$system, where cell volume decrease with the increase doping concentration

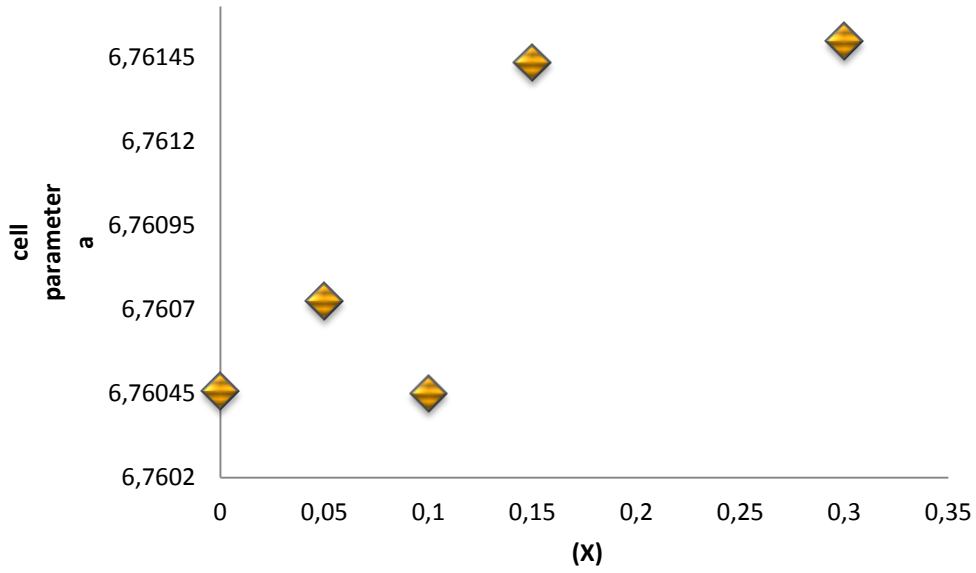

Figure 44: Cell parameter function of Ca^{2+} doping concentration curve for $Nd_{2-x}Ca_xBaZnO_{5-\delta}$ system, where value of cell parameter increase with the increasing doping concentration Exception observed at X=0.1.

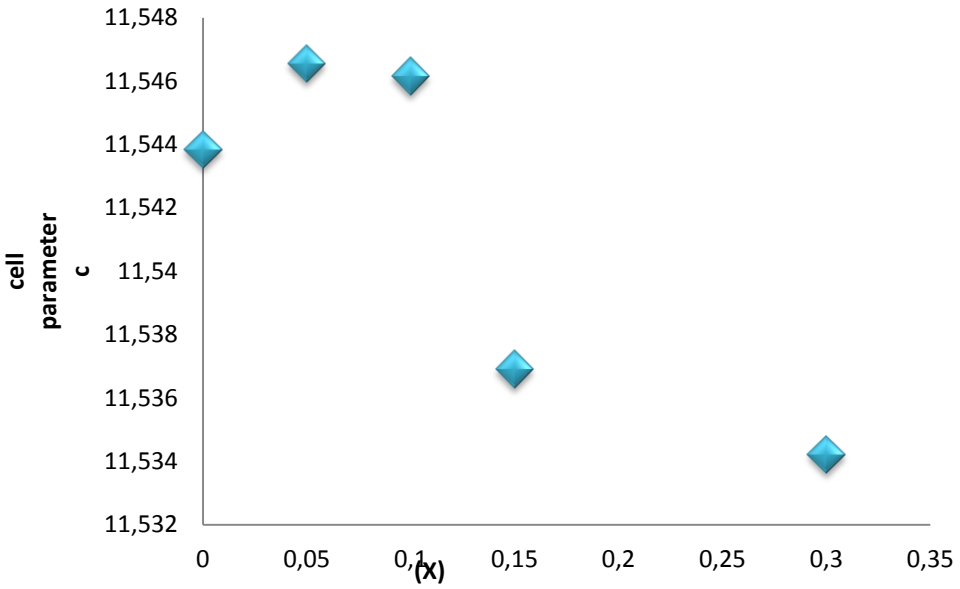

Figure 45: Cell parameter c function of Ca^{2+} doping concentration curve for $Nd_{2-x}Ca_xBaZnO_{5-\delta}$ system, where value of cell parameter decrease with the increasing doping concentration

For $Nd_{2-x}Ca_xBaZnO_{5-\delta}$ system cell volume decreased with the increased of Ca^{2+} doping concentration. Exception was observed for undoped sample and impurity phase was found in long scan diffraction pattern of undoped system (figure 43).according to figure, 44, 45 cell parameter (a) decreased and cell parameter (c) increased with increasing Ca^{2+} concentration. Although ionic radius of CN 8 Ca^{2+} (1,12Å) was higher than ionic radius of CN 8 Nd^{3+} (1.109Å), unit cell was contracted. It can be explained in a way that Initially Ca^{2+} replaced Nd^{3+} at lower doping and later Ba^{2+} was substituted by Ca^{2+} that's why cell parameter and cell volume initially increased and later decreased.

Thermo gravimetric analysis (TGA) was performed on as prepared and hydrated samples. Mass loss in hydrated samples much higher than as prepared samples.

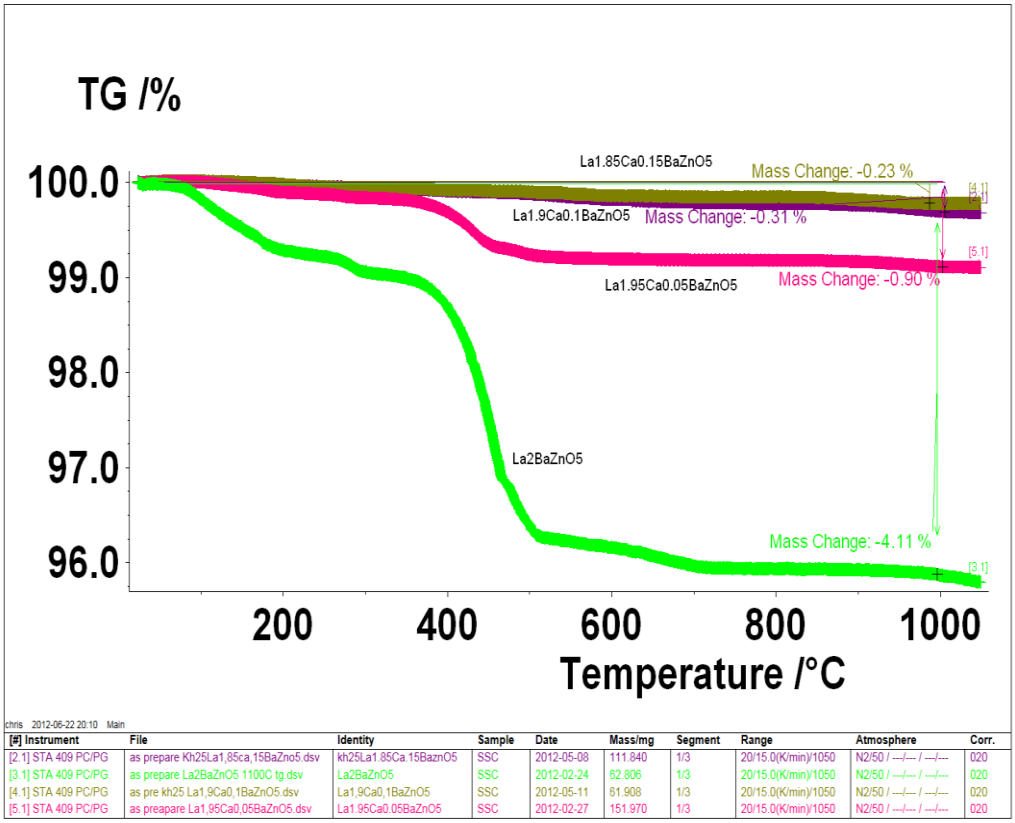

Figure 46: TGA data for $La_{2-x}Ca_xBaZnO_{5-\delta}$ system showing amount of mass loss in as prepared samples. Amount of mass is inconsistent.

Table7: Summary of TGA data for $La_{2-x}Ca_xBaZnO_{5-\delta}$ and $Nd_{2-x}Ca_xBaZnO_{5-\delta}$ system with as prepared and hydrated samples.

Sample	TEMP REGION(°C)	Mass change for As prepared samples	Mass change for hydrated samples
La_2BaZnO_5	82-1000	4.11%	12,95%
$La_{1.95}ca_{0.05}BaZnO_{5-\delta}$	82-1000	0.9%	12,50%
$La_{1.9}ca_{0.1}BaZnO_{5-\delta}$	82-1000	0.24%	12,72%
$La_{1.85}ca_{0.15}BaZnO_{5-\delta}$	82-1000	0.31%	12,28%
$Nd_2BaZnO_{5-\delta}$	82-1000	0.11%	6,33%
$Nd_{1.95}ca_{0.05}BaZnO_{5-\delta}$	82-1000	0.11%	6,34%
$Nd_{1.9}ca_{0.05}BaZnO_{5-\delta}$	82-1000	0.42%	6,64%
$Nd_{1.85}ca_{0.05}BaZnO_{5-\delta}$	82-1000	0.2%	6,83%

Mass loss was inconsistent for as prepared $La_{2-x}Ca_xBaZnO_{5-\delta}$ system .Mass loss decreased with the increased of doping level. However in perovskite systems mass loss increase with the doping level. Hydrated samples have higher mass loss than as prepared samples. During hydration these materials continuously decomposed results higher mass loss. $Ln(OH)_3$ was showed in XRD pattern of hydrated samples(figure 39). The obtained mass loss for both Ln-Zn (Ln=Nd,La)was given in table 7.

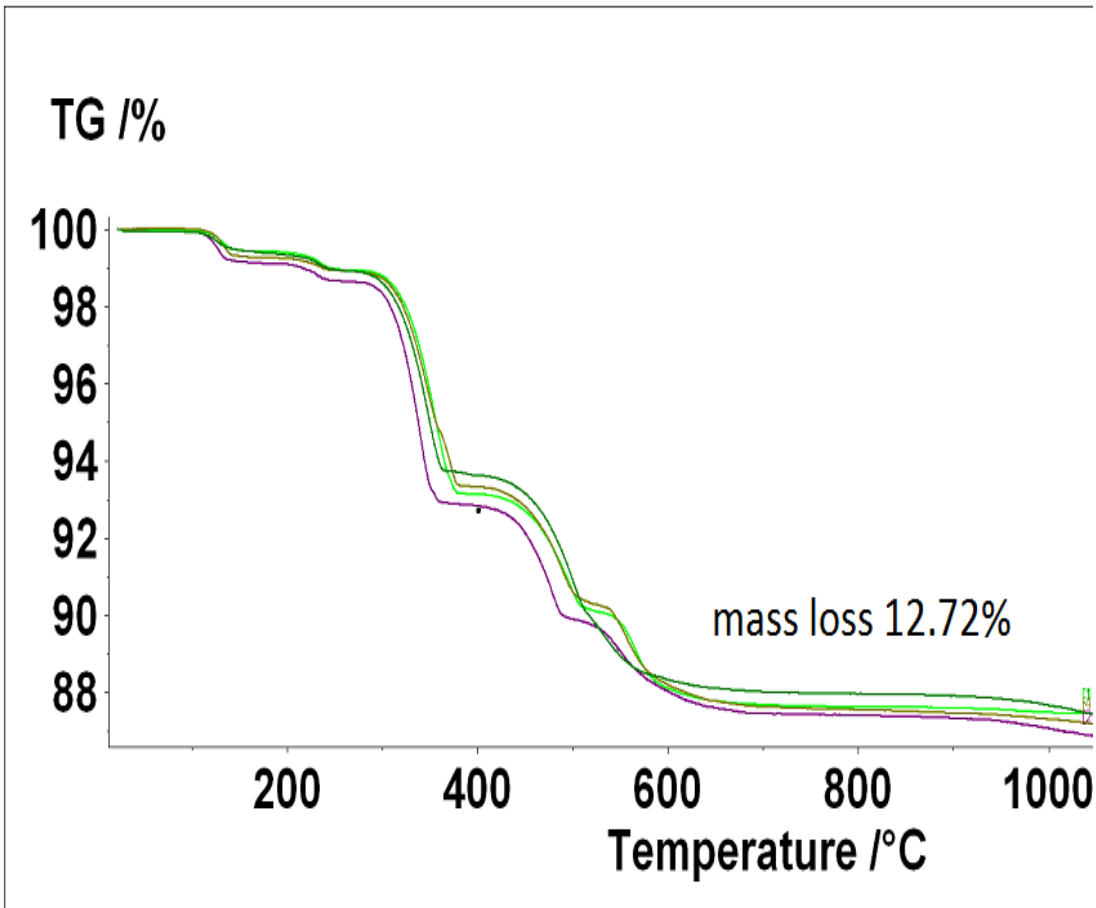

chris 2012-06-22 20:37 Main

[#] Instrument	File	Identity	Sample	Date	Mass/mg	Segment	Range	Atmosphere	Co
[1.1] STA 409 PC/PG	hydrated kh25 La1.85Ca0.15BaZno5.dsv	La1.85Ca0.15BaZno5	SSC	2012-05-21	50.868	1/3	20/15.0(K/min)/1050	N2/50 / ---/--- / ---/---	02
[2.1] STA 409 PC/PG	hydrated kh01 La2BaZno5.dsv	kh01la2BaZnO5	SSC	2012-05-18	25.406	1/3	20/15.0(K/min)/1050	N2/50 / ---/--- / ---/---	02
[3.1] STA 409 PC/PG	hydrated kh02 La1.95Ca0.05BaZno5.dsv	la1.95Ca.05BaZnO5	SSC	2012-05-20	58.132	1/3	20/15.0(K/min)/1050	N2/50 / ---/--- / ---/---	02
[4.1] STA 409 PC/PG	hydrated kh24 La1.9Ca0.1BaZno5.dsv	La1.9Ca0.1BaZnO5	SSC	2012-05-22	38.016	1/3	20/15.0(K/min)/1050	N2/50 / ---/--- / ---/---	02

Figure 47: TGA data for $La_{2-x}Ca_xBaZnO_{5-\delta}$ system showing amount of mass loss in hydrated samples. Amount of mass loss is same for all systems.

Total conductivity for the system $La_{2-x}Ca_xBaZnO_{5-\delta}$ were investigated and plotted in the figure 48.Conductivity experiment was run under dry Argon. Magnitude of the total conductivity increases with the increase of acceptor doping level. There is huge conductivity difference between the curve with undoped and the curve with doped system. That means

small amount of acceptor doping has great influence on conductivity level. At higher doped systems conductivity increase with small extent. However conductivity level was found even lower in $La_{1.7}Ca_{0.3}BaZnO_{5-\delta}$ system due to impurity. This sample was not completely pure according to XRD.

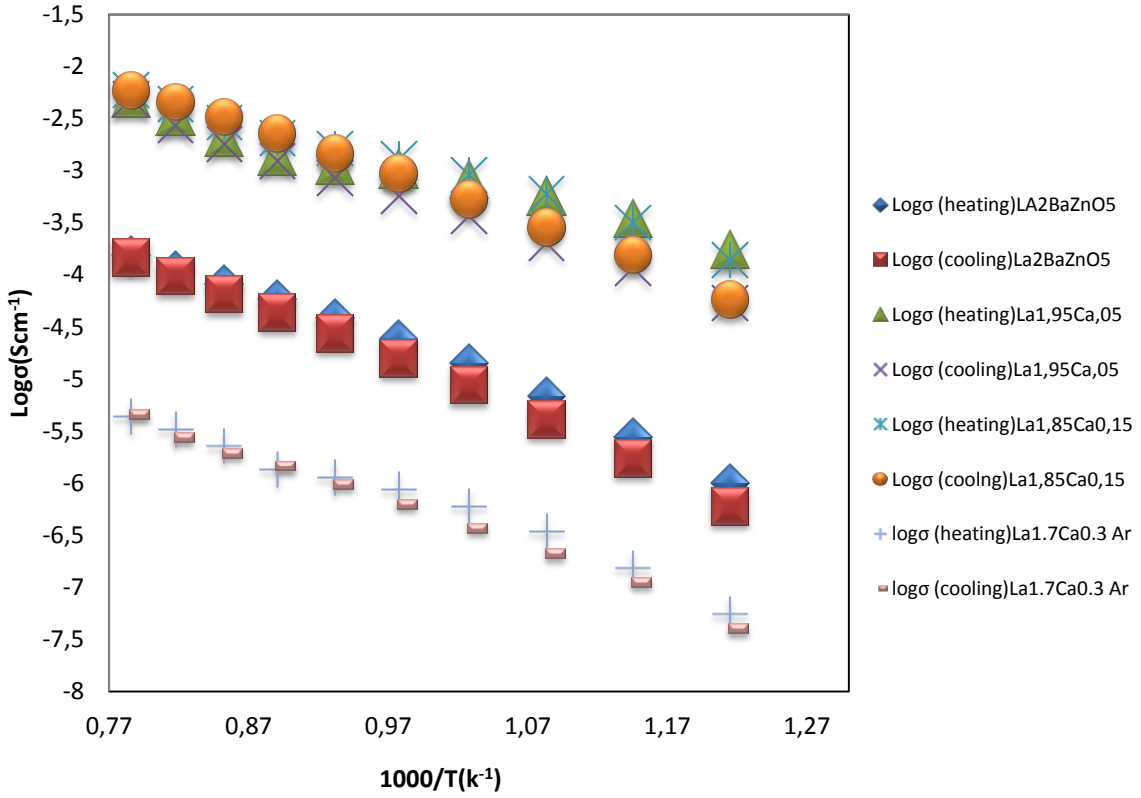

Figure 48: A typical plot of log of conductivity function of inverse temperatures under dry argon flow as prepared samples of $La_{2-x}Ca_xBaZnO_{5-\delta}$ system. The conductivity increased with the increase of doping level. Exception was observed for $La_{1.7}Ca_{0.3}BaZnO_{5-\delta}$ system**.**

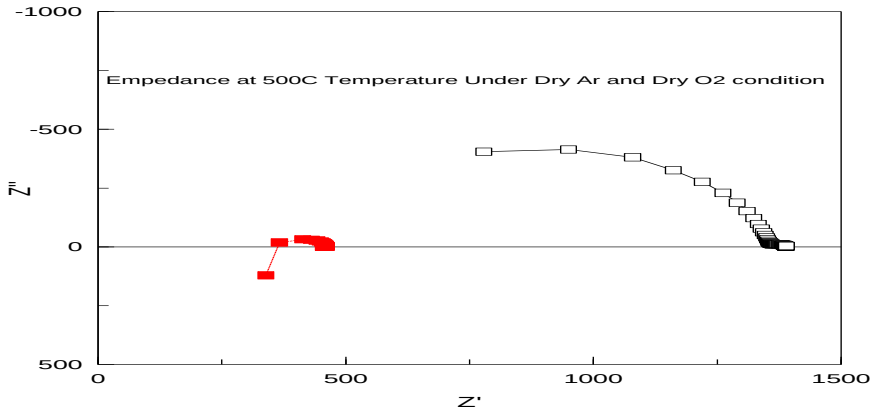

Figure 49: A z-view generated Impedance plot for $La_{1.85}ca_{0.15}$ $BaZnO_{5-\delta}$ at 500^0C under Dry Argon (black semicircle) and Dry oxygen (Red semicircle) flow.

Figure 49 is impedance plot of $La_{1.85}ca_{0.15}$ $BaZnO_{5-\delta}$ system under dry oxygen and dry Argon flow. The impedance value under oxygen run was much lower than Argon run at same temperature. That's why conductivity was also calculated higher under O_2 run than Argon run at 500^0C.

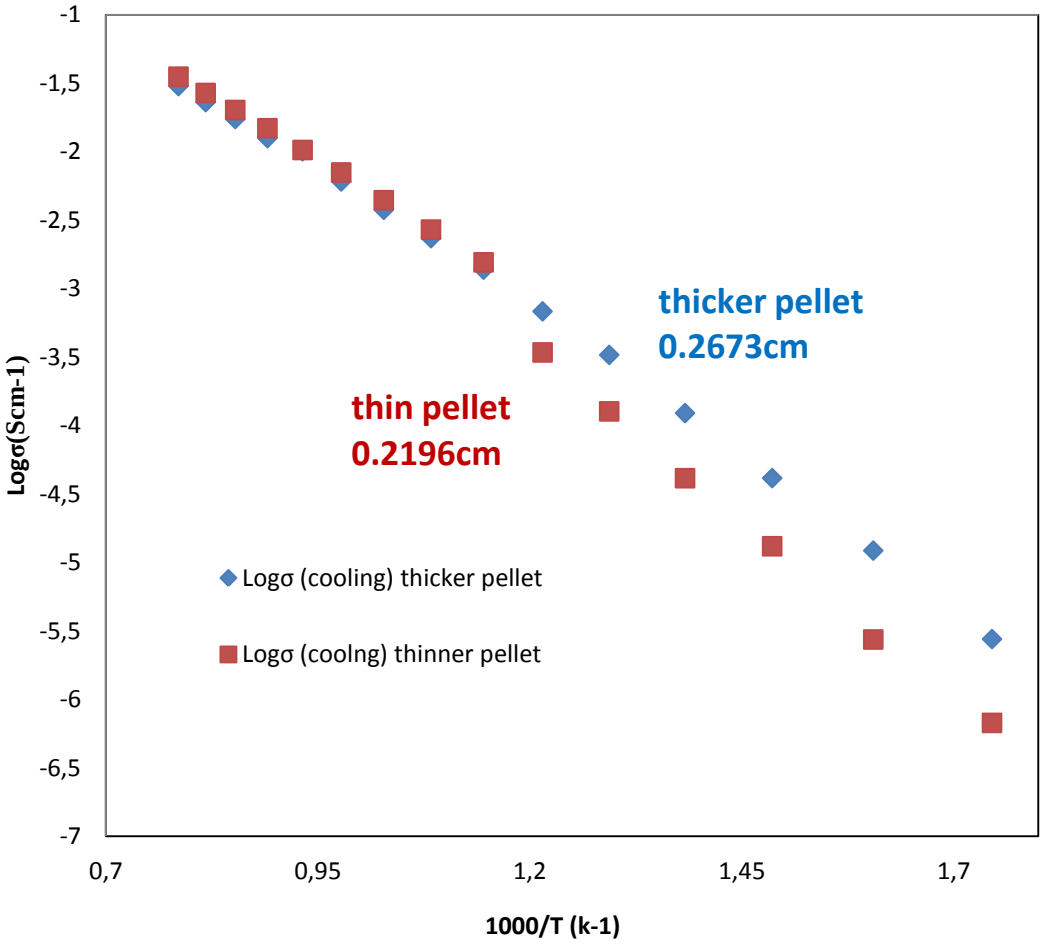

Figure 50: A total conductivity plot for $La_{1.85}Ca_{0.15}$ $BaZnO_{5-\delta}$ system of thicker and thinner pellet under dry O_2 flow (cooling).

Conductivity experiment was repeated on of $La_{1.85}Ca_{0.15}$ $BaZnO_{5-\delta}$ system and plotted in figure 50.Conductivity is consistent for repeated experiment.

Total conductivity plot of $La_{1.85}Ca_{0.15}$ $BaZnO_{5-\delta}$ system under dry O_2 and dry Argon flow is shown in figure 51.Under dry O_2 flow oxide ion could move fast and impedance dropped and high conductivity was observed .Conductivity under O_2 flow was higher than in Argon flow condition. Activation energy was calculated 0,7474eV at temperature $(600\text{-}1000)^0$C, 1,0379 eV at$(400\text{-}550)^0$C and 0,7318eV at $(250\text{-}350)^0$C under dry O_2 flow condition Under dry

Argon flow condition activation energy was calculated respectively 0,8843 eV 1,0973eV and 0,8818 eV. At higher temperature activation energy dropped because energy barrier decreased and oxide ion moved rapidly and conductivity increased.

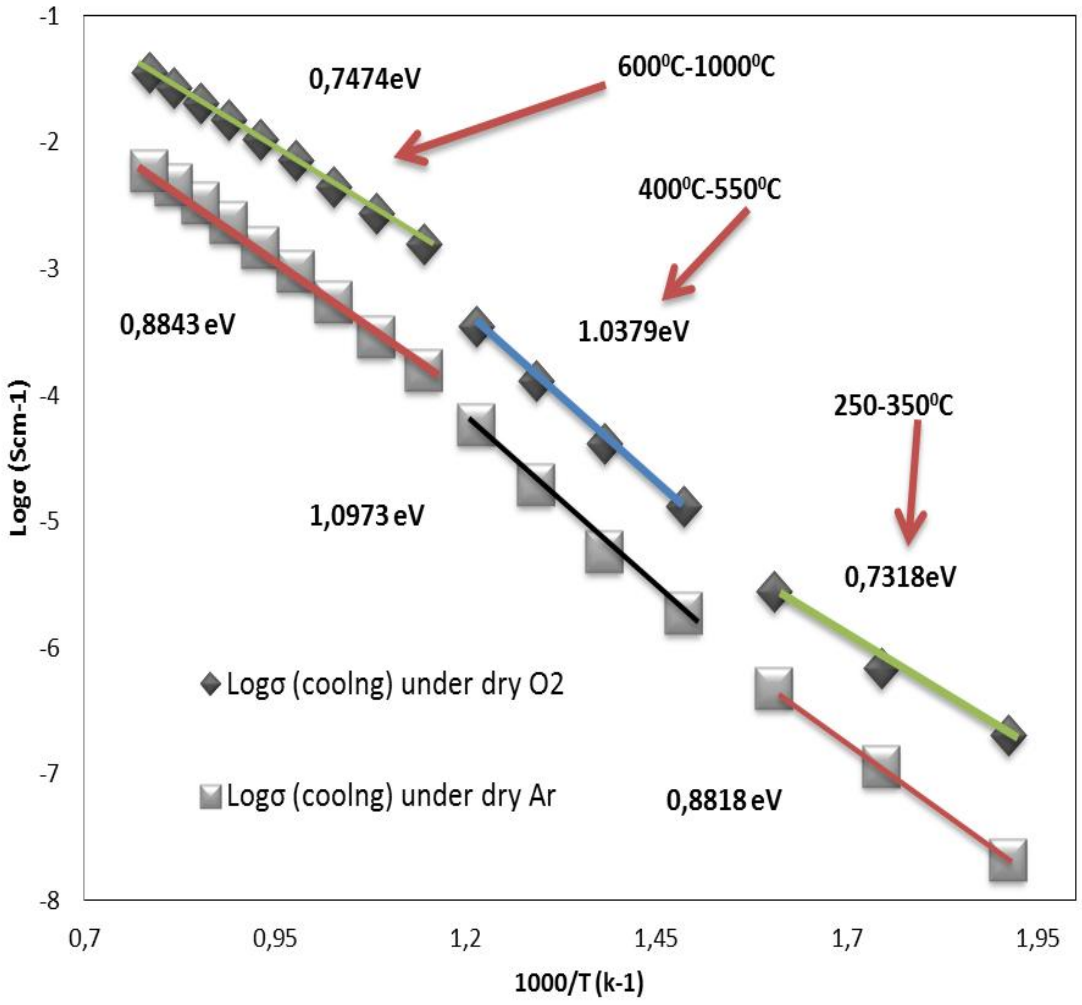

Figure 51: A total conductivity plot for $La_{1.85}Ca_{0.15}$ $BaZnO_{5-\delta}$ system under dry O_2 and dry Argon flow (cooling)

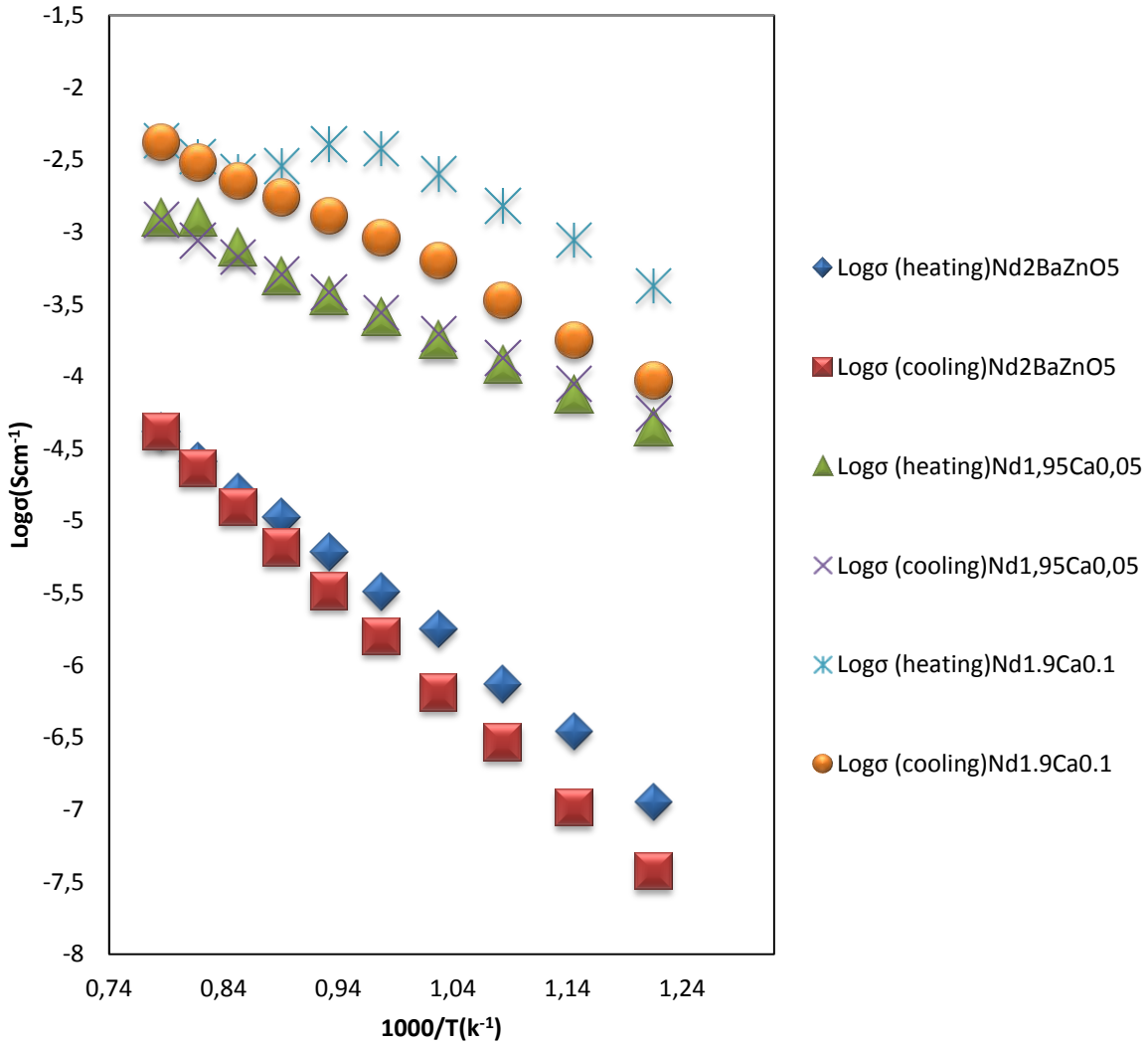

Figure 52: Log of conductivity as a function of inverse temperature showing conductivity of $Nd_{2-x}Ca_xBaZnO_{5\,\delta}$ system. The conductivity increase with the increase of acceptor doping level.

Total conductivity for $Nd_{2-x}Ca_xBaZnO_{5-\delta}$ systems were investigated and plotted in the figure 52.Acceptor doping has effect on conductivity. Conductivity level was increased with the increase of doping level. Conductivity of $Nd_{1.9}Ca_{0.1}BaZnO_{5-\delta}$.system was higher than undoped and lower doped systems.

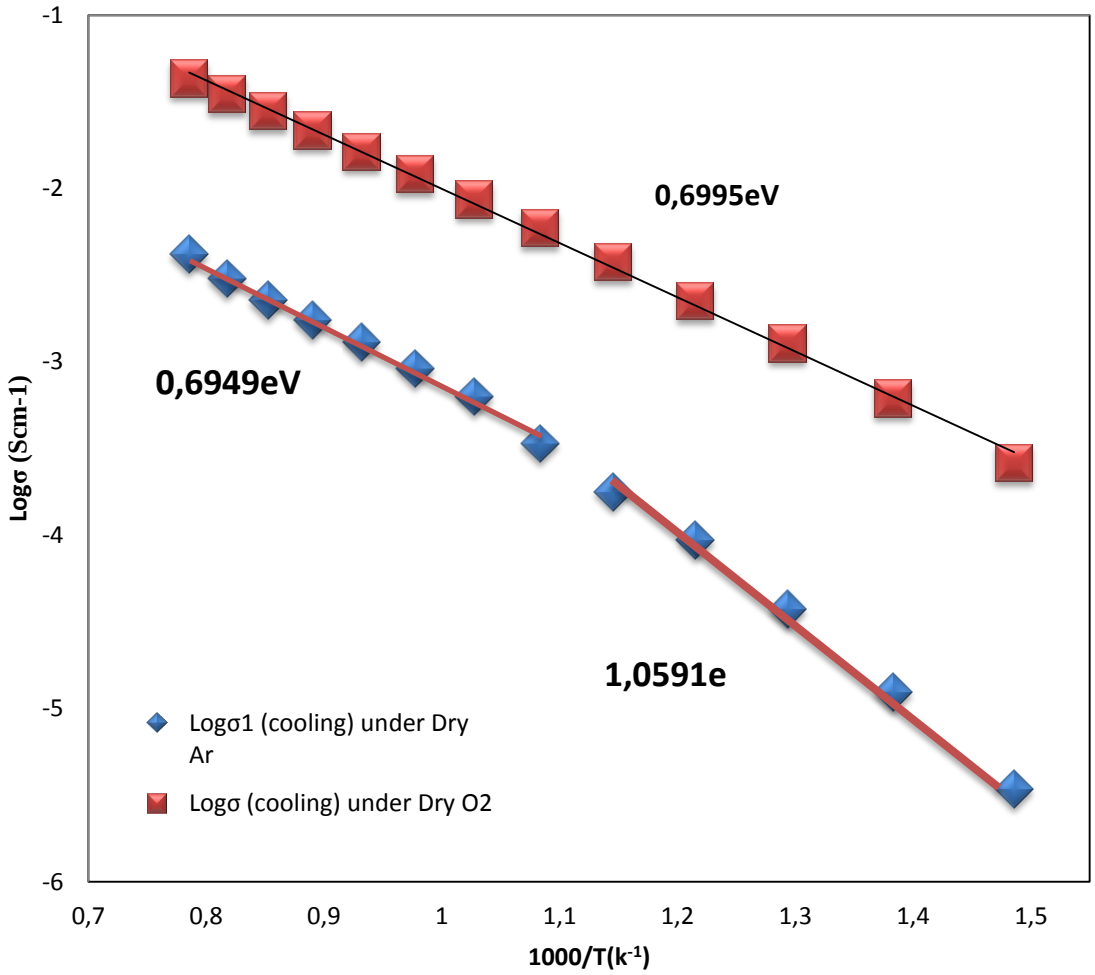

Figure 53: A total conductivity plot for $Nd_{1.9}Ca_{0.1}$ $BaZnO_{5-\delta}$ system under dry O_2 cooling and dry Argon cooling .Conductivity difference is clearly observed under different condition.

A clear difference of conductivity was observed under different condition (figure 53). Under dry O_2 condition conductivity level of $Nd_{1.9}Ca_{0.1}$ $BaZnO_{5-\delta}$ system showed higher value than under dry Argon condition. Under dry O_2 condition impedance dropped and that means conductivity increased. Activation energy was respectively 1,0591eV at $(400\text{-}600)^0$C, 0,6949eV at $(650\text{-}1000)^0$C under dry Argon condition and 0, 6995 eV under dry O_2 condition.

Activation energy of $La_{-x}Ca_xBaZnO_{5\,\delta}$ and $Nd_{2-x}Ca_xBaZnO_{5\,\delta}$ system under Dry Argon and O_2 condition at different temperature given in table 8. Arrhenius plot of total conductivity was used to calculate activation energy for different system. At $600\text{-}1000^0$C temperature region activation energy for $La_{1.85}Ca0.15BaZnO_{5-\delta}$ system was 0, 8843 eV under dry Argon condition

and 0, 7474 eV under dry O_2 condition. That means under O_2 condition oxide ions were easily moving because energy barrier decreased.

Table 8: Activation energy chart for $La_{2-x}Ca_xBaZnO_{5\,\delta}$ and $Nd_{2-x}Ca_xBaZnO_{5\,\delta}$ system under Dry Argon and O_2 condition.

Formula	**Temperatures (^{0}C)**	**Activation energy(eV) dry Argon**	**Activation energy(eV) dry O_2**
$La_2BaZnO_{5-\delta}$	**450-1000**	**1,0957**	
$La_{1.95}Ca_{0.05}BaZnO_{5-\delta}$	**650-1000**	**0,8685**	
	450-600	**1,1423**	
$La_{1.85}Ca0.15BaZnO_{5-\delta}$	**600-1000**	**0,8843**	**0,7474**
	400-550	**1,0973**	**1,0379**
	250-350	**0,8818**	**0,7318**
Nd_2BaZnO_5	**150-1000**	**1,3982**	
$Nd_{1.95}Ca_{0.05}BaZnO_{5-\delta}$	**150-1000**	**0,6809**	
$Nd_{1.9}Ca_{0.1}BaZnO_{5-\delta}$	**400-600**	**1,0591**	**0,6995**
	650-1000	**0,6949**	**0,6995**

$Ln_{2-x}Ca_xBaZnO_{5-\delta}$ where Ln=La, Nd; x=0 to 0.3 structure based materials were successfully synthesized by solid state sintering method. These materials were not stable in wet condition and during hydration H_2O react with (La, Nd) to form $Ln(OH)_3$.TGA results confirm that these materials uptake lots of water during hydration consistent with the decomposing to hydroxide. Cell expansion of these materials was proved by Reitveld analysis. With the increase of acceptor doping level total conductivity of $Ln_{2-x}Ca_xBaZnO_{5-\delta}$ system increased .Higher doped materials (x≥0.3) has lower conductivity due to impurity. In O_2 conductivity is dominated by p-type electron holes. In Argon the conductivity is lower and it is oxide ion

conduction. Undoped La_2BaZnO_5 has one order of higher magnitude of total oxide ion conductivity than Nd_2BaZnO_5 (figure 48, 52) .The oxide ion conductivity is still pretty good. At 1000^0C the conductivity of $La_{1.85}Ca_{0.15}BaZnO_{5-\delta}$ is 3, $4\times10^{-2}Scm^{-1}$ and $Nd_{1.9}Ca_{0.1}BaZnO_{5-\delta}$ is $4.3\times10^{-}2Scm^{-1}$one order of magnitude lower than YSZ ($1\times10^{-1}Scm^{-1}$)(42).

Conclusion

The proton conductivity in acceptor doped pyrochlores $Nd_{2-x}Ca_xInMO_{7-\delta}$ where M=Ta, Nb; $0\leq x\leq 0.05$, $Ln_{2-x}Ca_xBaZnO_{5-\delta}$ structure based where Ln=Nd, La; $0\leq x\leq 0.3$ and brownmillerite structure based materials $Ba_2In_{2-x}MxO_{5-\delta}$ where M=Ga, Y; $0\leq x\leq 0.85$ have been investigated. $Ln_{2-x}Ca_xBaZnO_{5-\delta}$ possessed tetragonal structure with I4/mcm space group, $Nd_{2-x}Ca_xInMO_{7-\delta}$ possessed cubic structure with Fd-3m space group and $Ba_2In_{2-x}MxO_{5-\delta}$ possessed orthorhombic with Ibm2.All of these samples were synthesized successfully by solid state sintering method's and XRD data showed these materials synthesized successfully.

In order to make conclusion further study (more synthesis, TGA, conductivity) is needed for pyrochlore $Nd_2Ca_xInMO_{7-\delta}$ systems however initial conductivity was low. Acceptor doping Ca^{2+}enhanced the ionic conductivity of Ln_2BaZnO_5 (where Ln=La, Nd) structure based materials, and $Nd_{1.9}Ca_{0.1}BaZnO_{5-\delta}$ and $La_{1.85}Ca_{0.15}BaZnO_{5-\delta}$ are good oxide ionic conductors. However, these phases were unstable in wet condition making them unsuitable as proton conductors. Under dry Argon condition at 800^0C conductivity of $1{,}29x10^{-3}Scm^{-1}$ was obtained in $Nd_{1.9}Ca_{0.1}BaZnO_{5-\delta}$ system and $1{,}45x10^{-3}Scm^{-1}$ was obtained for $La_{1.85}Ca_{0.15}BaZnO_{5-\delta}$ system, where YSZ showed conductivity of $6{,}71x10^{-2}Scm^{-1}$ at 800^0C(43). Although lower than YSZ and other fluorites Ca^{2+} doped $Ln_2BaZnO_{5-\delta}$ show promising oxide conductivity.

Cell expansion was clearly observed for $Ba_2In_{2-x}Y_xO_{5-\delta}$ and cell contraction was observed for $Ba_2In_{2-x}Ga_xO_{5-\delta}$ system. Hydrated brownmillerite $Ba_2In_{2-x}M_xO_{5-\delta}$ (where M=Ga, Y and $0\leq x\leq 0.3$) adopts tetragonal structure. Neutron diffraction will be done on $Ba_2In_{2-x}M_xO_{5-\delta}$ (where M= Ga, Y $0\leq x\leq 0.3$) to follow the structural transition that occurs on hydration.

Appendix I

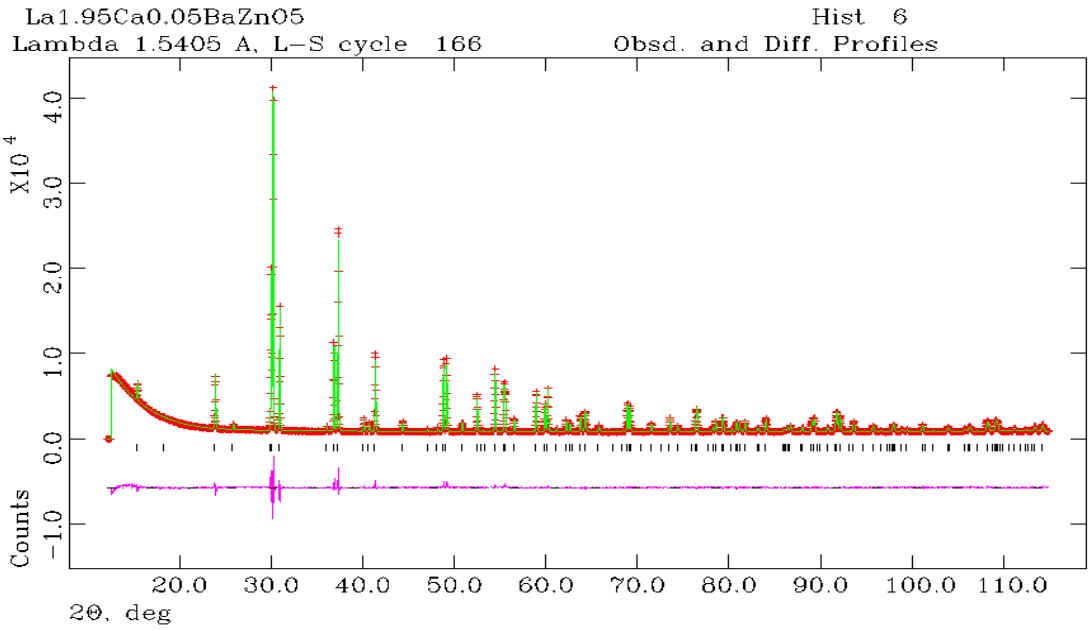

Figure 1 Rietveld fit of XRD data for the $La_{1.95}Ca_{0.05}BaZnO_{5-\delta}$. The difference curve (pink), calculated pattern as solid lines and the model (green) on the observed pattern (red).

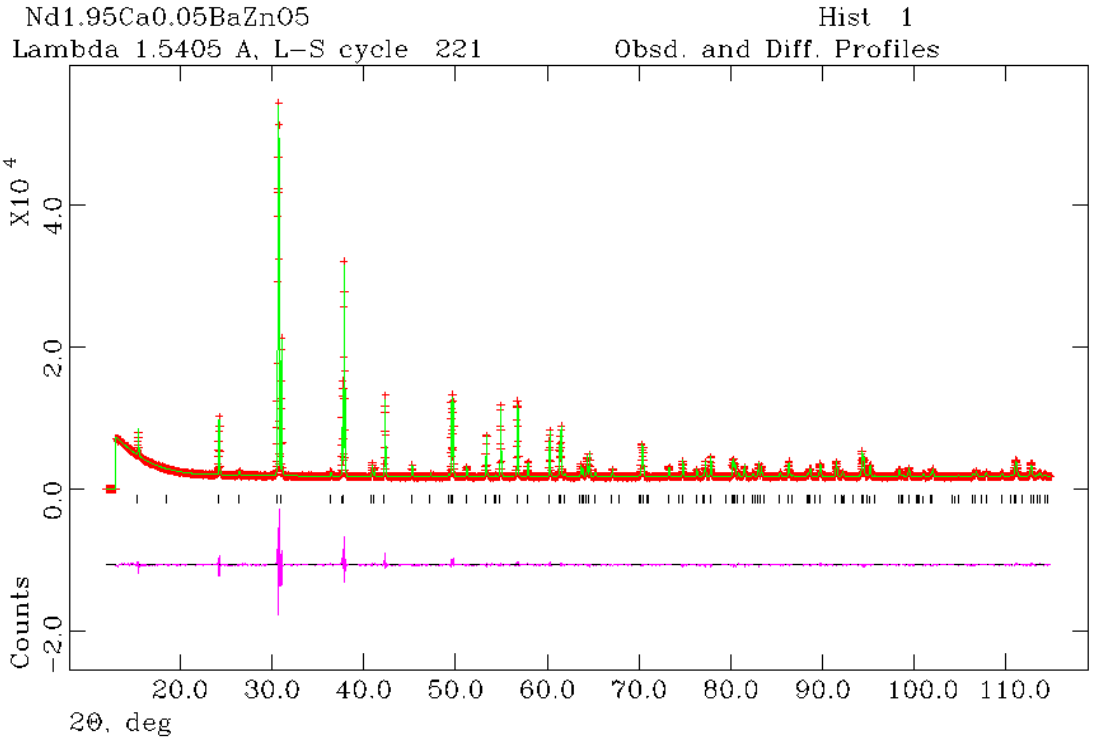

Figure 2: Rietveld fit of XRD data for the $Nd_{1.95}Ca_{0.05}BaZnO_{5-\delta}$. The difference curve (pink), calculated pattern as solid lines and the model (green) on the observed pattern (red).

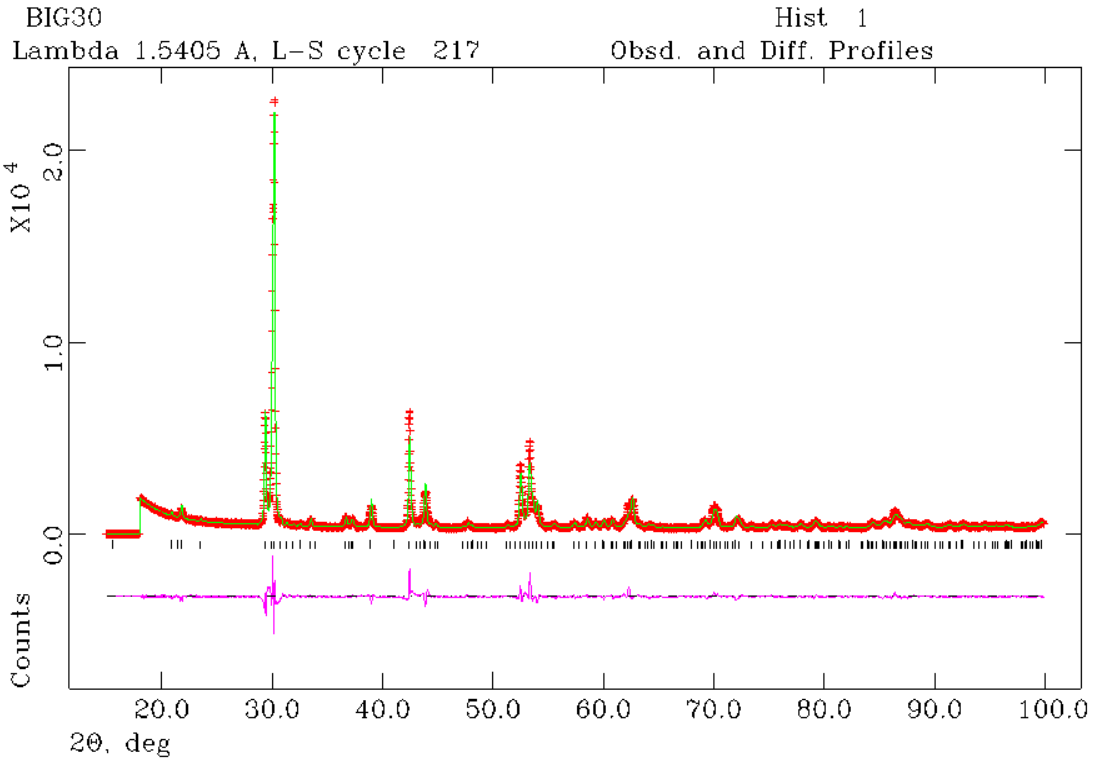

Figure 3: Rietveld fit of XRD data for the $Ba_2In_{1.7}Ga0.3O_{5-\delta}$. The difference curve (pink), calculated pattern as solid lines and the model (green) on the observed pattern (red).

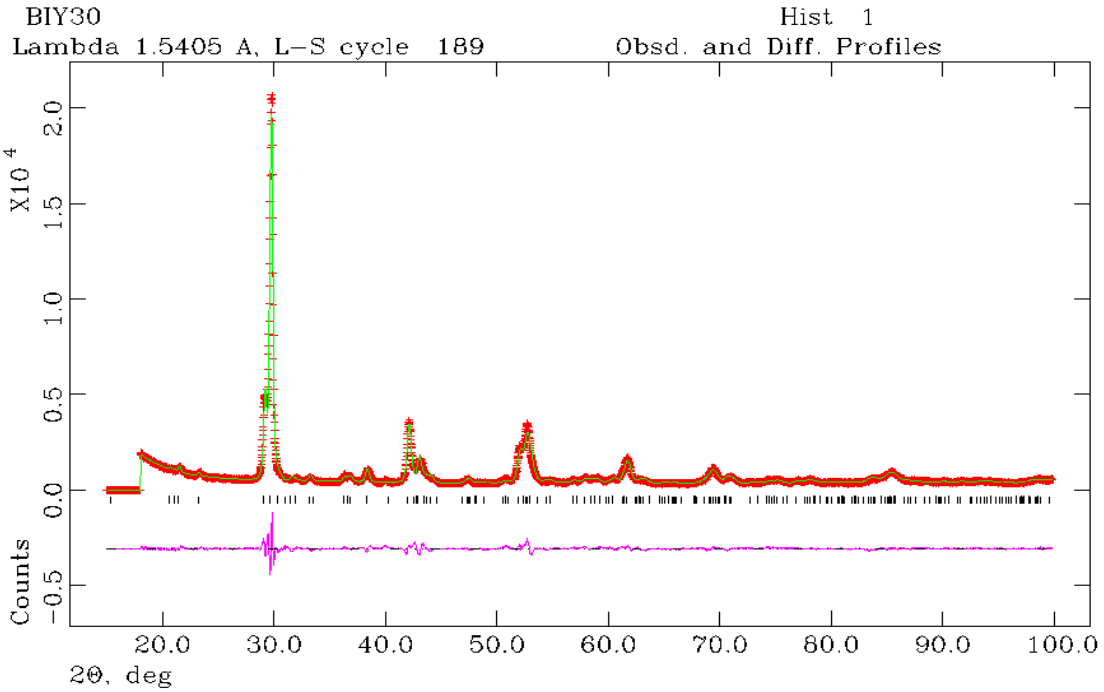

Figure 4: Rietveld fit of XRD data for the $Ba_2In_{1.7}Y_{0.3}O_{5-\delta}$. The difference curve (pink), calculated pattern as solid lines and the model (green) on the observed pattern (red).

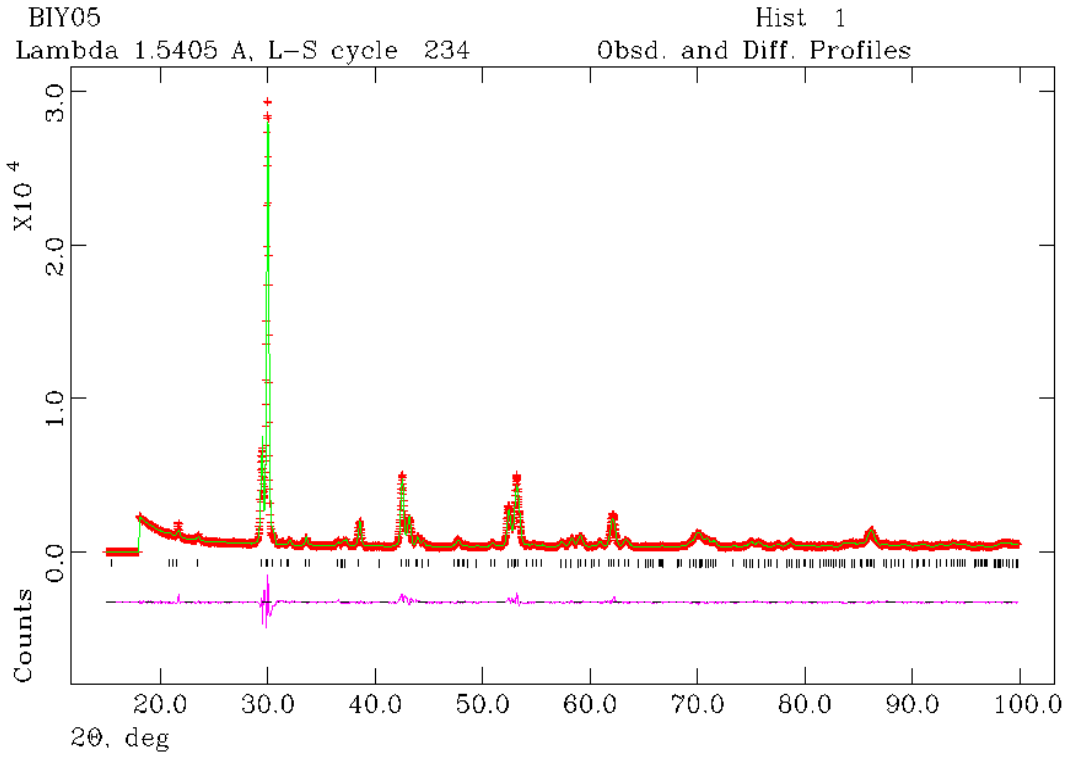

Figure 5: Rietveld fit of XRD data for the $Ba_2In_{1.95}Y_{0.05}O_{5-\delta}$. The difference curve (pink), calculated pattern as solid lines and the model (green) on the observed pattern (red).

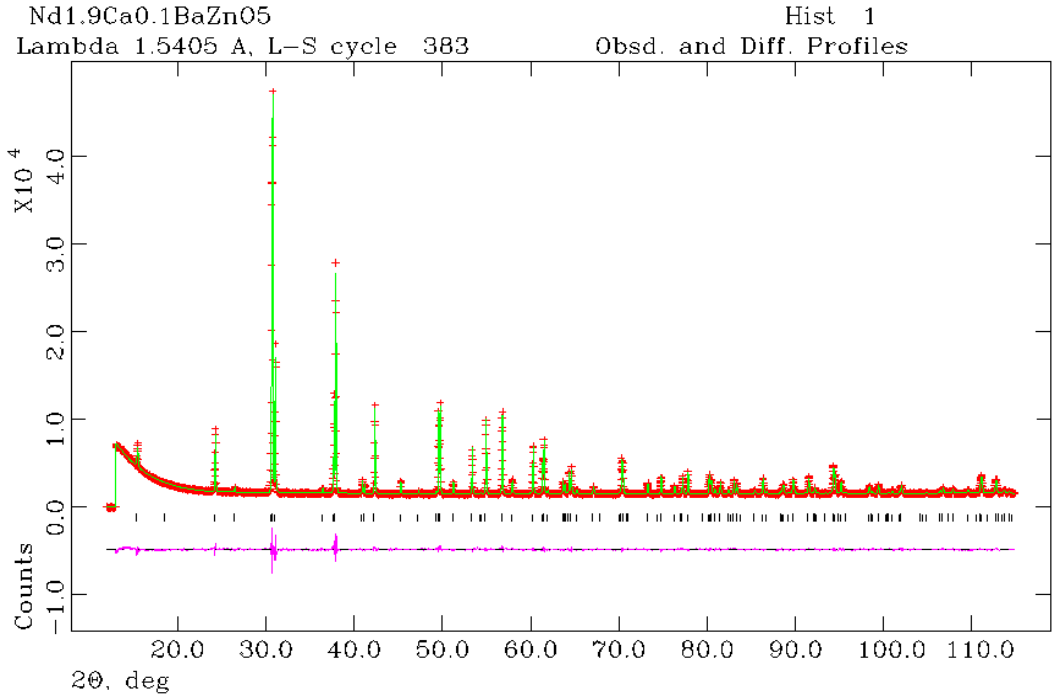

Figure 6: Rietveld fit of XRD data for the $Nd_{1.9}Ca_{0.1}BaZnO_{5-\delta}$. The difference curve (pink), calculated pattern as solid lines and the model (green) on the observed pattern (red).

Appendix II

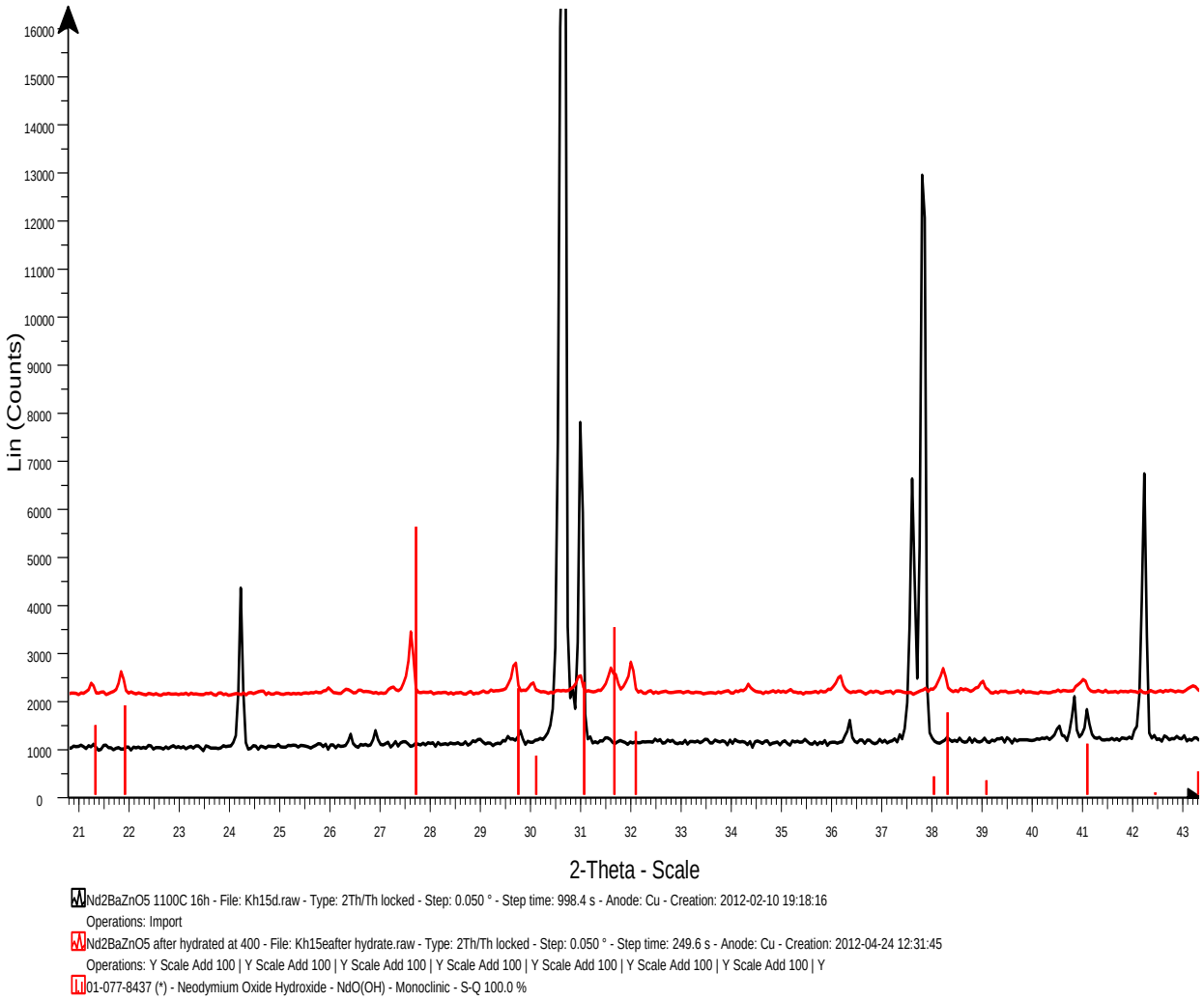

Figure7: XRD pattern for Nd_2BaZnO_5 where red curve is for hydrated sample and black curve is for as prepare sample. Hydrated curve is showing some $Nd(OH)_3$ peaks

Acknowledgements

This work has been done in the Laboratory of inorganic chemistry department. I would like to sincerely thank my supervisor Christopher Knee for his constructive help in theoretical and practical studies. Without his help it would not have been possible to successfully done this project. I would also like to thank my examiner Professor StenEriksson for giving me an opportunity to work in oxide group. I have learned a lot when I did his course during my Master's thesis.

Seikh M H Rahman and Francis Kinyanjui helped me a lot during my experimental work. I am also very grateful for their help. If I will get chance to work here I will overcome any scientific challenges that come our way.

I also thanks to my colleagues at the oxide group for their help and cooperation in lab

References

1. Larminie, J. & Dicks, A. Fuel Cell Systems Explained ,John Wiley & Son, 2003, 2nd edition,2003.

2. Lorenzo Malavasi, Craig A. J. Fisher and M. Saiful Islam, Oxide-ion and proton conducting electrolyte materials for clean energy applications: structural and mechanistic features, The Royal Society of Chemistry, Chem. Soc. Rev., 2010, 39, 4370–4387.

3. I. Kosacki and H. L. Tuller, Solid State Ionics, 1995, 80, 223.

4. N. Bonanos,B. Ellis and M.N.Mahmood,Solid State Ionics ,1988,28-30,579-584

5. Porter D.L., Heuer A.H., Journal of American Ceramic Society, 1979, 62, 298.

6. Yanzhong Wang, Synthesis and characterisation of acceptor-doped BaSnO3 compounds as proton conductors,Phd thesis,2009,05

7. T. Norby, Nature,2001, 410, 877.

8. A. J. Appleby, F. R. Foulkes, Fuel Cell handbook, Van Nostrand Reinhold ,1989.

9. B. C. H. Steele and A. Heinzel, Nature,2001, 414, 345-352.

10. M. Nagao, T. Kamiya, P. Heo, A. Tomita, T. Hibino, M. Sano, Journal of the Electrochemical Society. 153(2006), A1604-A1609.

11. K. D. Kreuer, Annual Review of Materials Research,2003, 33, 333.

12: T. Norby and Y. Larring, Current Opinion in Solid State and Material Science, 1997,2, 593.

13. A. Lashtabeg and S. J. Skinner, J. Material Chemistry, 16 (2006), 3161.

14. S. Nakayama, H. Aono and Y. Sadaoka. Chemistry Letters, 1995,431.

15. N. Zhou, G. Chen, H. J. Zhang and C. Zhou, Phys. B, 404(2009),4150-4154

16. R. Punn, A. M. Feteira, D. C. Sinclair and C. Greaves, J. Am.Chem. Soc., 2006, 128, 15386.

17. Stephen J. Skinner and John A. Kilner, oxygen ion conductor, Materials Today, 2003

18. Feng, M., and Good enough, J. B., Eur. J. Solid State Inorganic Chemistry, 1994, 31, 663

19. Huang, K. Q., et al., J. Electrochem. Soc. (1997), 144, 3620

20. T. Ishihara, H. Matsuda and Y. Takata, J. Am. Chem. Soc., 1994,116, 3801.

21. Coors, W. G., and Ready, D. W., J. Am. Ceram. Soc.,2002, 85, 2637.

22. T. Ishihara, H. Matsuda, M. Azmi Bin Bustam and Y. Takita, Solid State Ionics, 1996, 86–88, 197;

23. A. Sinha, H. Na¨ fe, B. P. Sharma and P. Gopalan, J. Electrochem.Soc., 2008, 155, B309.

24. Tealdi, G. Chiodelli, L. Malavasi and G. Flor, J. Mater. Chem., 2004, 14, 3553.

25. S. Nakayama, H. Aono and Y. Sadaoka, Chem. Lett., 1995,431

26. S. Nakayama, T. Kagayama, H. Aono and Y. Sadoaka, J. Mater. Chem., 1995, 5, 1801.

27. M. C. Steil, J. Fouletier, M. Kleitz and P. Labrune, J. Eur. Ceram. Soc., 1999, 19, 815

28. H. Iwahara, H. Uchida, K. Ono and K. Ogaki, J. Electrochem.Soc., 1988, 135, 529.

29. G. B. Zhang and D. M. Smyth, Solid State Ionics, 1995, 82, 153

30. T. Norby, Solid State Ionics, 1999, 125, 1.

31. Anthony R.West.Solid State Chemistry and its Application. John Wiley & Sons Ltd.,1984

32. H. M. Rietveld, Journal of Applied Crystallography, 1969, 2 ,65.

33. Lesley E smart, Elaine A. Moore.Solid State Chemistry: An Introduction,3rd edition, Taylor & Francis, 2005.

34. Evgenij Barsoucov, J. Ross Macdonald. Impedance spectroscopy Theory, experiment and Applications, 2nd edition, A John Wiley & Sons, 2005.

35.I Ahmeh, Phd thesis,ISBN:978-91-7385-101-5.

36. Karin Emma Josephina Eurenius,Phd thesis,ISBN:978-91-628-7897-9

37. Xinde Tang, Hongqi Ye, Zhi Zhao, Hui Liu, Chenxia Ma, Photocatalytic Splitting of Water Over a Novel Visible-Light-Response Photocatalyst Nd2InTaO7,2009, 133:362–369.

38. Kai Han, Hong-Qiye, Xin-De Tang, Zhi Zhao, Hui Liu, You-Feng Li , Preparation and photocatalytic activity of novel visible light driven photocatalyst Nd2InNbO7,2011 Vol. 5, p. 639 -642.

39 Berlaut, P. E. F.; Blum. P.:Sagninsa. A. A m Cr,rrollor. 1959.12,149.

40. S. A. Klimin*, M. N. Popova*, and B. V. Mill Infrared Spectroscopy of the Nd3+ Ion in Nd2BaCuO5 and Nd2BaZnO5, 2001, Vol. 44 pp. 1492–1497.

41. M.Taibi, J. Aride',J. Darriet, A. Moqine, A. Boukhari. Structure cristalline de l'oxyde Nd2BaZn05. Journal of Solid State Chemistry, 1990, 86, 233-237

42. Osamu Yamamoto. Solid oxide fuel cells: fundamental aspects and prospects, Electrochimica Acta, 2000, 45, 2423–2435.

43. Keiji Yamahara, Tal Z. Sholklapper, Craig P. Jacobson+, Steven J. Visco, LuTGArd C. De Jonghe. Ionic conductivity of stabilized zirconia networks in composite SOFC electrodes2004.LBNL-54801

44. Farheen Nasir Sayed, Balaji Prasad Mandal, Dheeraj Jain, Chirakarumpil Gopalan Nair Sivan Pillai, Avesh Kumar Tyagi, Journal of the European Ceramic Society,2012,32,3221-3228.